Oxidative Medicine and Cellular Longevity

Oxidative Stress and Inflammation in Cardiovascular Disease

Guest Editors: Noemí García, Cecilia Zazueta, and Leopoldo Aguilera-Aguirre

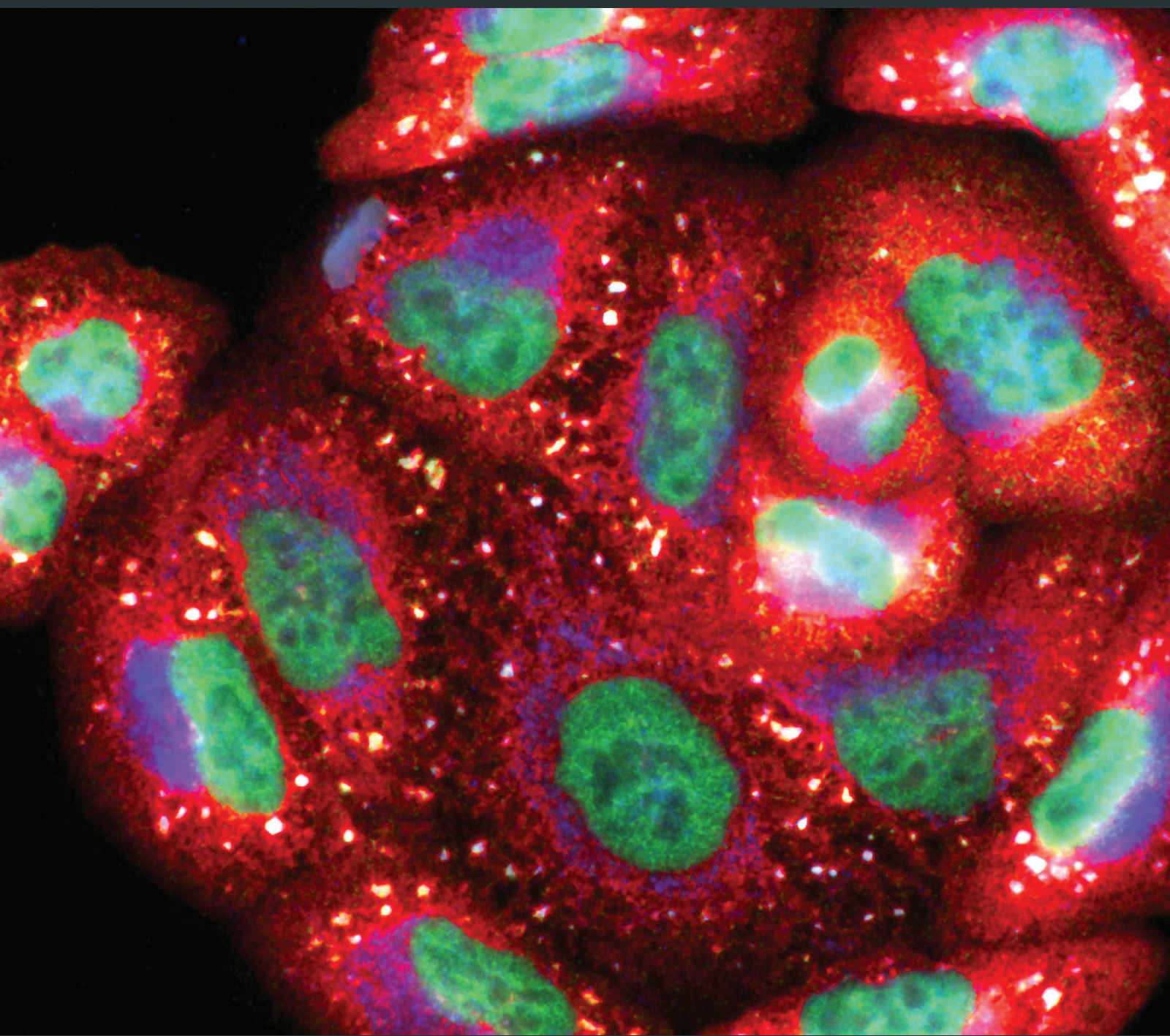

Oxidative Stress and Inflammation in Cardiovascular Disease

Oxidative Medicine and Cellular Longevity

Oxidative Stress and Inflammation in Cardiovascular Disease

Guest Editors: Noemí García, Cecilia Zazueta, and Leopoldo Aguilera-Aguirre

Editorial Board

Contents

Hindawi
Oxidative Medicine and Cellular Longevity
Volume 2017, Article ID 5853238, 2 pages
https://doi.org/10.1155/2017/5853238

Editorial
Oxidative Stress and Inflammation in Cardiovascular Disease

Noemí García,[1] Cecilia Zazueta,[2] and Leopoldo Aguilera-Aguirre[3]

[1]*Escuela de Medicina, Tecnológico de Monterrey, Monterrey, NL, Mexico*
[2]*Departamento de Biomedicina Cardiovascular, Instituto Nacional de Cardiología-Ignacio Chávez, Ciudad de México, Mexico*
[3]*Department of Microbiology and Immunology, University of Texas Medical Branch, Galveston, TX, USA*

Correspondence should be addressed to Noemí García; garcianr@itesm.mx

Received 9 March 2017; Accepted 9 March 2017; Published 27 April 2017

Evidence from experimental and clinical studies have shown that oxidative/nitrosative stress and inflammation associated with metabolic disorders such as obesity, hypertension, and diabetes conduce to left ventricular hypertrophy, fibrosis, diastolic dysfunction, heart failure, and ischemia/reperfusion damage [1, 2].

In this special issue, original researches on the causative effect of oxidative stress and inflammation on pathologies such as mitral valve prolapse (MVP), arteriosclerosis, hypertension, and ischemia/reperfusion (IR) injury are presented. Also, the evidence of the effect of NLRP3-inflammasome and reactive oxygen species (ROS) production by Ca2+ overload on mitochondrial function, along with the demonstration of the regulatory properties of MG132, demetoxicurcumin, and lycopene on signaling pathways that activate either nuclear factor E2-related factor 2 (Nrf2) or NFκB, are shown. Information in this issue also includes findings on the relationship between ROS and the activation/maturation of dendritic cells (DCs) that might trigger cardiovascular and metabolic pathologies.

The strong association between osteoprotegerin (OPG) levels and oxidative stress status in patients affected by MVP with severe regurgitation opens its possible use as a serum marker of this pathology according to P. Songia et al. On the other hand, R. Mastrocola et al. demonstrate that the inhibition of NLP3-inflammasome reduces IR injury by activating prosurvival RISK pathway and preserving mitochondrial function. This is interesting and is related to the article presented by Y. Oropeza-Alamazán et al., which demonstrates that silencing of MCU decreases ROS production and mitochondrial dysfunction induced by Ca2+ overload in reperfusion injury.

Pharmacological regulation of oxidative stress and inflammation is also included in this special issue. Y. Li et al. demonstrated that the downregulation of cyclooxygenase (COX-2) by demethoxycurcumin (DMC) favors nitric oxide (NO) production via e-NOS activation, preventing endothelial dysfunction, whereas L. Kong et al. demonstrated that MG132 administration inhibits Nrf2 and IkB proteolysis via the proteasome, preventing endothelial dysfunction associated with cardiovascular disease in animals with diabetic nephropathy. The antioxidant and anti-inflammatory properties of lycopene are shown to be related with the downregulation of Rho-associated kinases and the activation of key factor expression in the study described by Y. He et al., who propose that this compound might by a potentially effective method for transplant arteriosclerosis in clinical organ transplantation. Finally, J. Stein et al. show that Nox2-derivated oxidative stress and PKC activation play relevant roles in DCs activation and the atherothrombotic processes that might impinge on cardiovascular and metabolic pathologies.

We hope that the research articles included in this issue contribute to the understanding of mechanisms related to the development of cardiovascular diseases and increase the possibility to find novel specific markers and the proposal of new potential therapeutic treatment with the use of new drugs that regulated pathway risk related with the trigger of cardiovascular disease.

Acknowledgments

It is our pleasure to thank all the authors and the referees for their time and invaluable work that made this special issue possible.

Noemí García
Cecilia Zazueta
Leopoldo Aguilera-Aguirre

References

[1] A. L. Sverdlov, A. Elezaby, F. Qin et al., "Mitochondrial reactive oxygen species mediate cardiac structural, functional, and mitochondrial consequences of diet-induced metabolic heart disease," *Journal of the American Heart Association*, vol. 5, no. 1, pp. 1–13, 2016.

[2] X. Yao, D. Carlson, Y. Sun et al., "Mitochondrial ROS induces cardiac inflammation via a pathway through mtDNA damage in a pneumonia-related sepsis model," *PLoS ONE*, vol. 10, no. 10, pp. 1–29, 2015.

Hindawi
Oxidative Medicine and Cellular Longevity
Volume 2017, Article ID 4157213, 12 pages
https://doi.org/10.1155/2017/4157213

Research Article

Role of Protein Kinase C and Nox2-Derived Reactive Oxygen Species Formation in the Activation and Maturation of Dendritic Cells by Phorbol Ester and Lipopolysaccharide

Judith Stein,[1] Sebastian Steven,[2,3] Matthias Bros,[1] Stephan Sudowe,[1] Michael Hausding,[2,3] Matthias Oelze,[2] Thomas Münzel,[2,3] Stephan Grabbe,[1] Angelika Reske-Kunz,[1] and Andreas Daiber[2,3]

[1]*Department of Dermatology, Medical Center of the Johannes Gutenberg University, Mainz, Germany*
[2]*Center for Cardiology/Cardiology 1, Laboratory of Molecular Cardiology, Medical Center of the Johannes Gutenberg University, Mainz, Germany*
[3]*Center for Thrombosis and Hemostasis (CTH), Medical Center of the Johannes Gutenberg University, Mainz, Germany*

Correspondence should be addressed to Angelika Reske-Kunz; a.reske-kunz@uni-mainz.de and Andreas Daiber; daiber@uni-mainz.de

Received 18 November 2016; Revised 7 February 2017; Accepted 8 February 2017; Published 28 March 2017

Academic Editor: Leopoldo Aguilera-Aguirre

Aims. Activation/maturation of dendritic cells (DCs) plays a central role in adaptive immune responses by antigen processing and (cross-) activation of T cells. There is ongoing discussion on the role of reactive oxygen species (ROS) in these processes and with the present study we investigated this enigmatic pathway. *Methods and Results*. DCs were cultured from precursors in the bone marrow of mice (BM-DCs) and analyzed for ROS formation, maturation, and T cell stimulatory capacity upon stimulation with phorbol ester (PDBu) and lipopolysaccharide (LPS). LPS stimulation of BM-DCs caused maturation with moderate intracellular ROS formation, whereas PDBu treatment resulted in maturation with significant ROS formation. The NADPH oxidase inhibitors apocynin/VAS2870 and genetic gp91phox deletion both decreased the ROS signal in PDBu-stimulated BM-DCs without affecting maturation and T cell stimulatory capacity of BM-DCs. In contrast, the protein kinase C inhibitors chelerythrine/Gö6983 decreased PDBu-stimulated ROS formation in BM-DCs as well as maturation. *Conclusion*. Obviously Nox2-dependent ROS formation in BM-DCs is not always required for their maturation or T cell stimulatory potential. PDBu/LPS-triggered BM-DC maturation rather relies on phosphorylation cascades. Our results question the role of oxidative stress as an essential "danger signal" for BM-DC activation, although we cannot exclude contribution by other ROS sources.

1. Introduction

Immune cells provide protection of the organism from invading microbial pathogens. The immune system with its various cell types can be divided into innate immune system (e.g., PMN or NK cells) and adaptive immune response (e.g., lymphocytes). Dendritic cells (DCs) serve as a messenger between adaptive and innate immune response [1]. A key event in the adaptive immune response consists of the priming or sensitization of resting T cells, which is a prerequisite for any antigen-induced cellular adaptive immune response. T cell activation largely depends on efficient presentation of antigen fragments by antigen-presenting cells such as DCs. The latter are located in tissues with close contact to the external environment like skin (Langerhans cells) or epithelium of lungs and intestines. DC-dependent activation of T cells also contributes to the development of arterial hypertension [2]. This underlines the clinical relevance of DC activation/maturation for cardiovascular disease. It is known that platelet activation during the course of vascular injury or bleeding and subsequent CD40L release provides a "danger signal" that activates DCs at the site of blood vessel damage and thus facilitates the induction of local T cell-mediated immune responses. In addition, other "danger signals" such

as bacterial or fungal endotoxins (e.g., lipopolysaccharide [LPS] or zymosan A), tissue injury markers (e.g., uric acid, hyaluronic acid), immune activation (e.g., CD40L, inflammatory cytokines), and even angiotensin II cause potent activation/maturation of DC [2, 3]. Therefore, an inflammatory and thrombotic environment represents a major trigger for DC activation, maturation, and infiltration, and subsequent immune responses leading to atherothrombotic events in the vasculature.

In addition to the above-described classical "danger signals," DCs may also become activated by oxidative stress, either via direct immunomodulatory actions of ROS on proteins in immune cells or on mediators of inflammation (e.g., oxLDL, isoketals, and other lipid peroxidation products) [4–11]. In support of this notion, it was shown that oxidative stress in the bone marrow upregulates TNFα leading to activation of DCs [12] and that vascular oxidative stress leads to DC activation, adhesion, and transmigration [13]. However, cigarette smoke-induced oxidative stress suppressed the generation of key cytokines by maturing DCs through the activation of ERK-dependent pathways [14]. In turn, ROS have been demonstrated to activate NADPH oxidases in a protein kinase C-dependent fashion [15] opening the opportunity to activate the DC NADPH oxidase (Nox2 isoform). Several publications ascribe an important role of Nox2-derived ROS in antigen processing and presentation by controlling the pH of the phagosome [16–18]. Protein kinase C (isoform α) not only is an essential activator of Nox2 activity but also regulates cytokine production of DCs in a MyD88- and toll-like receptor- (TLR-) dependent fashion [19].

With the present study we sought to investigate the role of protein kinase C and Nox2-derived ROS in DC maturation and T cell stimulatory capacity.

2. Materials and Methods

2.1. Animals and Treatment Protocol. C57BL/6, BALB/cJ, and *gp91*^{phox} knockout mice were obtained from the Translational Animal Research Center of the University Medical Center Mainz and maintained under pathogen-free conditions on a standard diet.

Hemizygous *gp*91$^{phox-/y}$ mice (Nox2 knockout (#2365), C57BL/6 background, Jackson Laboratories, Bar Harbor, ME) were generated as described previously [20] and C57BL/6 mice were used as the corresponding wild type controls. Mice were sacrificed under isoflurane anesthesia and femurs and tibias were recovered for generation of BM-DCs. Animal treatment was in accordance with the Guide for the Care and Use of Laboratory Animals as adopted and promulgated by the US National Institutes of Health and was approved by the Ethics Commission according to the German Law on the Protection of Animals (Landesuntersuchungsamt Rheinland-Pfalz, Koblenz, Germany: #23 177-07/G 10-1-054, #23 170-07/G 07-1-023).

2.2. Bone Marrow-Derived DCs. BM-DCs were generated as first described by Scheicher et al. [21] and modified by Bros et al. [22]. Shortly, bone marrow cells (2×10^6 cells/10 ml) were cultured in IMDM supplemented with 5% heat-inactivated FCS (Gibco, Paisley, UK), 2 mM L-glutamine (Roth, Karlsruhe, Germany), 100 U/ml penicillin, 100 μg/ml streptomycin (both PAA, Pasching, Austria), 50 μM β-mercaptoethanol (Roth), and 5% GM-CSF-containing cell culture supernatant derived from X63.Ag8-653 myeloma cells stably transfected with a murine GM-CSF expression construct [23] on bacterial dishes (Greiner Bio-One, Frickenhausen, Germany). BM-DC culture medium was replenished on day 3 and day 6 of culture. On day 7, immature BM-DCs were harvested, centrifuged, reseeded in 6-well nontissue culture treated plates (1×10^6 cells/2 ml), and cultured for another 24 hours.

2.3. Detection of Extracellular and Intracellular ROS Formation of Cultured BM-DCs. Oxidative burst of cultured BM-DCs (24-well, 1×10^6 cells/well, day 8) was induced by phorbol ester dibutyrate (PDBu, 10 μM) (Sigma-Aldrich, Steinheim, Germany) or LPS (50 μg/ml) (Calbiochem) using L-012- (100 μM-) enhanced chemiluminescence (ECL) in PBS (1 mM Ca^{2+}/Mg^{2+}) on a Centro plate reader (Berthold Technology, Bad Wildbad, Germany). In some experiments, inhibitors of NADPH oxidase, apocynin (150 or 300 μM, Sigma-Aldrich) or VAS2870 (20 μM, Sigma-Aldrich), or the protein kinase C inhibitors chelerythrine (10, 50, and 100 μM, Sigma-Aldrich) or Gö6983 (0.1, 1, 10 μM, Sigma-Aldrich) were added to the cells 20 min before addition of the L-012 dye and stimulation with PDBu or LPS. ROS formation by BM-DCs (24-well, 2×10^5 cells/well) was also tested by dichlorofluorescein-diacetate (DCF-DA, 20 μM) or dihydroethidium (DHE, 1 μM) fluorescence using a Mithras 2 fluorescence plate reader for DCF-DA (Berthold Techn., Bad Wildbad, Germany; filters for excitation: 485 ± 10 nm, emission: 535 ± 10 nm) and fluorescence microscopy for DHE (Axiovert, Zeiss). DCF-DA was added with the inhibitor to the cells 20 min before stimulation with PDBu or LPS.

2.4. Detection of Intracellular ROS Generation by Flow Cytometry (FACS). On day 8 of culture, an aliquot of BM-DCs was incubated with the dye CM-DCF-DA (5 μM/1×10^6/ml) (Thermo Fisher Scientific, Waltham, MA) for 30 min, while another aliquot was left untreated. Cells were stimulated with LPS (1.5 μg/ml), various concentrations of PDBu (0.1 μM, 1 μM, or 10 μM), PMA (50 ng/ml, Sigma-Aldrich), zymosan A (50 μg/ml, life technologies), lipoteichoic acid (10 μg/ml, Sigma-Aldrich), activating antiCD40 Ab (10 μg/ml), mouse recombinant soluble CD40L (0.5 μg/ml, ImmunoTools, Frisoythe, Germany), TNF-α/IL-1β (10 ng/mg each, ImmunoTools), or remained unstimulated as a control for the time points indicated. Cells were harvested and washed in staining buffer (PBS/2% FCS). To avoid Fc receptor-mediated nonspecific binding of antibodies (Ab), cells were incubated for 15 min on ice with a rat anti-mouse CD16/CD32 Ab (clone 2.4G2, purified from hybridoma supernatant). Cell surface was stained with a phycoerythrin- (PE-) conjugated Ab recognizing CD11c (clone N418, Miltenyi Biotec, Bergisch-Gladbach, Germany) and a phycoerythrin-cyanine 5- (PE-Cy5-) conjugated Ab recognizing MHCII

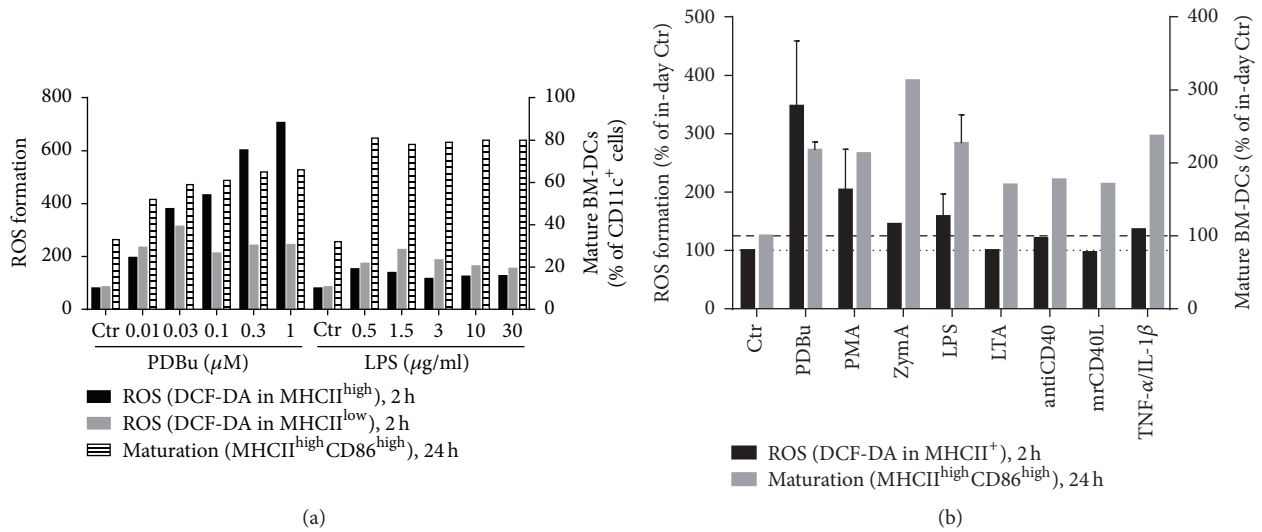

Figure 1: Analysis of ROS formation 2 h and maturation (high MHCII and CD86 expression) 24 h after stimulation of BM-DCs with (a) increasing concentrations of PDBu (0.01–1 μM) or LPS (0.5–30 μg/ml) or (b) PDBu (0.1 μM), PMA (50 ng/ml), zymosan A (ZymA, 50 μg/ml), LPS (1.5 μg/ml), lipoteichoic acid (LTA, 10 μg/ml), antiCD40 (10 μg/ml), mrCD40L (0.5 μg/ml) or TNF-α/IL-1β (10 ng/ml each) by flow cytometry. Representative data of one single experiment are shown (a) and mean ± SEM of n = 1–3 experiments (b).

(clone M5/114, eBioscience, San Diego, CA). Suitable isotype control Abs were used. Flow cytometry measurement was performed using a FACS Canto II flow cytometer (BD Biosciences) and analyzed using FlowJo software. In particular, DCs were identified by the expression of the surface marker CD11c (named CD11c$^+$ cells), and these were subsequently subdivided into MHCII^{high} expressing DCs and MHC^{low} expressing DCs as indicated in suppl. Figure 1S available online at https://doi .org/10.1155/2017/4157213. ROS generation was analyzed in both subpopulations.

2.5. Detection of Maturation Using FACS. Stimulated and unstimulated BM-DCs were harvested and Fc-receptor block was performed as described above. Cell surface was stained with the following Abs: fluorescein isothiocyanate- (FITC-) conjugated anti-CD11c (clone N418, Miltenyi Biotec), PE-conjugated anti-CD86 (clone GL1, eBioscience), and PE-Cy5-conjugated anti-MHCII (clone M5/114, eBioscience). Cells were fixed with 0.7% paraformaldehyde (Merck, Darmstadt, Germany) in PBS and subjected to FACS analysis as described above. As described above, DCs were defined as CD11c$^+$ cells, and expression of MHCII^{high} and CD86^{high} characterized these cells as mature DCs as indicated in suppl. Figure 2S.

2.6. Allogeneic T Cell Stimulation Assays. Splenic BALB/cJ T cells (3×10^5) enriched by nylon wool adherence as described [24] were cocultured with serially diluted C57BL/6 or $gp91^{phox-/y}$ BM-DCs (start concentration: 5×10^4) in triplicates in 200 μl culture medium without GM-CSF in 96-well flat-bottom plates for 4 days. Proliferation was assessed by measuring the genomic incorporation of [^{3}H] thymidine (0.25 μCi/well), which was added for the last 16 h of the culture. Cells were harvested onto glass fiber filters and retained radioactivity was measured in a liquid scintillation counter (1205 Betaplate, LKB Wallac, Turcu, Finland).

2.7. Statistical Analysis. Data are expressed as mean ± SEM. Statistically significant differences were assessed by using one-way ANOVA for comparisons of groups followed by pairwise comparison analysis using Holm-Sidak. p values < 0.05 were considered statistically significant ($^*p < 0.05$, $^{**}p < 0.01$, and $^{***}p < 0.001$). Analysis was performed for most data by using SigmaPlot 12.3 (Systat Software, San Jose, CA) and for chemiluminescence and fluorescence data of ROS formation by employing Prism 6 for Windows, version 6.05, GraphPad Software.

3. Results

3.1. LPS and the PKC-Activator PDBu Promote BM-DC Maturation, but Only PDBu Increases Intracellular ROS Formation in BM-DCs. In a set of pilot experiments, we observed that the phorbol ester PDBu induced a concentration-dependent increase in ROS formation in MHCII^{high} cells, whereas maturation was augmented by the lowest concentration of PDBu and showed only marginal further increase at higher concentrations of PDBu (Figure 1(a)). In contrast, the endotoxin LPS at all concentrations employed increased the maturation of BM-DCs to a similar extent but led to a less pronounced augmentation of the ROS formation rate as compared to PDBu (Figure 1(a)). Puzzled by this obvious dissociation between ROS formation and maturation in BM-DCs we tested a set of different stimulators of BM-DC maturation. We found that only phorbol esters induced ROS formation and maturation, whereas all other classical stimulators induced maturation without significant ROS formation (Figure 1(b)). In order to exclude artificial ROS signals by FACS analysis,

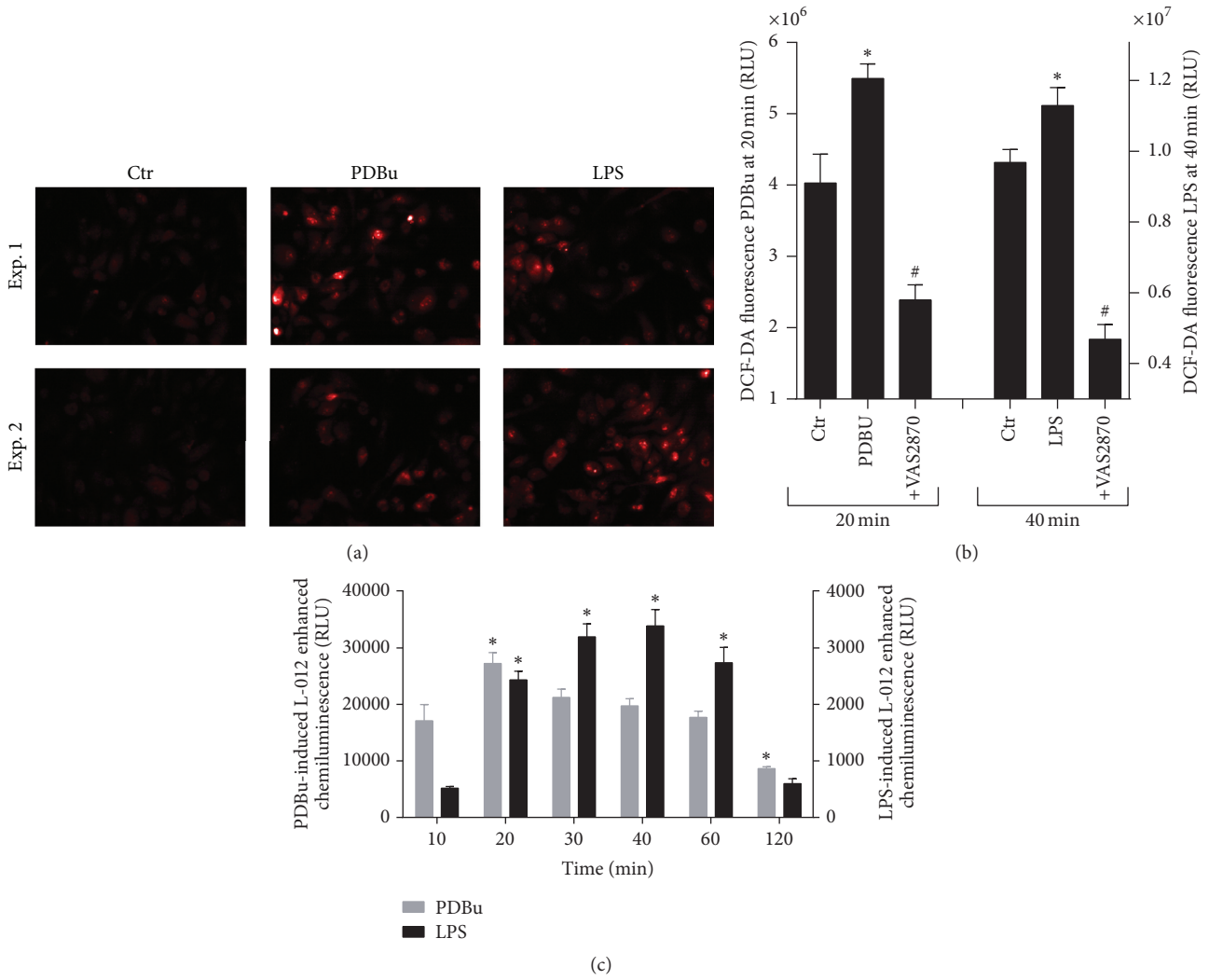

FIGURE 2: Treatment of BM-DCs (2×10^5 cells/well) with PDBu (10 μM) and analysis of the formation of intra- and extracellular ROS measured by (a) DHE (1 μM) fluorescence microscopy 20 min after addition of PDBu (10 μM) or LPS (50 μg/ml) (magnification 200x), (b) DCF-DA (20 μM) fluorescence in a plate reader 20 min after addition of PDBu, or 40 min after addition LPS in the presence or absence of the NADPH oxidase inhibitor VAS2870 (20 μM). (c) Kinetics of ROS formation were measured by L-012 (100 μM) ECL upon addition of PDBu or LPS. Representative images of 2 independent experiments (a) and mean ± SEM of 8 (b) and 8 (c) experiments are shown. $^*p < 0.05$ versus Ctr (w/o PDBu or LPS) or $^\#p < 0.05$ versus stimulated (with PDBu or LPS) (b) and $^*p < 0.05$ versus time point 10 min (c).

we tested other ROS detection methods. Staining of cultured BM-DCs with the fluorescence dyes dihydroethidium (DHE) or dihydrodichlorofluorescein diacetate (DCF-DA) revealed a quite similar increase in intracellular ROS formation upon stimulation of BM-DCs with PDBu or LPS (Figures 2(a) and 2(b)). Due to a high background signal, the increase in ROS formation upon stimulation with PDBu or LPS was less obvious with DCF-DA but was significantly suppressed by the NADPH oxidase inhibitor VAS2870. Using the luminol analogue and chemiluminescence dye L-012 we established a time course for PDBu- and LPS-induced extracellular ROS formation by BM-DCs with maxima at 20 and 40 min, respectively (Figure 2(c)). Maximal ROS formation revealed by L-012 ECL was approximately 10-fold more pronounced with PDBu stimulation as compared with the LPS-treated group. Therefore, the overall ROS signal induced by the two stimulators largely depends on the site of ROS measurement and the employed dye.

More detailed FACS analysis confirmed these initial findings on the dissociation between ROS formation and maturation of BM-DCs. Only PDBu, but not LPS, resulted in a significant increase in ROS formation by BM-DCs at 15 and 120 min (Figures 3(a) and 3(b)), whereas both stimuli increased the maturation at 24 h after stimulation to a similar degree (Figure 3(c)). Furthermore, T cell stimulatory capacity of BM-DCs was increased by PDBu and LPS (Figure 3(d)).

3.2. PDBu-Induced Maturation of BM-DCs Can Be Blocked by PKC-Inhibition and Does Not Depend on Nox2-Derived ROS Formation. Since previous studies identified the NADPH oxidase system (mainly the Nox2 isoform) as a potent source of ROS in activated BM-DCs, we tested the effect of the

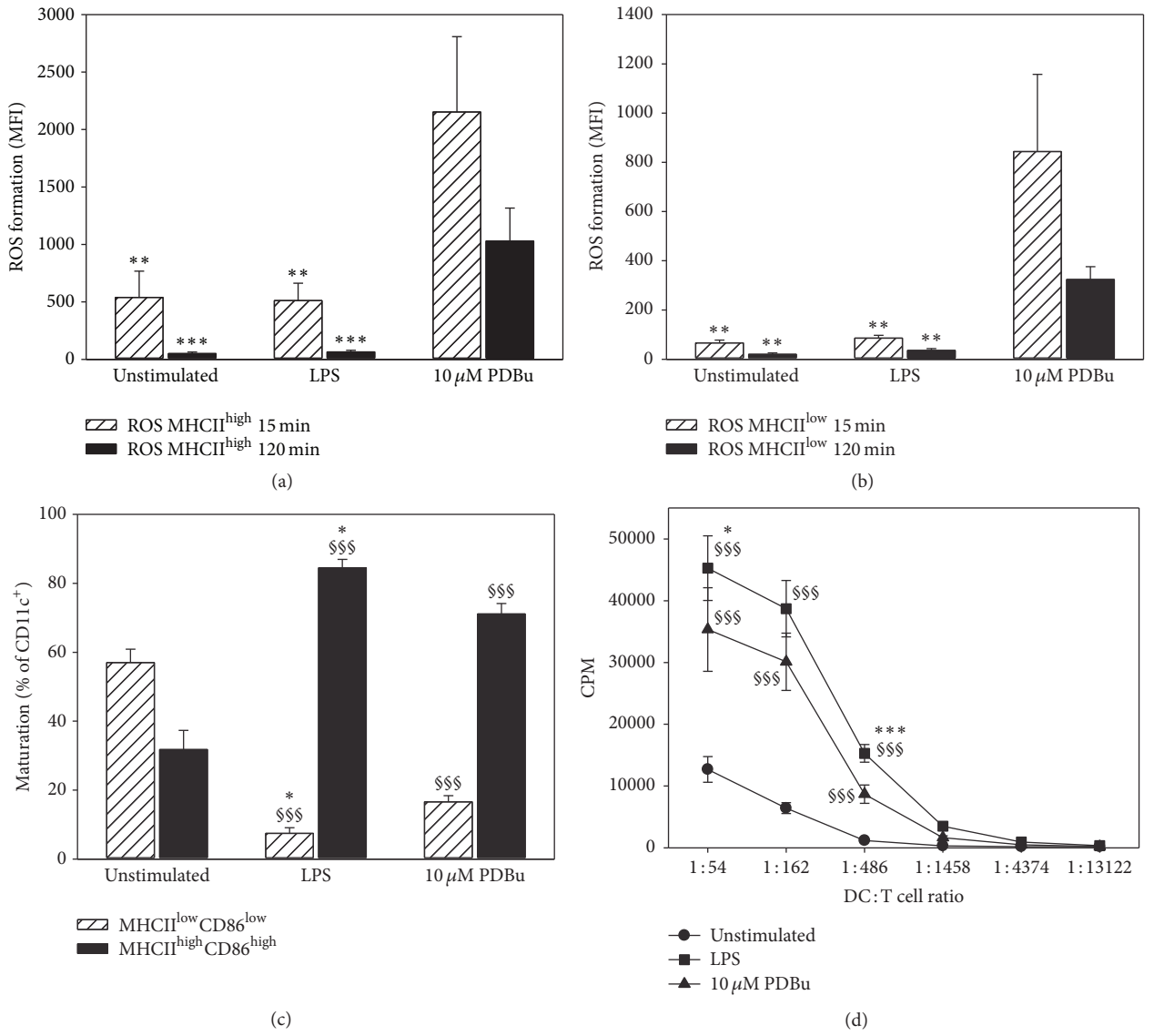

Figure 3: Analysis of intracellular ROS formation upon activation of BM-DCs, of maturation at 24 h after stimulation, and of their T cell stimulatory capacity. (a) 1×10^6 BM-DCs were stimulated with LPS (1.5 μg/ml) or PDBu (10 μM). ROS formation (a) in MHCII^{high} and (b) MHCII^{low} expressing CD11c$^+$ cells was analyzed by flow cytometry after 15 or 120 min. (c) Maturation was characterized by high MHCII and CD86 expression after 24 h using flow cytometry. (d) T cell stimulatory capacity was compared in a proliferation assay with a constant number of T cells (3×10^5) cocultured with decreasing numbers of differentially stimulated BM-DCs, and on day 4 proliferation of T cells was measured by incorporation of [^{3}H] thymidine. Data are mean ± SEM of (a) 4-5, (b) 4-5, (c) 5, and (d) 3 experiments. $^{***}p < 0.001$; $^{**}p < 0.01$ versus PDBu (a, b); $^{§§§}p < 0.001$ versus unstimulated; $^{*}p < 0.05$; $^{***}p < 0.001$ versus PDBu (c, d).

pharmacological inhibitor of NADPH oxidase-derived ROS formation, apocynin, on the ROS signal, and maturation of BM-DCs. We established a concentration-dependent inhibition of BM-DC-derived extracellular ROS formation by apocynin and the known Nox2 inhibitor nebivolol [25, 26] (Figure 4(a)). Also, LPS-induced extracellular ROS formation by BM-DCs was decreased by apocynin in a dose-dependent fashion (Figure 4(b)). In contrast, apocynin only caused a minor inhibition of maturation (Figure 4(c)) but a more pronounced loss of T cell stimulatory capacity (Figure 4(d)) of PDBu-stimulated BM-DCs. The latter would be compatible with numerous reports on a role of Nox2 in antigen presentation by BM-DCs that is based on pH modulation in the phagosome [16–18].

Since apocynin, especially at higher concentrations, has direct antioxidant properties [27], we also tested genetic deletion of the Nox2 subunit gp91phox in order to characterize the role of Nox2-derived ROS in BM-DC maturation and T cell stimulatory capacity. Although we observed a significant decrease in ROS formation by PDBu-stimulated BM-DCs of gp91phox-deficient as compared with control mice (Figures 5(a) and 5(b)), neither maturation nor T cell

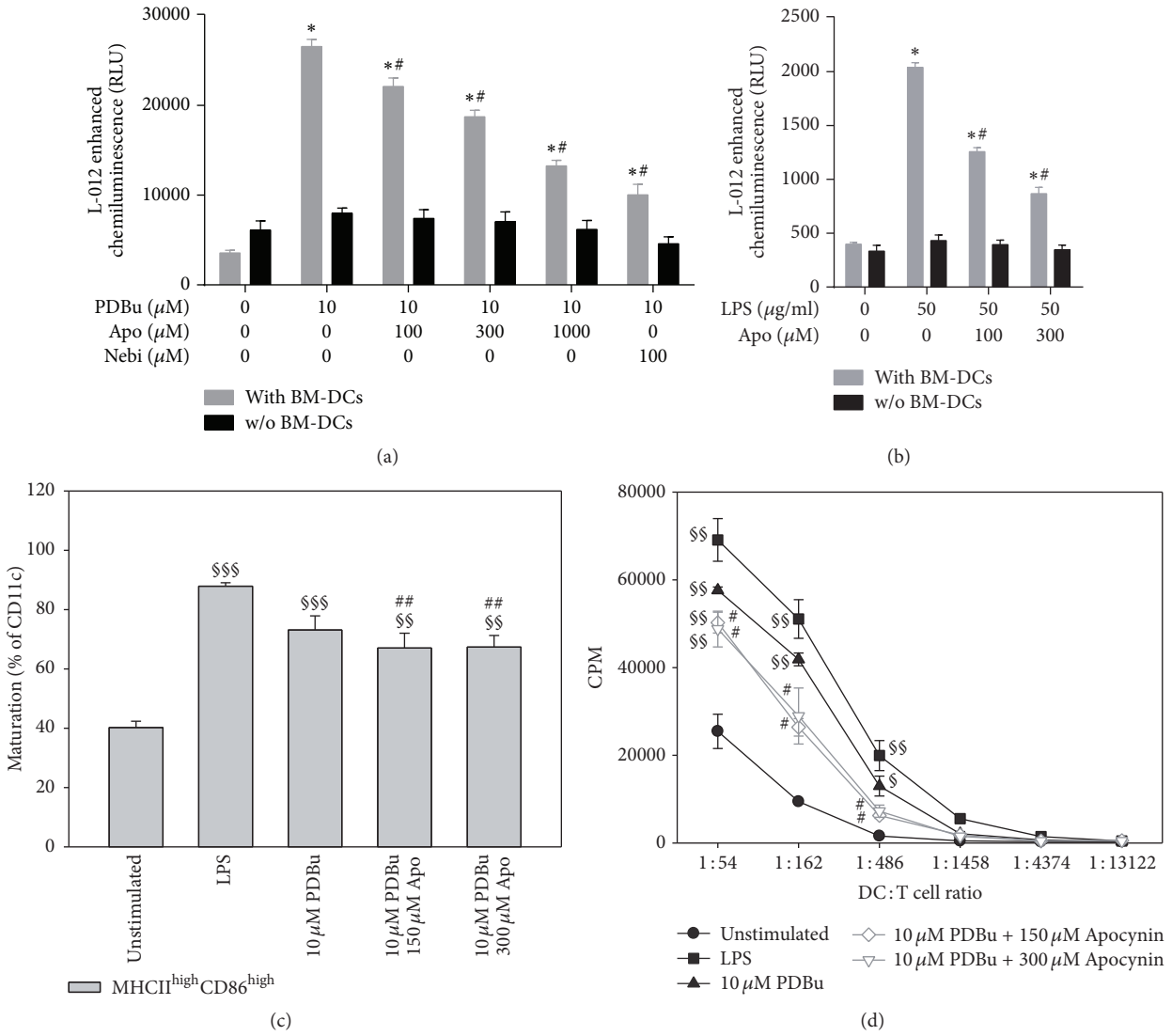

Figure 4: Analysis of the effects of apocynin treatment on the formation of ROS, maturation, and the T cell stimulatory capacity of BM-DCs upon activation by PDBu or LPS. (a) BM-DCs (1×10^6 cells/well) were stimulated with PDBu (10 μM) and additionally treated with different concentrations of apocynin (100–1000 μM) or with the potent inhibitor of Nox2 activity nebivolol (100 μM), and ROS generation was measured by L-012 chemiluminescence at 10 min after stimulation. (b) ROS formation after stimulation of BM-DCs (1×10^6 cells/well) with LPS (50 μg/ml) and cotreatment with apocynin (100–300 μM) was measured by L-012 chemiluminescence at 40 min after stimulation. (c) Maturation of BM-DCs (expression of MHCII and CD86 at high level) was analyzed after stimulation with LPS (1.5 μg/ml) or PDBu (10 μM) and treatment with apocynin (150–300 μM) after 24 h via flow cytometry. (d) T cell stimulatory capacity after apocynin treatment was compared in a proliferation assay (see legend to Figure 3). Data are mean ± SEM of 8 (a, b) and 3 (c) experiments. (d) One representative experiment of two is shown. (a, b) $^{*}p < 0.05$ versus Ctr (w/o PDBu or LPS); $^{\#}p < 0.05$ versus PDBu or LPS treated sample; (c) $^{\S\S\S}p < 0.001$; $^{\S\S}p < 0.01$ versus unstimulated; $^{\#\#}p < 0.01$ versus LPS. (d) $^{\S\S}p < 0.01$; $^{\S}p < 0.05$ versus unstimulated; $^{\#}p < 0.05$ versus PDBu.

stimulatory capacity was significantly impaired in gp91phox-deficient animals upon PDBu stimulation (Figures 5(c) and 5(d)). However, since PDBu-induced ROS formation was not completely absent in BM-DCs without gp91phox, we cannot exclude contribution of other sources of ROS (e.g., mitochondria or other Nox isoforms) to BM-DC maturation and T cell stimulatory capacity.

Nox2 activation is mainly mediated by PKC [28], which in turn was reported to essentially contribute to DC cytokine production [19]. We therefore tested the effect of the PKC inhibitor chelerythrine on BM-DC-derived ROS formation and maturation. Chelerythrine induced a concentration-dependent inhibition of PDBu- and LPS-induced BM-DC-derived extracellular ROS formation (Figures 6(a) and 6(b)). Also PDBu-induced intracellular ROS formation by BM-DCs (measured by FACS analysis) was decreased by chelerythrine in a dose-dependent fashion (Figure 6(c)). LPS-triggered ROS formation was clearly less pronounced as compared to the PDBu-treated group. PDBu-triggered BM-DC maturation was completely abolished by chelerythrine (Figure 6(d)).

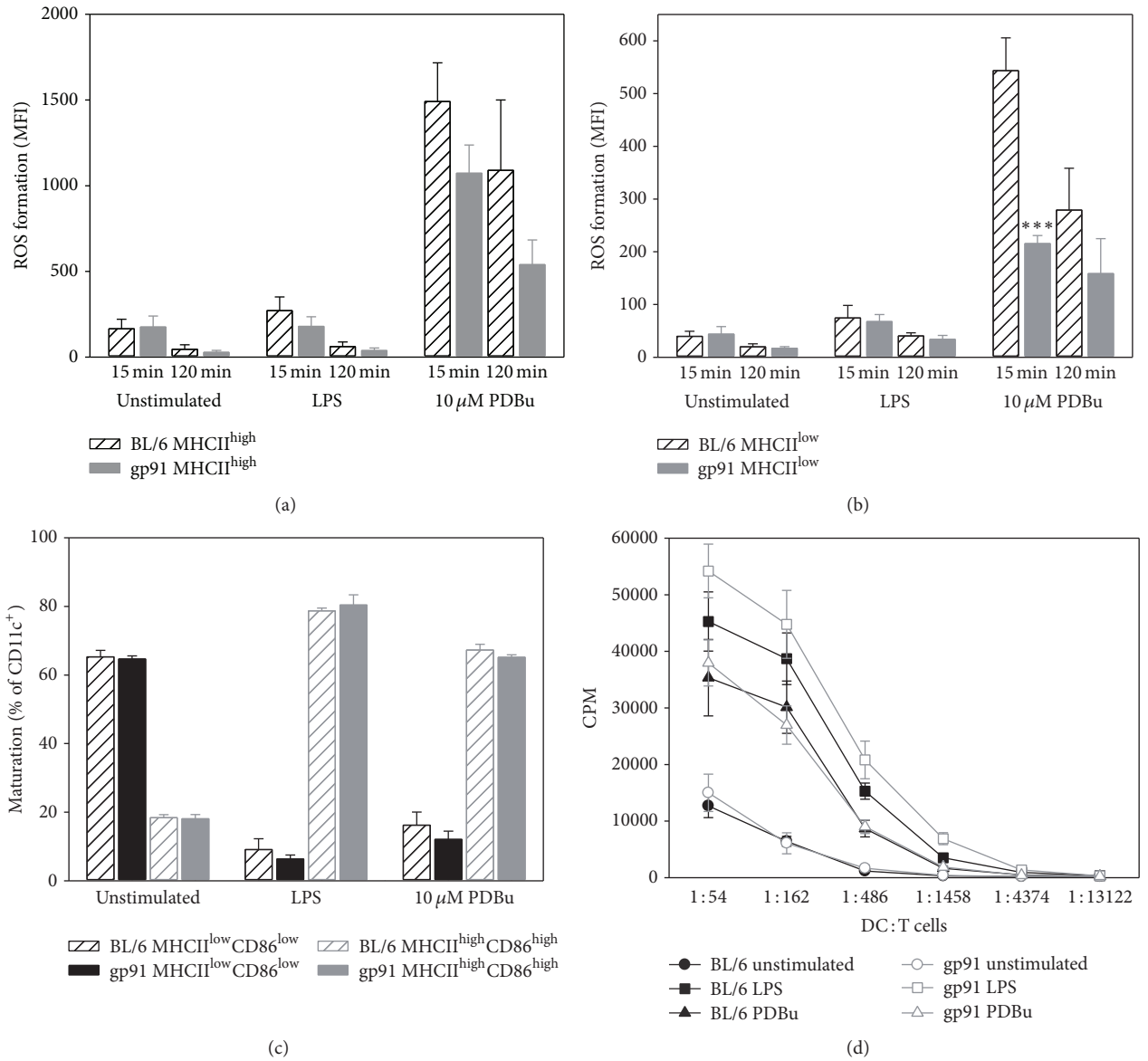

FIGURE 5: Analysis of the effects of genetic knock out of the gp91^{phox} subunit of the phagocytic NADPH oxidase on ROS formation, maturation, and T cell stimulatory capacity of PDBu- or LPS-activated BM-DCs. BM-DCs of control mice (C57BL/6) and gp91$^{phox-/y}$ mice were stimulated with LPS (1.5 μg/ml) or PDBu (10 μM). ROS formation was measured after 15 and 120 min in MHCII^{high} (a) or MHCII^{low} (b) expressing CD11c^{+} cells. (c) Analysis of maturation represented by high expression of MHCII and CD86 24 h after stimulation. (d) Analysis of T cell stimulatory capacity on day 4. Data are mean ± SEM of (a) 3, (b) 3, (c) 3, and (d) 3 experiments. $^{***}p < 0.001$ versus C57BL/6 PDBu at 15 min.

In an independent experiment we showed that the Nox2 inhibitor VAS2870 as well as the alternative PKC inhibitor Gö6983 inhibited the PDBu or LPS-stimulated extracellular ROS signal in BM-DCs (Figures 7(a) and 7(b)). As shown for chelerythrine, also Gö6983 decreased the PDBu-triggered BM-DC maturation (Figure 7(c)).

4. Discussion

The results of the present study demonstrate that the phorbol ester PDBu like LPS, which are classical stimulators for oxidative burst in PMN, trigger BM-DC maturation and T cell stimulatory capacity. We aimed to identify the role of oxidative stress in BM-DC maturation and found that PDBu and to a minor extent also LPS induced intracellular ROS formation in BM-DCs. Interestingly, inhibition of NADPH-oxidase by apocynin, VAS2870, or genetic knock-out of Nox2 subunit gp91phox had only minor or no effect on BM-DC maturation and T cell stimulatory capacity. However, inhibition of protein kinase C by chelerythrine or Gö6983 inhibited both PDBu-induced maturation and ROS formation. Taken together, we here provide evidence against an essential role of intracellular Nox2-derived ROS formation in BM-DC maturation by PDBu and LPS.

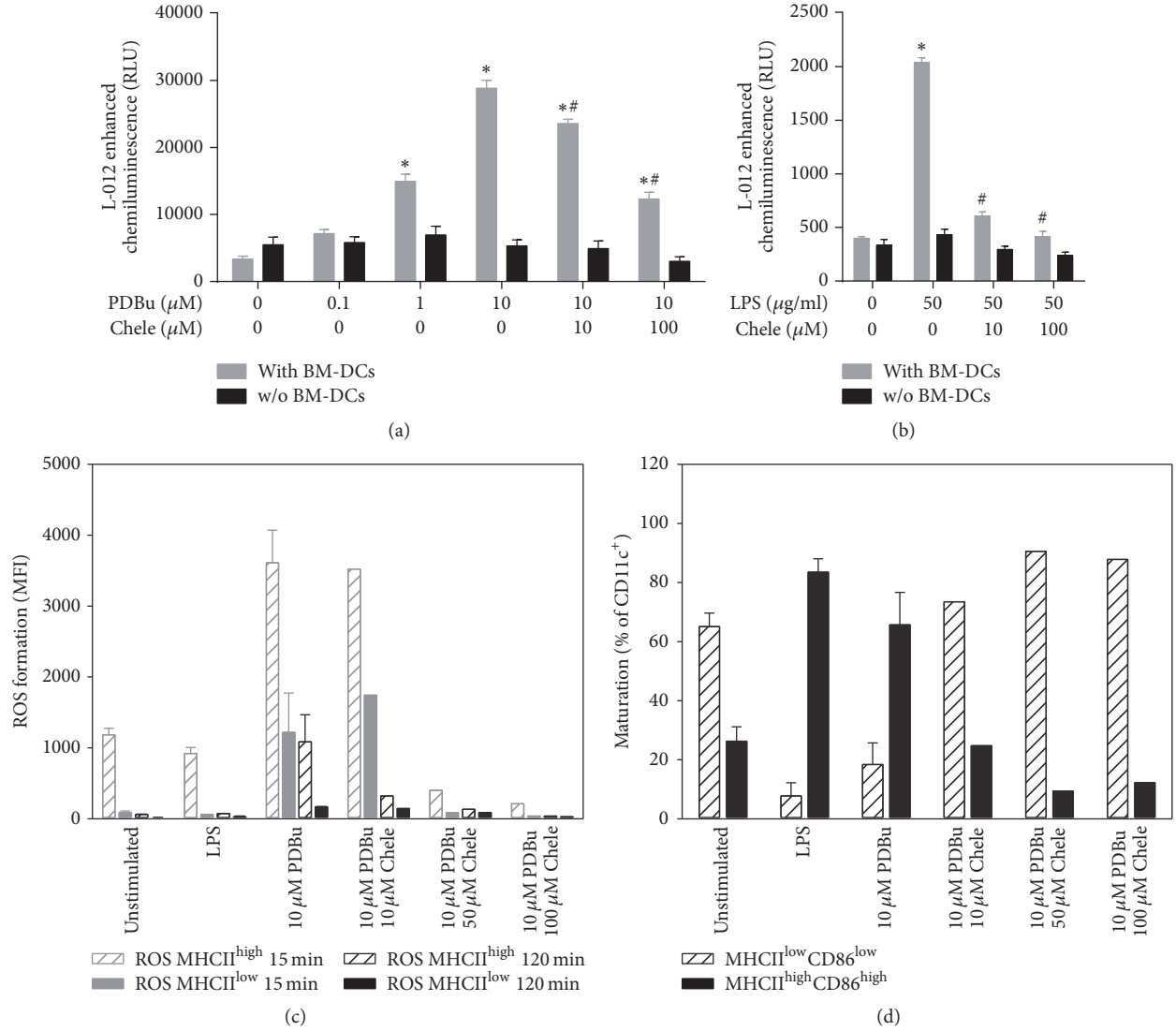

Figure 6: Analysis of the effects of chelerythrine treatment on the formation of ROS and maturation of BM-DCs upon activation by PDBu or LPS. (a) BM-DCs (1×10^6 cells/well, 24-well plate) were stimulated with PDBu (0.1, 1, and 10 μM) and additionally treated with different concentrations of chelerythrine (10 and 100 μM), and ROS generation was measured by L-012 chemiluminescence at 20 min after stimulation. (b) ROS formation after stimulation of BM-DCs (1×10^6 cells/well, 24-well plate) with LPS (50 μg/ml) and cotreatment with chelerythrine (10 and 100 μM) was measured by L-012 chemiluminescence at 40 min after stimulation. Analysis of ROS generation (c) and maturation (d) after stimulation with LPS (1.5 μg/ml) or PDBu (10 μM) and cotreatment with chelerythrine (10–100 μM) using flow cytometry. Synthesis of 2 experiments (controls were merged) with different chelerythrine concentrations. Data are mean ± SEM of 8 (a, b) and 1-2 (c, d) experiments. $^*p < 0.05$ versus Ctr (w/o PDBu or LPS); $^\#p < 0.05$ versus PDBu- or LPS-treated sample.

The phagocyte NADPH oxidase Nox2 is a well-known player in host defense of the innate immune system, and there is increasing evidence for a role of Nox2 in adaptive immunity [29–31]. Patients suffering from chronic granulomatous disease (CGD) have a higher susceptibility to autoimmune diseases like lupus erythematosus or rheumatoid arthritis [32, 33]. Maturation of DCs is part of the pathogenesis of such autoimmune diseases [34]. Nox2-deficient mice crossed onto a lupus-prone genetic background (MRL.Fas^{lpr}) develop higher antibody titer and a more severe clinical picture of the disease than control mice [35]. Furthermore, Nox2 is involved in antigen presentation by BM-DCs, which is based on pH modulation in the phagosome [16–18].

However, the role of Nox2-derived ROS in autoimmune disease is not clear until now and the literature data reflect a quite contradictory picture of the role of ROS formation in DC maturation. It was shown that ROS-low DCs displayed a more pronounced response to TLR agonists like LPS and zymosan, followed by accelerated maturation and T cell stimulatory capacity as compared with ROS-high DCs, which showed increased MAPK signaling, adhesion and hydrogen peroxide release indicating their role in immediate microbial

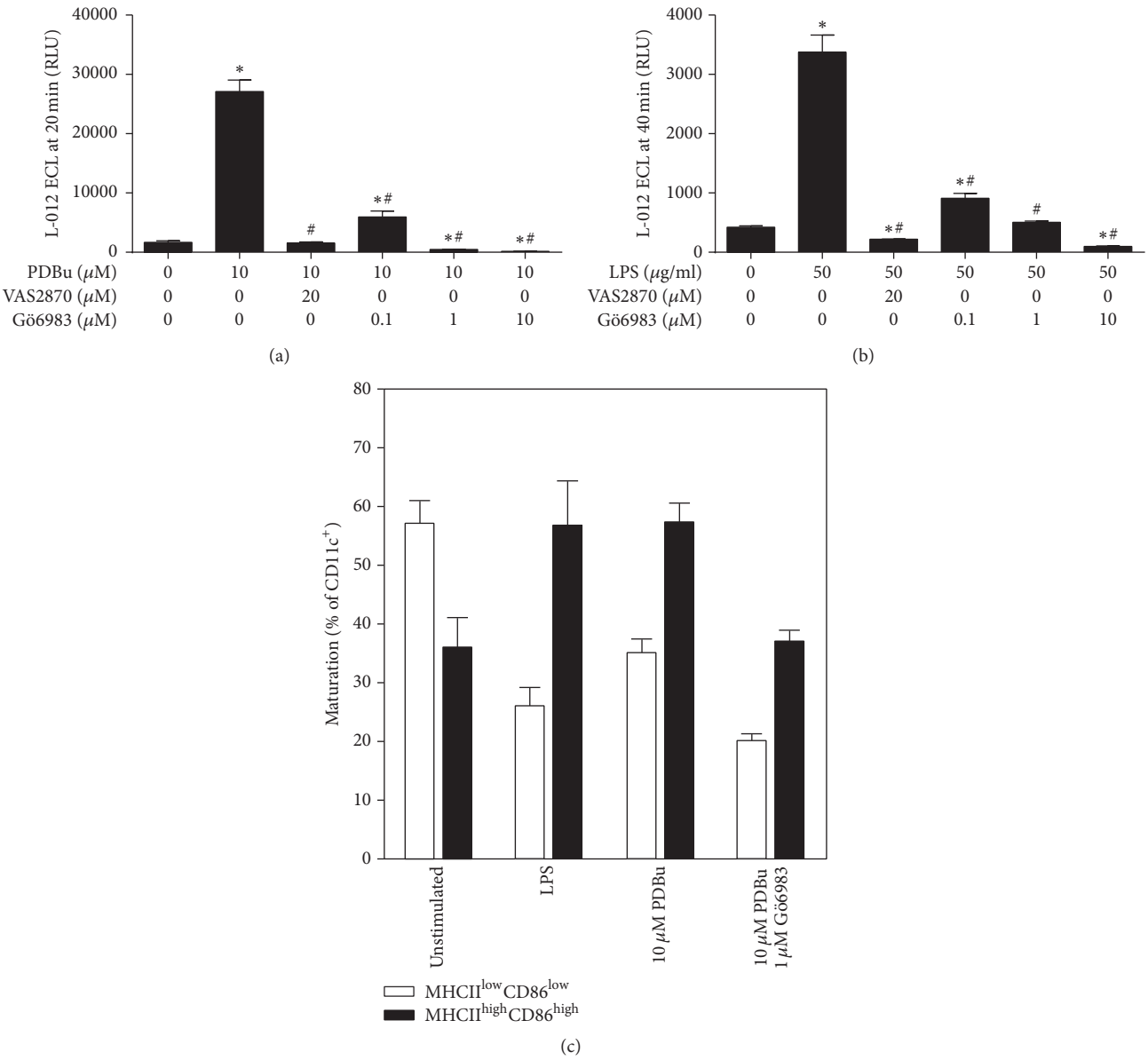

Figure 7: Analysis of the effects of the treatment with the NADPH oxidase inhibitor VAS2870 and the PKC inhibitor Gö6983 on the formation of ROS and maturation of BM-DCs upon activation by PDBu or LPS. (a) BM-DCs (2×10^5 cells/well, 96-well plate) were stimulated with PDBu and additionally treated with VAS2870 and Gö6983, and ROS generation was measured by L-012 (100 μM) chemiluminescence at 20 min after stimulation. (b) ROS formation after stimulation of BM-DCs (2×10^5 cells/well, 96-well plate) with LPS and cotreatment with VAS2870 and Gö6983 was measured by L-012 chemiluminescence at 40 min after stimulation. (c) Analysis of maturation of BM-DCs (1×10^6 cells/well, 24-well plate) after stimulation with LPS (1.5 μg/ml) or PDBu (10 μM) and cotreatment with Gö6983 using flow cytometry. Data are mean ± SEM of 8 (a, b) and 2 (c) experiments. $^*p < 0.05$ versus Ctr (w/o PDBu or LPS); $^\#p < 0.05$ versus PDBu- or LPS-treated sample.

targeting [36]. In contrast, liposome-driven ROS formation and chemokine (ERK-dependent)/cytokine (MAPK-dependent) production were all prevented by unspecific antioxidants (TEMPO and ebselen), an inhibitor of flavin-dependent oxidoreductases including NADPH oxidases (diphenyl iodonium) and a MAPK inhibitor (SB203580) [37]. Although representing an unspecific approach, cigarette smoke extract induced ROS formation, production of the chemokines CCL3 and CXCL2, and NFκB activation in a TLR-dependent fashion, all of which were prevented by the antioxidant N-acetylcysteine [38]. Another unspecific approach was based on LPS-triggered ROS formation by DCs and their activation (maturation, cytokine production, and T cell stimulatory potential), all of which were prevented by the antioxidant ebselen [39], however, keeping in mind that this compound is an unspecific inhibitor of thiol-dependent enzymes [40]. Also, treatment with a glutathione ester successfully prevented LPS-induced mitochondrial ROS formation (measured by electron spin resonance spectroscopy) and cytokine production [41]. Mitochondrial ROS formation

was demonstrated to be an essential contributor to DC differentiation since the complex I inhibitor rotenone but also catalase in the culture medium decreased DC-derived ROS levels and markers of differentiation, pointing towards an essential role of mitochondrial hydrogen peroxide in this process [41]. This is in line with the observation that mitochondrial ROS can trigger hypoxia-inducible factor 1-dependent reprogramming and switch to glycolysis in various cell types including DC [42, 43].

Previously it was shown that NADPH oxidase-derived ROS did not contribute to DC differentiation, maturation, cytokine production, and induction of T cell proliferation, since DC generated from patients with chronic granulomatous disease (CGD) displayed normal function [44]. Likewise, treatment with a ROS scavenger also had no effect in the hands of these authors. In contrast, NADPH oxidase activation was essential for DC-mediated killing of intracellular *E. coli* [44], which is supported by various cases indicating exacerbated inflammatory reactions upon bacterial infections of CGD patients [45]. In line with this previous observations, our data indicate a minor role of Nox2-derived ROS formation for BM-DC maturation and T cell stimulatory capacity upon activation by PDBu or LPS. Nevertheless, since neither PDBu-induced nor LPS-induced ROS formation was completely absent in BM-DCs without gp91phox, it might be speculated whether other sources of ROS (e.g., mitochondria or other Nox isoforms) contribute to BM-DC maturation and T cell stimulatory capacity. Also, as shown in multiple studies on experimental sepsis (endotoxemia), LPS-dependent activation of immune cells is associated with appreciable levels of ROS formation, which most likely originate from mitochondria and NADPH oxidases [46, 47]. In general, it is also well known that ROS over production in immune cells leads to cell dysfunction and impaired/unregulated immune response and end organ damage [48–51], although in some rare diseases also insufficient ROS production may contribute to uncontrolled inflammatory conditions [52]. In most cases, this implies that even in LPS models ROS may play a role in the activation of immune cells as well as resolution of inflammation, as shown for mitochondrial ROS in LPS-primed bone marrow-derived macrophages [53]. In support of this it was shown in several experimental sepsis models that LPS-induced ROS formation is decreased and survival is improved in endotoxemic gp91phox knockout mice or by pretreatment with apocynin [54–56]. In contrast, in human genetic gp91phox deficiency (like in CGD patients) even exacerbation of LPS-induced inflammation was reported [45].

In conclusion, we provide evidence for an important role of protein kinase C in BM-DC maturation, since PKC blockade by chelerythrine or Gö6983 inhibited PDBu-dependent BM-DC maturation. There are only few reports on PKC stimulatory effects on BM-DC maturation, but it was reported to essentially contribute to DC cytokine production [19].

5. Limitations

A major problem in the comparison of the different studies on DC-dependent ROS production and its impact on maturation might be the exact time point of measurement. As long as no kinetics of ROS formation are provided it is hard to assign the signal to a certain source of ROS. Also the fact that FACS analyses are restricted to the measurement of intracellular ROS formation represents a major limitation of the previous studies on effects of ROS on DC maturation and T cell stimulatory capacity.

Moreover, in vivo activation and maturation of DC are multifactorial and antigen/disease specific [3, 57]. Of note, other sources of ROS (e.g., mitochondria) as well as oxidation products generated by ROS (e.g., oxLDL, reactive aldehydes, and isoketals) are known to contribute to DC activation and maturation [6, 9–11]. Likewise, ROS from external Nox2 sources (e.g., other activated immune cells) could trigger BM-DC maturation in vivo. These "external" factors could be missing in our BM-DC cell culture model. In fact, our present data indicate that not all DC activation and maturation require ROS but may solely depend on the toll-like receptor activation and cell signaling pathways such as PKC.

The identification of the specific PKC isoform(s) that contribute to this ROS independent signaling by future experiments would provide important molecular insights in the activation mechanisms of DCs.

6. Conclusions and Clinical Implications

Our findings question the concept that Nox2-dependent ROS formation in BM-DCs is required for their maturation or their T cell stimulatory potential (based on the absence of any effect of gp91phox deficiency or the NADPH oxidase inhibitor apocynin). The observed phorbol ester-triggered BM-DC maturation seems to rather depend on phosphorylation cascades than on Nox2-derived ROS formation (based on the observed effects with the PKC inhibitors chelerythrine and Gö6983). However, we cannot exclude that other sources of ROS in DCs (e.g., mitochondria) or ROS coming from external Nox2 sources (e.g., other immune cells) or ROS-generated oxidized DC activators such as lipid oxidation products contribute to BM-DC maturation and their T cell stimulatory potential in vivo. Since DCs provide an essential link between adaptive and innate immune response and confer the priming or sensitization of resting T cells, which is a prerequisite for any antigen-induced cellular adaptive immune response, their activation represents a fundamental mechanism in all kinds of immune responses but also progression of autoimmune diseases and low-grade inflammation triggered cardiovascular, metabolic, and neurodegenerative pathologies. Our results question the role of oxidative stress as an essential "danger signal" for BM-DC activation.

Competing Interests

The authors have no financial conflict to declare.

Authors' Contributions

Judith Stein, Sebastian Steven, Angelika Reske-Kunz, and Andreas Daiber contributed equally and should be considered as joint first and senior authors.

Acknowledgments

The authors acknowledge Jörg Schreiner and Evelyn Montermann for their excellent technical assistance. This work was supported by funds from the Federal Ministry of Education and Research (BMBF 01EO1003, TRP A3 and a Virchow Fellowship) to Andreas Daiber and Sebastian Steven and Stephan Grabbe.

References

[1] G. Nace, J. Evankovich, R. Eid, and A. Tsung, "Dendritic cells and damage-associated molecular patterns: endogenous danger signals linking innate and adaptive immunity," *Journal of Innate Immunity*, vol. 4, no. 1, pp. 6–15, 2012.

[2] L. Xiao, A. Kirabo, J. Wu et al., "Renal denervation prevents immune cell activation and renal inflammation in Angiotensin II-induced hypertension," *Circulation Research*, vol. 117, no. 6, pp. 547–557, 2015.

[3] C. Reis E Sousa, "Dendritic cells in a mature age," *Nature Reviews Immunology*, vol. 6, no. 6, pp. 476–483, 2006.

[4] A. Abderrazak, T. Syrovets, D. Couchie et al., "NLRP3 inflammasome: from a danger signal sensor to a regulatory node of oxidative stress and inflammatory diseases," *Redox Biology*, vol. 4, pp. 296–307, 2015.

[5] Y. Lei, K. Wang, L. Deng, Y. Chen, E. C. Nice, and C. Huang, "Redox regulation of inflammation: old elements, a new story," *Medicinal Research Reviews*, vol. 35, no. 2, pp. 306–340, 2015.

[6] W. G. McMaster, A. Kirabo, M. S. Madhur, and D. G. Harrison, "Inflammation, immunity, and hypertensive end-organ damage," *Circulation Research*, vol. 116, no. 6, pp. 1022–1033, 2015.

[7] C. Janko, M. Filipović, L. E. Munoz et al., "Redox modulation of HMGB1-related signaling," *Antioxidants and Redox Signaling*, vol. 20, no. 7, pp. 1075–1085, 2014.

[8] P. Wenzel, S. Kossmann, T. Münzel, and A. Daiber, "Redox regulation of cardiovascular inflammation—immunomodulatory function of mitochondrial and Nox-derived reactive oxygen and nitrogen species," *Free Radical Biology and Medicine*, 2017.

[9] A. Kirabo, V. Fontana, A. P. C. De Faria et al., "DC isoketal-modified proteins activate T cells and promote hypertension," *Journal of Clinical Investigation*, vol. 124, no. 10, pp. 4642–4656, 2014.

[10] J. Frostegard, Y. Zhang, J. Sun, K. Yan, and A. Liu, "Oxidized Low-Density Lipoprotein (OxLDL)-treated dendritic cells promote activation of T cells in human atherosclerotic plaque and blood, which is repressed by statins: microRNA let-7c is integral to the effect," *Journal of the American Heart Association*, vol. 5, no. 9, 2016.

[11] L. Perrin-Cocon, F. Coutant, S. Agaugué, S. Deforges, P. André, and V. Lotteau, "Oxidized low-density lipoprotein promotes mature dendritic cell transition from differentiating monocyte," *Journal of Immunology*, vol. 167, no. 7, pp. 3785–3891, 2001.

[12] F. Grassi, G. Tell, M. Robbie-Ryan et al., "Oxidative stress causes bone loss in estrogen-deficient mice through enhanced bone marrow dendritic cell activation," *Proceedings of the National Academy of Sciences of the United States of America*, vol. 104, no. 38, pp. 15087–15092, 2007.

[13] W.-G. Zhu, S. Li, L.-Q. Lin, H. Yan, T. Fu, and J.-H. Zhu, "Vascular oxidative stress increases dendritic cell adhesion and transmigration induced by homocysteine," *Cellular Immunology*, vol. 254, no. 2, pp. 110–116, 2009.

[14] P. R. Kroening, T. W. Barnes, L. Pease, A. Limper, H. Kita, and R. Vassallo, "Cigarette smoke-induced oxidative stress suppresses generation of dendritic cell IL-12 and IL-23 through ERK-dependent pathways," *Journal of Immunology*, vol. 181, no. 2, pp. 1536–1547, 2008.

[15] A. K. Doughan, D. G. Harrison, and S. I. Dikalov, "Molecular mechanisms of angiotensin II-mediated mitochondrial dysfunction: linking mitochondrial oxidative damage and vascular endothelial dysfunction," *Circulation Research*, vol. 102, no. 4, pp. 488–496, 2008.

[16] A. Savina, C. Jancic, S. Hugues et al., "NOX2 controls phagosomal pH to regulate antigen processing during crosspresentation by dendritic cells," *Cell*, vol. 126, no. 1, pp. 205–218, 2006.

[17] C. Jancic, A. Savina, C. Wasmeier et al., "Rab27a regulates phagosomal pH and NADPH oxidase recruitment to dendritic cell phagosomes," *Nature Cell Biology*, vol. 9, no. 4, pp. 367–378, 2007.

[18] A. R. Mantegazza, A. Savina, M. Vermeulen et al., "NADPH oxidase controls phagosomal pH and antigen cross-presentation in human dendritic cells," *Blood*, vol. 112, no. 12, pp. 4712–4722, 2008.

[19] C. Langlet, C. Springael, J. Johnson et al., "PKC-α controls MYD88-dependent TLR/IL-1R signaling and cytokine production in mouse and human dendritic cells," *European Journal of Immunology*, vol. 40, no. 2, pp. 505–515, 2010.

[20] J. D. Pollock, D. A. Williams, M. A. C. Gifford et al., "Mouse model of X-linked chronic granulomatous disease, an inherited defect in phagocyte superoxide production," *Nature Genetics*, vol. 9, no. 2, pp. 202–209, 1995.

[21] C. Scheicher, M. Mehlig, R. Zecher, and K. Reske, "Dendritic cells from mouse bone marrow: in vitro differentiation using low doses of recombinant granulocyte-macrophage colony-stimulating factor," *Journal of Immunological Methods*, vol. 154, no. 2, pp. 253–264, 1992.

[22] M. Bros, E. Montermann, A. Cholaszczyńska, and A. B. Reske-Kunz, "The phosphodiesterase 4 inhibitor roflumilast augments the Th17-promoting capability of dendritic cells by enhancing IL-23 production, and impairs their T cell stimulatory activity due to elevated IL-10," *International Immunopharmacology*, vol. 35, pp. 174–184, 2016.

[23] T. Zal, A. Volkmann, and B. Stockinger, "Mechanisms of tolerance induction in major histocompatibility complex class II-restricted T cells specific for a blood-borne self-antigen," *Journal of Experimental Medicine*, vol. 180, no. 6, pp. 2089–2099, 1994.

[24] M. Bros, F. Jährling, A. Renzing et al., "A newly established murine immature dendritic cell line can be differentiated into a mature state, but exerts tolerogenic function upon maturation in the presence of glucocorticoid," *Blood*, vol. 109, no. 9, pp. 3820–3829, 2007.

[25] M. Oelze, A. Daiber, R. P. Brandes et al., "Nebivolol inhibits superoxide formation by NADPH oxidase and endothelial dysfunction in angiotensin II-treated rats," *Hypertension*, vol. 48, no. 4, pp. 677–684, 2006.

[26] H. Mollnau, E. Schulz, A. Daiber et al., "Nebivolol prevents vascular NOS III uncoupling in experimental hyperlipidemia and inhibits NADPH oxidase activity in inflammatory cells," *Arteriosclerosis, Thrombosis, and Vascular Biology*, vol. 23, no. 4, pp. 615–621, 2003.

[27] S. Heumüller, S. Wind, E. Barbosa-Sicard et al., "Apocynin is not an inhibitor of vascular NADPH oxidases but an antioxidant," *Hypertension*, vol. 51, no. 2, pp. 211–217, 2008.

[28] R. P. Brandes, N. Weissmann, and K. Schröder, "Nox family NADPH oxidases: molecular mechanisms of activation," *Free Radical Biology and Medicine*, vol. 76, pp. 208–226, 2014.

[29] J. D. Lambeth and A. S. Neish, "Nox enzymes and new thinking on reactive oxygen: a double-edged sword revisited," *Annual Review of Pathology: Mechanisms of Disease*, vol. 9, pp. 119–145, 2014.

[30] J. Cachat, C. Deffert, S. Hugues, and K.-H. Krause, "Phagocyte NADPH oxidase and specific immunity," *Clinical Science*, vol. 128, no. 10, pp. 635–648, 2015.

[31] F. Kotsias, E. Hoffmann, S. Amigorena, and A. Savina, "Reactive oxygen species production in the phagosome: impact on antigen presentation in dendritic cells," *Antioxidants and Redox Signaling*, vol. 18, no. 6, pp. 714–729, 2013.

[32] J. M. van den Berg, E. van Koppen, A. Åhlin et al., "Chronic granulomatous disease: the European experience," *PLoS ONE*, vol. 4, no. 4, Article ID e5234, 2009.

[33] S. S. De Ravin, N. Naumann, E. W. Cowen et al., "Chronic granulomatous disease as a risk factor for autoimmune disease," *Journal of Allergy and Clinical Immunology*, vol. 122, no. 6, pp. 1097–1103, 2008.

[34] M. Wahren-Herlenius and T. Dörner, "Immunopathogenic mechanisms of systemic autoimmune disease," *The Lancet*, vol. 382, no. 9894, pp. 819–831, 2013.

[35] A. M. Campbell, M. Kashgarian, and M. J. Shlomchik, "NADPH oxidase inhibits the pathogenesis of systemic lupus erythematosus," *Science Translational Medicine*, vol. 4, no. 157, Article ID 3004801, 2012.

[36] K.-C. Sheng, G. A. Pietersz, C. K. Tang, P. A. Ramsland, and V. Apostolopoulos, "Reactive oxygen species level defines two functionally distinctive stages of inflammatory dendritic cell development from mouse bone marrow," *Journal of Immunology*, vol. 184, no. 6, pp. 2863–2872, 2010.

[37] W. Yan, W. Chen, and L. Huang, "Reactive oxygen species play a central role in the activity of cationic liposome based cancer vaccine," *Journal of Controlled Release*, vol. 130, no. 1, pp. 22–28, 2008.

[38] E. Mortaz, A. D. Kraneveld, J. J. Smit et al., "Effect of cigarette smoke extract on dendritic cells and their impact on T-cell proliferation," *PLoS ONE*, vol. 4, no. 3, Article ID e4946, 2009.

[39] H. Matsue, D. Edelbaum, D. Shalhevet et al., "Generation and function of reactive oxygen species in dendritic cells during antigen presentation," *Journal of Immunology*, vol. 171, no. 6, pp. 3010–3018, 2003.

[40] A. Daiber, M.-H. Zou, M. Bachschmid, and V. Ullrich, "Ebselen as a peroxynitrite scavenger *in vitro* and *ex vivo*," *Biochemical Pharmacology*, vol. 59, no. 2, pp. 153–160, 2000.

[41] H. Yamada, T. Arai, N. Endo et al., "LPS-induced ROS generation and changes in glutathione level and their relation to the maturation of human monocyte-derived dendritic cells," *Life Sciences*, vol. 78, no. 9, pp. 926–933, 2006.

[42] R. Requejo-Aguilar, I. Lopez-Fabuel, E. Fernandez, L. M. Martins, A. Almeida, and J. P. Bolaños, "Pink1 deficiency sustains cell proliferation by reprogramming glucose metabolism through HIF1," *Nature Communications*, vol. 5, article 4514, 2014.

[43] U. Fearon, M. Canavan, M. Biniecka, and D. J. Veale, "Hypoxia, mitochondrial dysfunction and synovial invasiveness in rheumatoid arthritis," *Nature Reviews Rheumatology*, vol. 12, no. 7, pp. 385–397, 2016.

[44] M. Vulcano, S. Dusi, D. Lissandrini et al., "Toll receptor-mediated regulation of NADPH oxidase in human dendritic cells," *Journal of Immunology*, vol. 173, no. 9, pp. 5749–5756, 2004.

[45] J. A. Winkelstein, M. C. Marino, R. B. Johnston Jr. et al., "Chronic granulomatous disease. Report on a national registry of 368 patients," *Medicine*, vol. 79, no. 3, pp. 155–169, 2000.

[46] S. Steven, M. Hausding, S. Kröller-Schön et al., "Gliptin and GLP–1 analog treatment improves survival and vascular inflammation/dysfunction in animals with lipopolysaccharide–induced endotoxemia," *Basic Research in Cardiology*, vol. 110, no. 6, 2015.

[47] S. Kröller-Schön, M. Knorr, M. Hausding et al., "Glucose-independent improvement of vascular dysfunction in experimental sepsis by dipeptidyl-peptidase 4 inhibition," *Cardiovascular Research*, vol. 96, no. 1, pp. 140–149, 2012.

[48] S. Karbach, A. L. Croxford, M. Oelze et al., "Interleukin 17 drives vascular inflammation, endothelial dysfunction, and arterial hypertension in psoriasis-like skin disease," *Arteriosclerosis, Thrombosis, and Vascular Biology*, vol. 34, no. 12, pp. 2658–2668, 2014.

[49] S. Karbach, P. Wenzel, A. Waisman, T. Münzel, and A. Daiber, "eNOS uncoupling in cardiovascular diseases-the role of oxidative stress and inflammation," *Current Pharmaceutical Design*, vol. 20, no. 22, pp. 3579–3594, 2014.

[50] M. Mittal, M. R. Siddiqui, K. Tran, S. P. Reddy, and A. B. Malik, "Reactive oxygen species in inflammation and tissue injury," *Antioxidants and Redox Signaling*, vol. 20, no. 7, pp. 1126–1167, 2014.

[51] Z. V. Varga, Z. Giricz, L. Liaudet, G. Haskó, P. Ferdinandy, and P. Pacher, "Interplay of oxidative, nitrosative/nitrative stress, inflammation, cell death and autophagy in diabetic cardiomyopathy," *Biochimica et Biophysica Acta (BBA)—Molecular Basis of Disease*, vol. 1852, no. 2, pp. 232–242, 2015.

[52] G. Aviello and U. G. Knaus, "ROS in gastrointestinal inflammation: rescue or sabotage?" *British Journal of Pharmacology*, 2016.

[53] R. Zhou, A. S. Yazdi, P. Menu, and J. Tschopp, "A role for mitochondria in NLRP3 inflammasome activation," *Nature*, vol. 469, no. 7329, pp. 221–225, 2011.

[54] H.-W. Clement, J. F. Vazquez, O. Sommer et al., "Lipopolysaccharide-induced radical formation in the striatum is abolished in Nox2 gp91phox-deficient mice," *Journal of Neural Transmission*, vol. 117, no. 1, pp. 13–22, 2010.

[55] V. Ben-Shaul, L. Lomnitski, A. Nyska, Y. Zurovsky, M. Bergman, and S. Grossman, "The effect of natural antioxidants, NAO and apocynin, on oxidative stress in the rat heart following LPS challenge," *Toxicology Letters*, vol. 123, no. 1, pp. 1–10, 2001.

[56] R. Zhou, D.-Y. Hu, L.-M. Liu, and X.-W. Zhou, "Protective effects of apocynin on 'two-hit' injury induced by hemorrhagic shock and lipopolysaccharide," *Acta Pharmacologica Sinica*, vol. 23, no. 11, pp. 1023–1028, 2002.

[57] S. Balkow, K. Loser, M. Krummen et al., "Dendritic cell activation by combined exposure to anti-CD40 plus interleukin (IL)-12 and IL-18 efficiently stimulates anti-tumor immunity," *Experimental Dermatology*, vol. 18, no. 1, pp. 78–87, 2009.

Hindawi
Oxidative Medicine and Cellular Longevity
Volume 2017, Article ID 3671751, 12 pages
https://doi.org/10.1155/2017/3671751

Research Article

Prevention of Streptozotocin-Induced Diabetic Nephropathy by MG132: Possible Roles of Nrf2 and IκB

Lili Kong,[1,2,3] Yangwei Wang,[1] Manyu Luo,[1] Yi Tan,[3] Wenpeng Cui,[1] and Lining Miao[1]

[1]*Department of Nephrology, The Second Hospital of Jilin University, Changchun, Jilin, China*
[2]*Department of Nephrology, The First Hospital of Jilin University, Changchun, Jilin, China*
[3]*Department of Pediatrics, University of Louisville, Louisville, KY, USA*

Correspondence should be addressed to Wenpeng Cui; wenpengcui@163.com

Received 10 October 2016; Accepted 14 February 2017; Published 8 March 2017

Academic Editor: Cecilia Zazueta

Our previous study showed that proteasomal inhibitor MG132 can prevent diabetic nephropathy (DN) along with upregulation of nuclear factor (erythroid-derived 2)-like 2 (Nrf2). The present study was to investigate whether MG132 can prevent DN in wild-type and Nrf2-KO mice. Type 1 diabetes was induced in wild-type and Nrf2-KO mice by multiple low doses of streptozotocin. Two weeks after streptozotocin injection, both wild-type and Nrf2-KO mice were randomly divided into four groups: control, MG132, DM, and DM/MG132. MG132 (10 μg/kg/day) or vehicle was administered intraperitoneally for 4 months. Renal function, morphology, and biochemical changes were measured after 4-month treatment with MG132. MG132 treatment suppressed proteasomal activity in the two genotypes. In wild-type mice, MG132 attenuated diabetes-induced renal dysfunction, fibrosis, inflammation, and oxidative damage along with increased Nrf2 and IκB expression. Deletion of *Nrf2* gene resulted in a partial, but significant attenuation of MG132 renal protection in Nrf2-KO mice compared with wild-type mice. MG132-increased IκB expression was not different between wild-type and Nrf2-KO mice. This work indicates that MG132 inhibits diabetes-increased proteasomal activity, resulting in Nrf2 and IκB upregulation and renal protection, which could be used as a strategy to prevent diabetic nephropathy.

1. Introduction

Diabetic nephropathy (DN) is the leading cause of end-stage renal failure worldwide. Additionally, DN is also linked to a high risk of cardiovascular disease. The risk factors include hyperglycemia, dyslipidemia, hypertension as well as elevation of homocysteine, and advanced glycation end products [1]. Moreover, albuminuria and glomerular filtration rate were also suggested to have relevant prognostic effects on cardiovascular morbidity and mortality, and the effect of albuminuria is especially pronounced when glomerular filtration rate is normal or near normal [2]. Both end-stage renal failure and cardiovascular disease brought us a heavy social burden. Current therapies for DN mainly including hypoglycemic agent and cotreatment with renoprotective drugs are not effective in blocking the progression of DN. Therefore, it is of vital importance and urgency to find more effective therapeutic strategies in countering the diabetes-associated renal injury.

Oxidative stress is induced by the imbalance of reactive oxygen species generation and endogenous antioxidant activity. Reactive oxygen species elicits inflammatory signaling pathways which in turn induces oxidative stress [3]. It is widely accepted that both oxidative stress and inflammation are main causes for DN [4, 5]. Thus, suppression of oxidative stress and inflammation may be an effective therapeutic strategy for DN.

The cell-permeable MG132 is a reversible, potent proteasome inhibitor. Reportedly, MG132 inhibited nuclear factor (erythroid-derived 2)-like 2 (Nrf2) and IkB proteasomal degradation, resulting in antioxidative stress and anti-inflammation function, respectively. Nrf2 is a transcription factor. By binding to the antioxidant-responsive element (ARE), Nrf2 could upregulate the expression of antioxidant genes and cytoprotective phase II detoxifying enzymes. Our previous study showed that nontoxic concentrations of MG132 could inhibit Nrf2 proteasomal degradation, leading to the renal protection of MG132 against diabetes-induced

renal dysfunction [6]. Besides, MG132 was reported to inhibit IkB proteasomal degradation in myocardium [7]. Under physiological conditions, IkB binds to NF-κB and retains NF-κB in the cytoplasm, which prevents NF-κB from activating the transcription of many inflammatory genes. MG132 upregulates IkB, resulting in transcriptional inactivation of NF-κB and cardiac protection [7]. Therefore, MG132 may have the potential to treat DN through resisting oxidative stress and inflammation.

In the present study, we tried to address the question of whether proteasomal inhibitor MG132 can prevent diabetic nephropathy model in wild-type and Nrf2-KO mice induced by multiple low-dose streptozotocin. Also, we want to know whether renoprotection of MG132 was totally Nrf2-dependent.

2. Materials and Methods

2.1. Animals. Wild-type ($Nrf2^{+/+}$), homozygote ($Nrf2^{-/-}$), and heterozygote ($Nrf2^{+/-}$) mice with C57BL/6J background were purchased from the Jackson Laboratory (Bar Harbor, Maine). Nrf2 knockout (KO, $Nrf2^{-/-}$) male mice were obtained by breeding of heterozygote ($Nrf2^{+/-}$) with homozygote ($Nrf2^{-/-}$). Only wild-type and age-matched Nrf2 KO male mice were used for the present study. All experimental procedures for these mice were approved by the Institutional Animal Care and Use Committee of the University of Louisville, which is compliant with National Institutes of Health standards.

For induction of type 1 diabetic mouse model, 8-week-old male wild-type and Nrf2-KO mice were injected with multiple low-dose streptozotocin (Sigma-Aldrich, St. Louis, MO, USA) intraperitoneally, dissolved in 0.1 M sodium citrate buffer (pH = 4.5) at 50 mg/kg body weight daily for 5 consecutive days, while age-matched control mice received multiple injections of the same sodium citrate buffer. Five days after the last injection, mice with hyperglycemia (blood glucose levels $\geq$ 250 mg/dL) were defined as diabetes mellitus (DM) as before [8]. Both wild-type and Nrf2-KO mice were randomly allocated into four groups ($n = 7$ at least per group): control, MG132, DM, and DM/MG132. Dose of MG132 was used based on our previous study [6]. MG132 (Sigma-Aldrich, St. Louis, MO) was dissolved in dimethyl sulfoxide at a concentration of 0.0025 μg/mL and diluted with saline for injection. Both nondiabetic and diabetic mice further received subcutaneous injection of MG132 at 10 μg/kg or vehicle daily for 4 months. At the end of the 4 months, the mice were euthanized, and their kidneys were harvested for analysis.

2.2. Mouse Urinary Albumin to Creatinine Ratio (UACR) Detection. Urinary albumin and urinary creatinine were measured according to manufacturers' procedures provided with these kits (Bethyl Laboratories Inc., Montgomery, TX; BioAssay Systems, Hayward, CA, resp.). Mouse UACR was calculated as UACR = urinary albumin/urinary creatinine (μg/mg).

2.3. Renal Histopathological Examination. Kidney tissues were fixed immediately in 10% buffered formalin solution after harvesting and were embedded in paraffin and sectioned into 5 μm-thick sections onto glass slides. The sections were processed for PAS and Masson's trichrome staining.

2.4. Isolation of Nuclei. The nuclei from kidney tissue were isolated according to manufacturers' procedures provided with the nuclei isolation kit (Sigma-Aldrich). Renal tissue from each mouse was homogenized in cold lysis buffer containing dithiothreitol (DTT) and Triton X-100. Then, Cushing solution (sucrose Cushion solution : sucrose Cushion buffer : dithiothreitol = 900 : 100 : 1) was added and the mixture was transferred to a new tube preloaded with sucrose Cushion solution followed by centrifugation at 13,000 rpm for 45 min. The supernatant fraction containing cytosolic components was aspirated and the nuclei were visible as a thin pellet at the bottom of the tube.

2.5. Real-Time PCR. Real-time PCR were performed as previously described [9] using primers for NQO-1, Nrf2, and actin (Life Technologies, Grand Island, NY).

2.6. Western Blotting Assay. Western blotting assay was conducted as previously described [10]. The primary antibodies were FN (1 : 200 dilution), TGF-β (1 : 1000 dilution), 3-NT (1 : 1000 dilution), 4-HNE (1 : 1000 dilution), IL-6 (1 : 500 dilution), NF-κB (1 : 1000 dilution), IκB-α (1 : 1000 dilution), Nrf2 (1 : 500 dilution), actin (1 : 3000 dilution), and α-tubulin (1 : 2000 dilution), all of which were purchased from Santa Cruz Biotechnology except for 3-NT (Millipore), 4-HNE (Alpha Diagnostic), and TGF-β, NF-κB, IκB-α, and α-tubulin (Cell Signaling).

2.7. 20S Proteasome Activity Assay. The 20S proteasome, the catalytic core of the 26S proteasome complex, is responsible for the degradation of short-lived regulatory proteins, including Nrf2 and IκB [7, 11, 12]. Since MG132 mainly inhibits proteasome chymotrypsin (ChT)-like activity [13], we detected 20S proteasome activity by quantifying the hydrolysis of SLLVY-AMC, a fluorogenic substrate for the ChT-like activity, according to the manufacturers' procedures of the 20S proteasome activity assay kit (Millipore). Detailed operation procedures have been described in our early studies [6].

2.8. Morphometric Analyses. Morphometric analyses were conducted using Image-Pro Plus 6.0 software (Media Cybernetics, Bethesda, MD, USA). Areas to be photographed were selected randomly by people blind to the identity of the samples.

2.9. Statistical Analysis. Data were collected from at least 7 mice each group and presented as means $\pm$ SD. Image Quant 5.2 was used to analyze western blotting. Comparisons among different groups were conducted by one-way ANOVA, followed by Tukey's post hoc test. In addition, a t-test was performed to compare the amount of decrease by MG132

Table 1: General changes after streptozotocin injection for 5 consecutive days.

	Control	MG132	DM	DM/MG132
UACR				
Wild type	25.21 ± 3.12	24.81 ± 3.12	28.65 ± 5.64	29.23 ± 5.87
Nrf2-KO	27.81 ± 3.76	27.32 ± 3.89	31.23 ± 5.92	30.89 ± 6.03
Blood glucose				
Wild type	98.89 ± 10.32	100.65 ± 11.20	280.46 ± 32.23*	290.85 ± 35.03*
Nrf2-KO	100.74 ± 12.32	96.15 ± 10.86	295.21 ± 35.23*	289.75 ± 34.98*
Body weight				
Wild type	19.65 ± 2.06	19.52 ± 2.16	19.32 ± 1.99	19.61 ± 2.03
Nrf2-KO	18.96 ± 1.96	19.32 ± 2.12	19.45 ± 2.15	19.1 ± 2.2

Notes. Data are presented as mean ± SD. * $p < 0.05$ versus wild type/control or Nrf2-KO/control correspondingly.

between wild-type and Nrf2-KO mice. Differences were significant if $p < 0.05$.

3. Results

3.1. General Changes after STZ Injection for 5 Consecutive Days. After STZ injection for 5 consecutive days, diabetic mice developed hyperglycemia. There was no significance in UACR and body weight among the four groups (Table 1).

3.2. MG132 Retained Partial Protection against Diabetes-Induced Albuminuria despite Deletion of the Nrf2 Gene. As an important index of renal function, UACR was measured at the end of the study. As shown in Figures 1(a) and 1(e), compared to their respective controls, a 4.95-fold increase in UACR for Nrf2-KO diabetic mice and a 3.38-fold increase in UACR for wild-type diabetic mice were found. The results revealed that streptozotocin-injected Nrf2-KO mice had a higher level of UACR than wild-type mice, indicating the essential role of Nrf2 in protecting against streptozotocin-induced renal injury. Next, kidney weight/tibia length (Figures 1(b) and 1(e)), which indicates enlargement of kidney, was calculated. The ratio was significantly increased in the diabetic groups in both strains but was decreased by MG132 treatment. MG132 decreased UACR and kidney weight/tibia length by 55.1% and 29.0% in wild-type diabetic mice and by 27.9% and 20.6% in Nrf2-KO mice, respectively; these effects were significantly lower in Nrf2-KO mice (Figure 1(e)). It not only confirmed the pivotal role of Nrf2 in MG132 protection, but also proved an Nrf2-independent protection against diabetes-induced renal injury. Blood glucose (Figure 1(c)) was increased in both wild-type and Nrf2-KO diabetic mice, and MG132 had no significant impact on blood glucose in the two genotypes. Diabetes reduced body weight in both wild-type and Nrf2-KO diabetic mice (Figure 1(d)). Interestingly, MG132 increased body weight in wild-type diabetic mice, but not in Nrf2-KO diabetic mice.

3.3. MG132 Retained Partial Protection against Diabetes-Induced Renal Fibrosis despite Deletion of the Nrf2 Gene. To investigate the effect of MG132 on diabetes-induced renal fibrosis, PAS staining (Figure 2(a)) was conducted to detect glycogen deposition and Masson's trichrome staining was conducted to measure the expression of fibronectin (FN) and collagens (Figure 2(b)). Diabetic kidney showed enlarged glomeruli, mesangial matrix expansion, and increased trichrome-positive area. MG132 significantly attenuated these changes in wild-type mice and still provided partial protection against diabetes-induced morphological changes in Nrf2-KO mice. Mesangial matrix expansion (Figure 2(c)) was quantified from PAS staining and fibrosis accumulation (Figure 2(d)) was quantified from Masson's trichrome staining.

Both FN and TGF-β, the two fibrosis indexes, were measured by western blotting assay in total proteins. The two kinds of protein were significantly increased in diabetic kidneys in the two genotypes, yet they were reduced by MG132 treatment. MG132 decreased FN (Figures 3(b) and 3(c)) and TGF-β (Figures 3(a) and 3(c)) by 51.2% and 48.9% in wild-type diabetic mice and by 29.6% and 20.0% in Nrf2-KO mice, respectively; these effects were significantly lower in Nrf2-KO mice.

3.4. MG132 Alleviated Diabetes-Induced Oxidative Stress in Wild-Type Diabetic Mice, but This Effect Was Completely Lost in Nrf2-KO Diabetic Mice. As shown in Figure 4, diabetes-induced oxidative damage was determined by 3-NT as an index of nitrosative damage and 4-HNE as an index of lipid peroxidation with western blotting assay in total proteins. Both 3-NT (Figures 4(a) and 4(c)) and 4-HNE (Figures 4(b) and 4(c)) were increased in diabetic kidney in the two genotypes, which was more obvious in Nrf2-KO mice. MG132 treatment significantly reduced 3-NT and 4-HNE accumulation in wild-type diabetic mice, but not in Nrf2-KO diabetic mice.

3.5. MG132 Retained Partial Protection against Diabetes-Induced Renal Inflammation despite Deletion of the Nrf2 Gene. As an important index of renal inflammation, IL-6 was determined by western blotting assay in total proteins, while NF-κB was determined by western blotting assay in nuclear proteins. As shown in Figure 5, in both wild-type and Nrf2-KO mice, diabetes increased the expression of IL-6 (Figures 5(a) and 5(c)) and NF-κB (Figures 5(b) and 5(c)) compared to control group, respectively. What is more, Nrf2-KO diabetic kidney expressed higher levels of IL-6 and NF-κB, compared to wild-type diabetic kidney. MG132

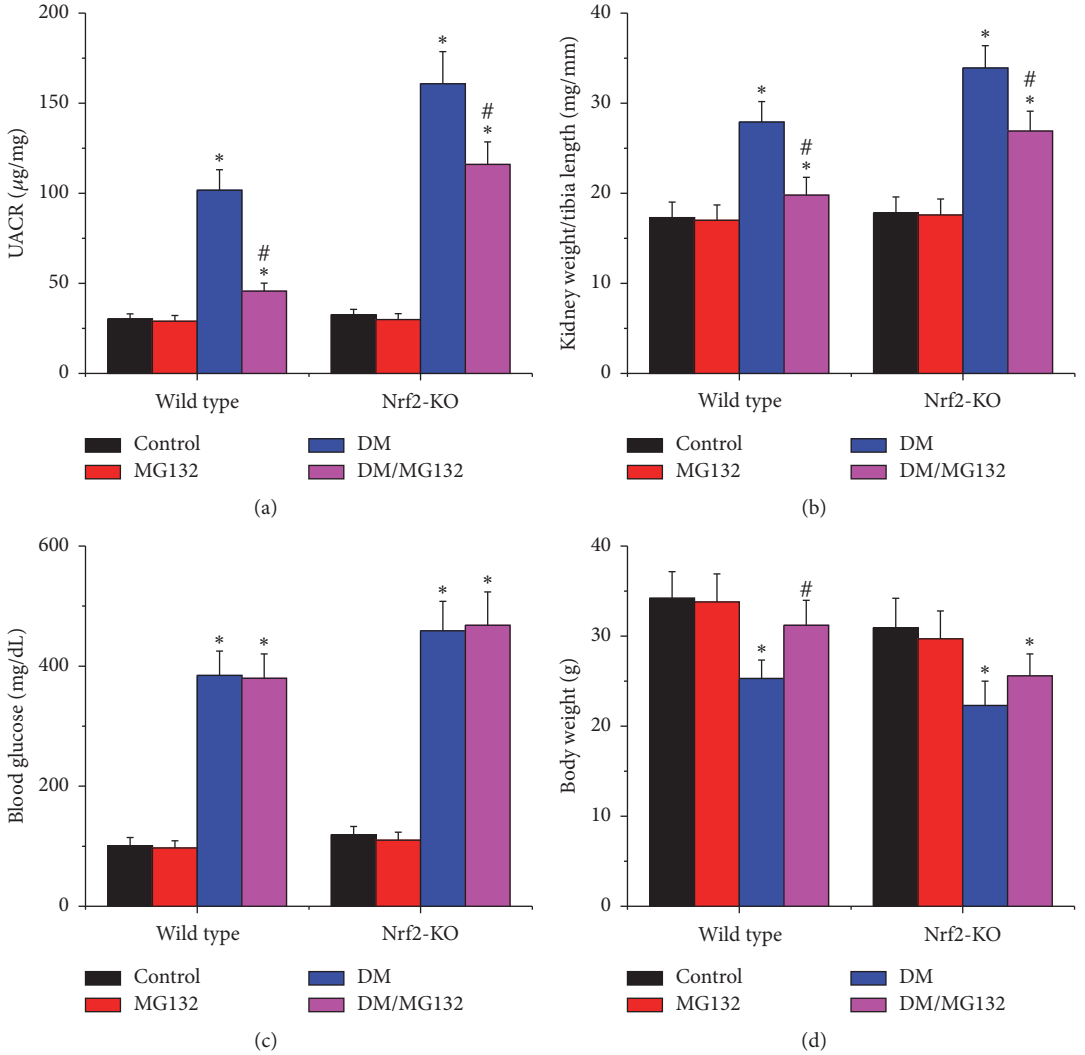

	Fold increased by diabetes		Percentage decreased by MG132	
	Wild type	Nrf2-KO	Wild type	Nrf2-KO
UACR	3.38	4.95$^{\&}$	55.1%	27.9%$^{\&}$
Kidney weight/tibia length	1.61	1.90$^{\&}$	29.0%	20.6%$^{\&}$

(e)

Figure 1: MG132 retained partial protection against diabetes-induced albuminuria despite deletion of the Nrf2 gene. UACR (a), kidney weight/tibia length (b), blood glucose (c), and body weight (d) were determined in all mice. Diabetes-induced pathological changes (fold) between wild-type and Nrf2-KO mice and the decreased percentages of these pathological changes with MG132 between WT and Nrf2-KO diabetic mice were compared (e). Data are presented as mean ± SD. $^{*}p < 0.05$ versus WT/control or Nrf2-KO/control correspondingly; $^{\#}p < 0.05$ versus WT/DM or Nrf2-KO/DM correspondingly; $^{\&}p < 0.05$ versus wild-type mice.

decreased IL-6 and NF-κB by 48.2% and 52.9% in wild-type diabetic mice and by 22.9% and 24.0% in Nrf2-KO mice, respectively; these effects were significantly lower in Nrf2-KO mice.

3.6. Possible Mechanisms by Which MG132 Attenuates DN. Diabetes increased renal proteasomal activity, which was reduced by MG132. As shown in Figure 6(a), compared to respective control group, renal proteasomal activity was increased in diabetic group in the two genotypes and was significantly reduced by MG132 treatment.

3.7. MG132 Inhibited Renal Proteasomal Activity, Resulting in Upregulation of Nrf2. Ubiquitination and subsequent degradation by the proteasome have been regarded as the main mechanism responsible for Nrf2's negative regulation. MG132 inhibited proteasomal activity, which may result in the reduction of Nrf2 degradation. Therefore, Nrf2 mRNA

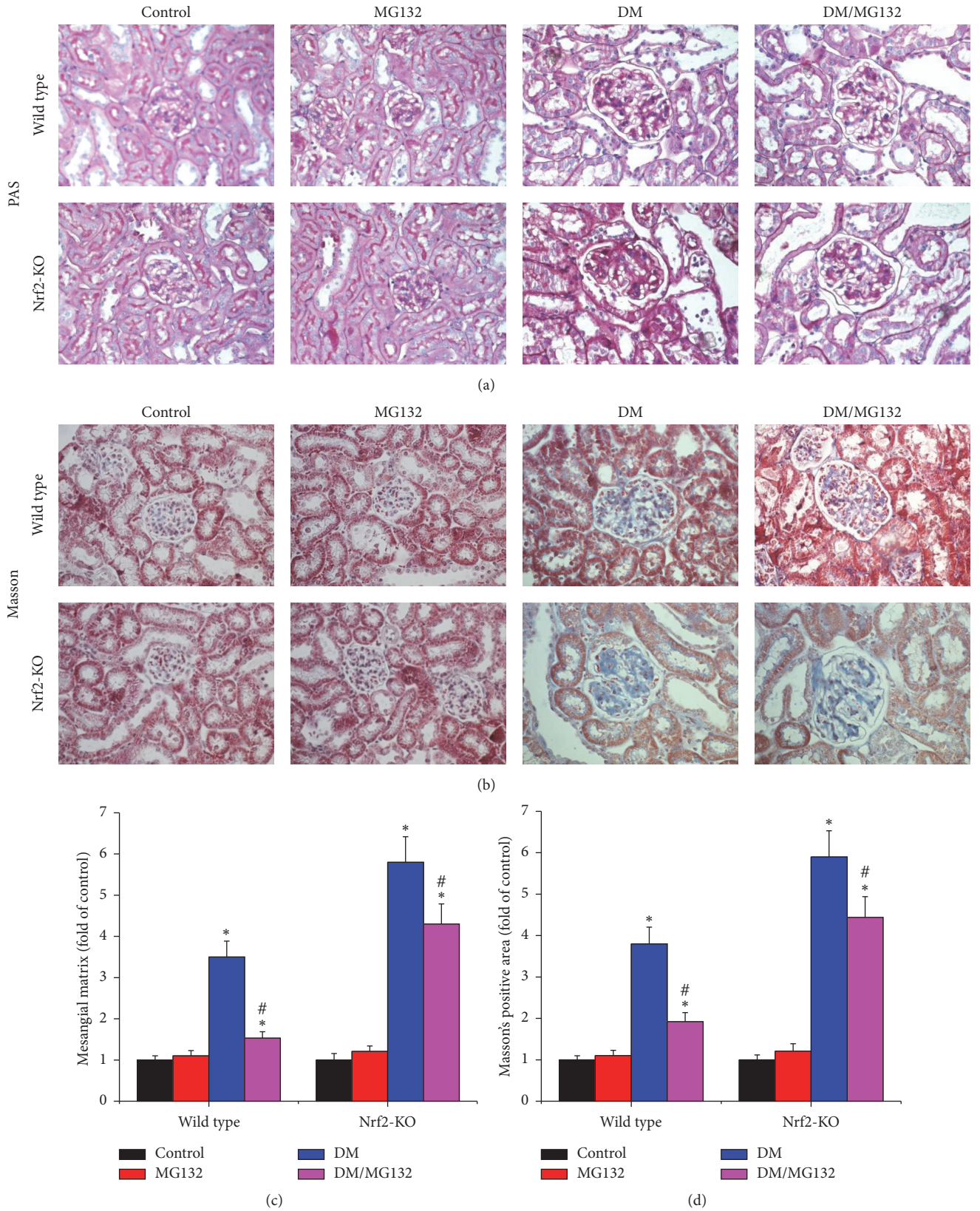

Figure 2: Effects of MG132 on diabetes-induced morphological changes were examined with PAS (a) and Masson's trichrome staining (b, ×400) in all mice. Mesangial matrix expansion (c) was quantified from PAS staining and fibrosis accumulation (d) was quantified from Masson's trichrome staining. Data are presented as mean ± SD. $^{*}p < 0.05$ versus WT/control or Nrf2-KO/control correspondingly; $^{\#}p < 0.05$ versus WT/DM or Nrf2-KO/DM correspondingly.

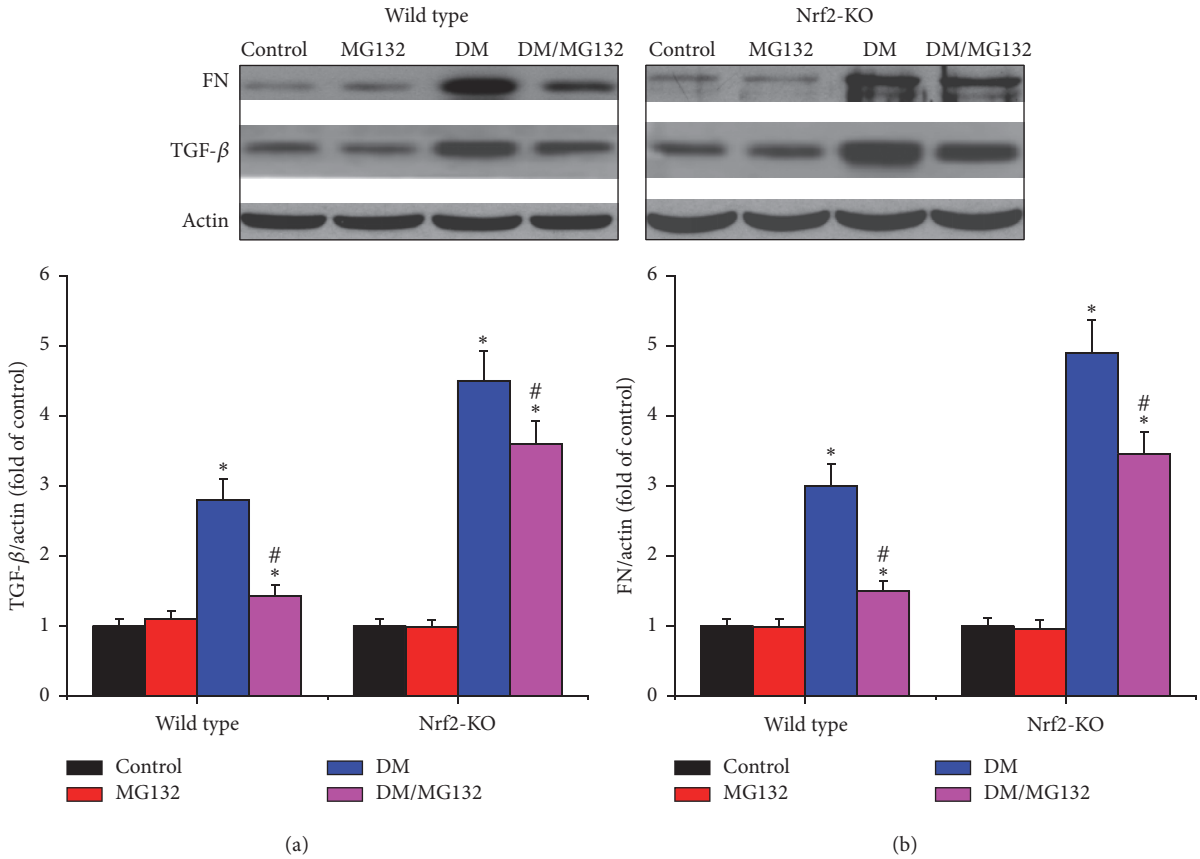

	Fold increased by diabetes		Percentage decreased by MG132	
	Wild type	Nrf2-KO	Wild type	Nrf2-KO
TGF-β	2.80	4.51$^{\&}$	48.9%	20.0%$^{\&}$
FN	3.01	4.90$^{\&}$	51.2%	29.6%$^{\&}$

(c)

Figure 3: Effects of MG132 on diabetes-induced renal fibrosis in wild-type mice (a) and Nrf2-KO mice (b) were determined by detecting the expression of FN and TGF-β with western blotting assay. Diabetes-induced fibrotic changes (fold) between wild-type and Nrf2-KO mice and the decreased percentages of these changes with MG132 between WT and Nrf2-KO diabetic mice were compared (c). Data are presented as mean ± SD. $^{*}p < 0.05$ versus WT/control or Nrf2-KO/control correspondingly; $^{\#}p < 0.05$ versus WT/DM or Nrf2-KO/DM correspondingly; $^{\&}p < 0.05$ versus WT mice.

(Figure 6(b)) and total protein levels (Figure 6(c)) were determined by real-time PCR and western blotting assay, respectively. Besides, NQO-1 expression, one of Nrf2 downstream genes, was also determined by real-time PCR (Figure 6(d)). In wild-type mice, diabetes increased Nrf2 expression at both mRNA and protein levels; MG132 treatment increased Nrf2 protein level, but not mRNA level. In Nrf2-KO mice, Nrf2 was almost undetectable by real-time PCR and western blotting assay. Consistent with Nrf2 protein levels, in wild-type mice, both diabetes and MG132 increased NQO-1 mRNA levels. However, Nrf2 deficiency disenabled MG132 to induce NQO-1 transcription.

3.8. MG132 Inhibited Renal Proteasomal Activity, Resulting in Upregulation of IκB and Downregulation of NF-κB. As a transcription factor, NF-κB can translocate into the nucleus and transcriptionally upregulate inflammatory cytokines. IκB is its negative regulator. Under basal conditions, IκB binds to NF-κB and retains NF-κB in the cytoplasm, which reduced the transcriptional activity of NF-κB. In order to determine the effect of MG132 on IκB, we detected its protein level by western blotting assay in total proteins. As shown in Figure 6(e), in both wild-type and Nrf2-KO mice, diabetes significantly reduced the expressions of IκB, which were significantly upregulated by MG132 treatment. This suggests that MG132 inhibited renal proteasomal activity, resulting in the reduction of IκB degradation. Consequently, MG132 increased IκB (Figure 6(e)) and reduced NF-κB (Figure 5(b)).

4. Discussion

The present study is the first to demonstrate that MG132 attenuates DN via suppression of proteasomal activity of diabetic kidney, which promotes degradation of Nrf2 and

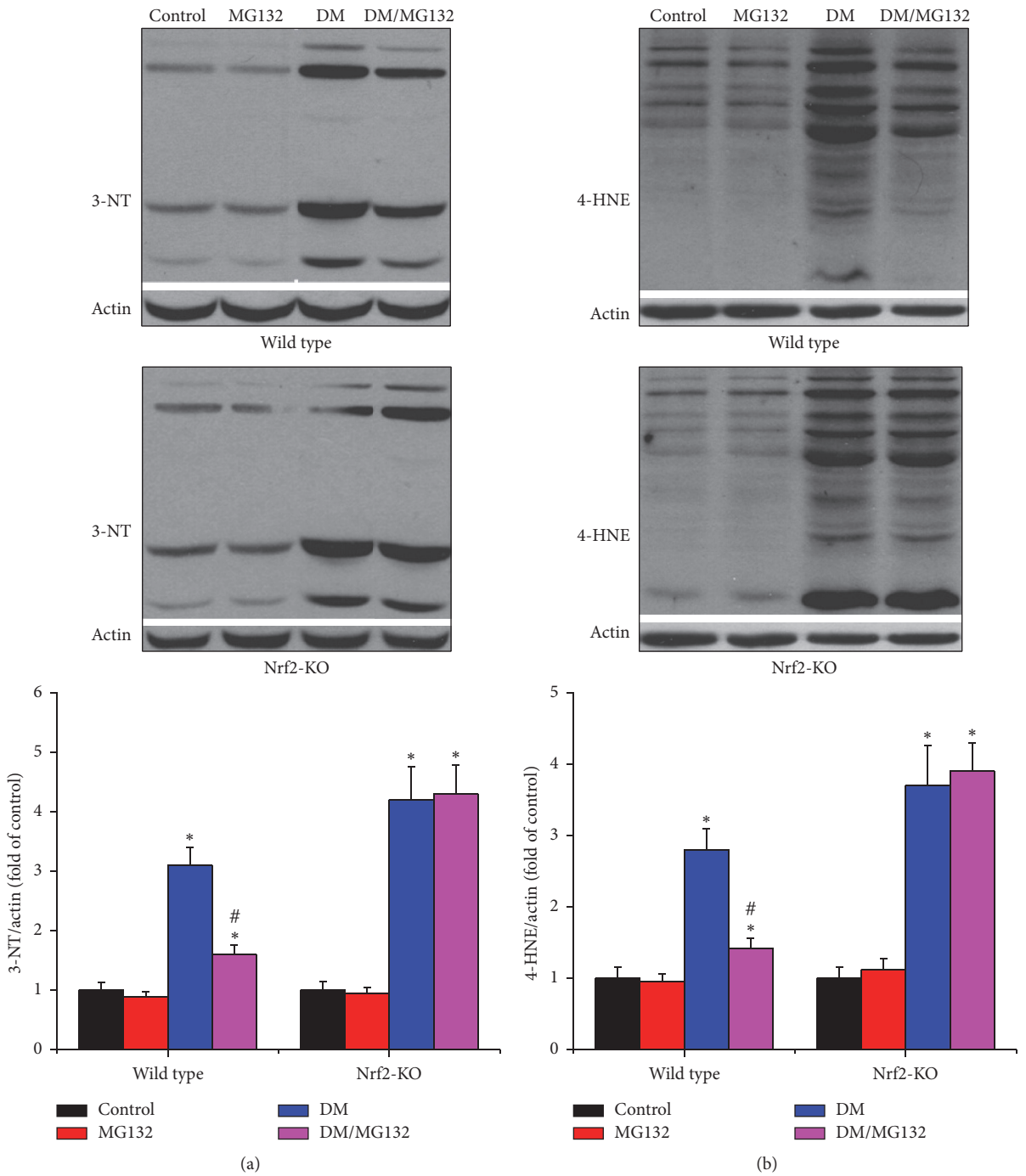

	Fold increased by diabetes		Percentage decreased by MG132	
	Wild type	Nrf2-KO	Wild type	Nrf2-KO
3-NT	3.11	4.22$^{\&}$	48.4%	−2.38%
4-HNE	2.81	3.73$^{\&}$	49.3%	−5.41%

(c)

Figure 4: Effects of MG132 on diabetes-induced renal oxidative damage were determined by detecting the expression of 3-NT (a) and 4-HNE (b) with western blotting assay. Diabetes-induced changes of oxidative damage (fold) between wild-type and Nrf2-KO mice and the decreased percentages of these changes with MG132 between WT and Nrf2-KO diabetic mice were compared (c). Data are presented as mean ± SD. $^{*}p < 0.05$ versus WT/control or Nrf2-KO/control correspondingly; $^{\#}p < 0.05$ versus WT/DM or Nrf2-KO/DM correspondingly; $^{\&}p < 0.05$ versus WT mice.

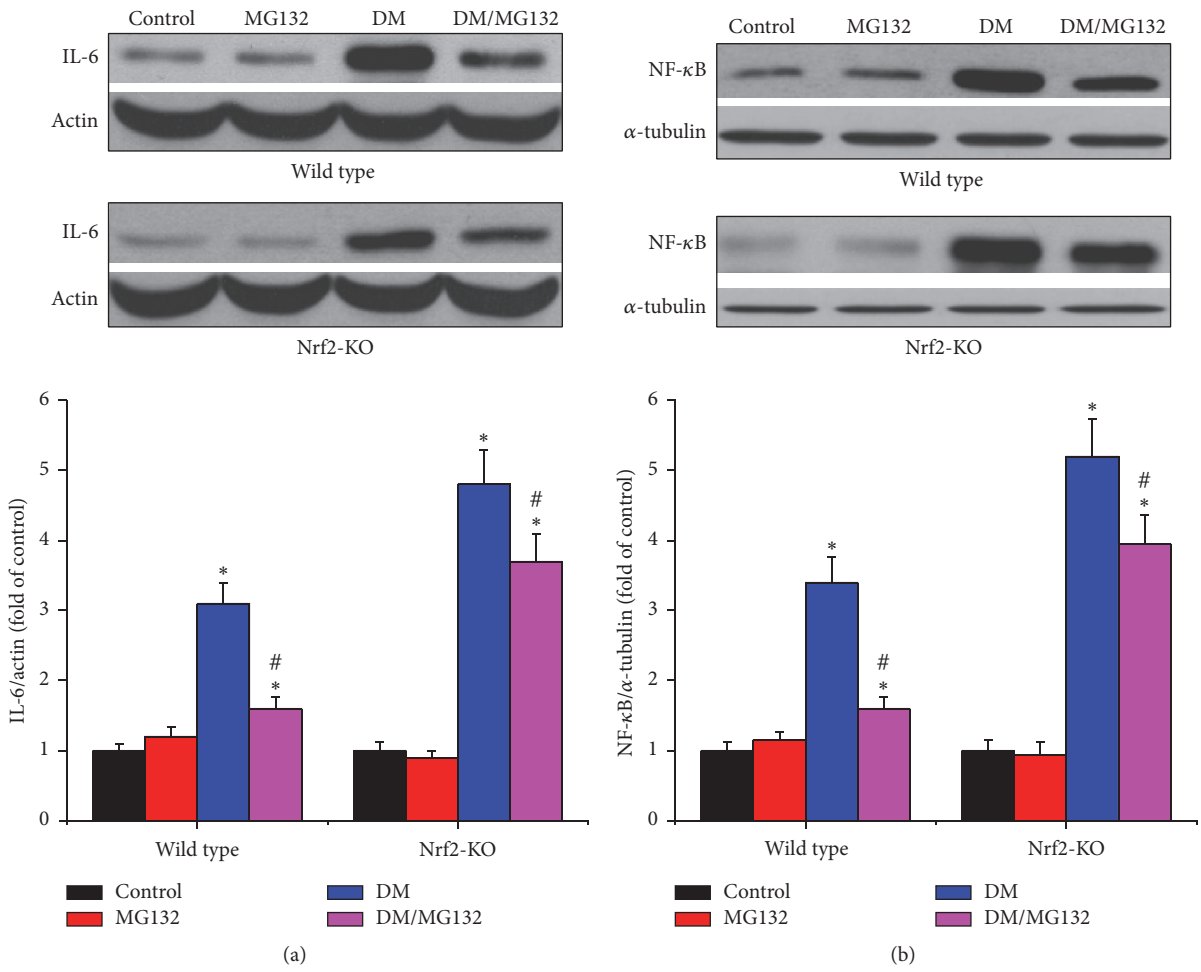

	Fold increased by diabetes		Percentage decreased by MG132	
	Wild type	Nrf2-KO	Wild type	Nrf2-KO
IL-6	3.11	4.82$^{\&}$	48.4%	22.9%$^{\&}$
NF-κB	3.4	5.2$^{\&}$	52.9%	24.0%$^{\&}$

(c)

Figure 5: Effects of MG132 on diabetes-induced renal inflammation were determined by detecting the expression of IL-6 (a) and NF-kB (b) with western blotting assay. Diabetes-induced inflammatory changes (fold) between wild-type and Nrf2-KO mice and the decreased percentages of these changes with MG132 between WT and Nrf2-KO diabetic mice were compared (c). Data are presented as mean ± SD. $^{*}P < 0.05$ versus WT/control or Nrf2-KO/control correspondingly; $^{\#}P < 0.05$ versus WT/DM or Nrf2-KO/DM correspondingly; $^{\&}P < 0.05$ versus WT mice.

IκB. We set up diabetic mouse model with multiple low-dose streptozotocin in both wild-type and Nrf2-KO mice and treated with MG132 for 4 months. In wild-type mice, MG132 inhibited proteasomal activity, resulting in the significant upregulation of Nrf2 and IκB. Consequently, MG132 significantly attenuated diabetes-induced renal dysfunction, fibrosis, inflammation, and oxidative damage. In Nrf2-KO mice, MG132 also inhibited proteasomal activity, resulting in the significant upregulation of IκB. However, Nrf2 deficiency resulted in partial loss of MG132 protection against DN.

DN is characterized by inflammation, oxidative stress, enlarged glomeruli, expansion of mesangial matrix, glomerular basement membrane thickening, glomerulosclerosis, and tubulointerstitial fibrosis. Inflammation and oxidative stress are considered as main pathogenesis of DN. Increasing evidence indicated that blocking oxidative stress could attenuate diabetic complications, such as DN [14], diabetic retinopathy [15], and diabetic cardiomyopathy [16]. As a transcription factor, Nrf2 is a master regulator of cellular redox status. Under unstressed conditions, Nrf2 is kept in the cytoplasm by Kelch-like-ECH-associated protein 1 (Keap1) and Cullin 3 which induces ubiquitination of Nrf2 [17]. Once Nrf2 is ubiquitinated, it is transported to the proteasome, where it is degraded and its components are recycled. Under oxidative conditions, oxidative stress disrupts critical cysteine residues in Keap1, disrupting the Keap1-Cul3 ubiquitination system.

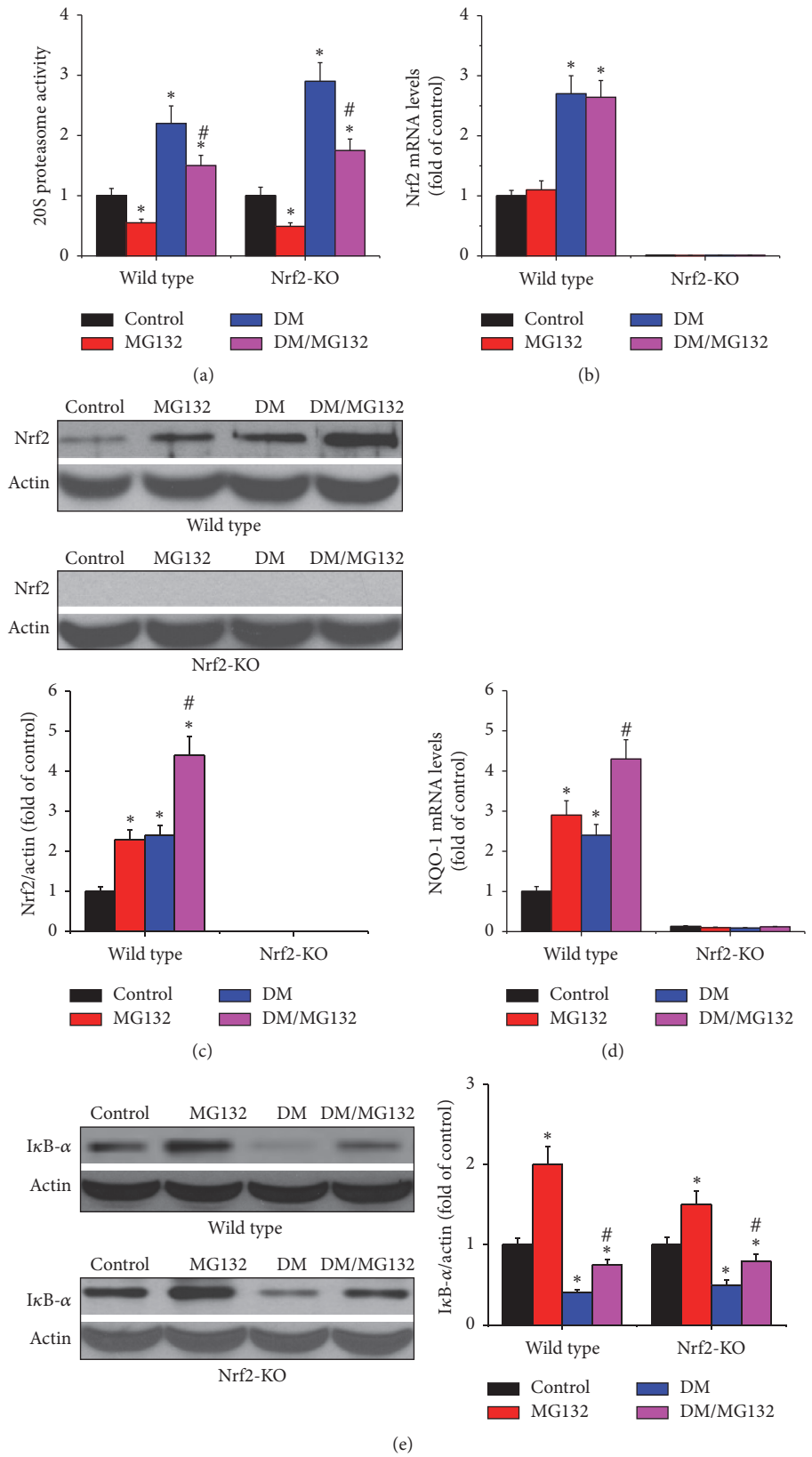

FIGURE 6: Possible mechanisms under which MG132 attenuates DN. 20S proteasome activity (a), Nrf2 expression at both mRNA (b) and protein levels (c), and Nrf2 downstream gene, NQO-1 mRNA (d) were examined in all mice. In addition, IkB-α protein level (e) was determined by western blotting assay. Data are presented as mean ± SD. $^{*}p < 0.05$ versus WT/control or Nrf2-KO/control correspondingly; $^{\#}p < 0.05$ versus WT/DM or Nrf2-KO/DM correspondingly.

Nrf2 is free from Keap1 and translocates from cytoplasm into the nucleus. In the nucleus, it combines with a small Maf protein and binds to the ARE in the upstream promoter region of genes encoding antioxidant enzymes and initiates their transcription [18]. Emerging evidence showed that upregulation of Nrf2 could alleviate oxidative injury and diabetic complications [19, 20]. Nrf2 is degraded by proteasome [21–24]; thus proteasomal inhibition might be a potent approach to upregulate Nrf2. Since the approval of the first proteasome inhibitor by the FDA [25], proteasome inhibitors have been used to treat several diseases. Due to the side effects and drug resistance, a new proteasome inhibitor without those disadvantages, namely, MG132, was discovered. It is reported that nontoxic concentrations of MG132 reduced Nrf2 proteasomal degradation, resulting in the upregulation of Nrf2 and its downstream antioxidants [26, 27]. Our previous study showed that MG132 prevents the development of DN in OVE26 mice via upregulation of Nrf2. Furthermore, silencing Nrf2 gene with siRNA disenabled MG132 to prevent renal tubule cells from high-glucose-induced profibrotic response. It suggested that therapeutic effect of MG132 on DN may be Nrf2-dependent. This present study also indicated the important role of Nrf2 in MG132 protection from DN. MG132, the proteasome inhibitor, upregulated Nrf2 and its downstream antioxidant genes, such as NQO-1, resulting in the alleviation of renal oxidative damage. In wild-type diabetic mice, MG132 reduced UACR by 55.1%. However, MG132 only reduced UACR in Nrf2-KO diabetic mice by 29.0%, demonstrating the beneficial effect of oxidative stress status alleviation on the renal protection afforded by MG132. Interestingly, MG132 retained partial protection against diabetes-induced renal injury in Nrf2-KO mice. That is, the renal protection of MG132 might not be Nrf2-dependent. There may be another mechanism underlying the protective effect of MG132 on DN. This inconsistence may be due to the discrepancy between in vivo and in vitro study. On one hand, exposure of renal tubule cells to high-glucose cannot fully mimic diabetes-induced renal injury. On the other hand, kidney is composed of several different kinds of cells, such as mesangial cells, tubular epithelial cells, endothelial cells, fibroblasts, and podocytes, not just tubule cells.

Several studies showed that diabetes increased proteasomal activity in vein endothelial cells, heart, and gastrocnemius muscles [28–32]. The present study also demonstrated diabetes increased renal proteasomal activity, companied by the decrease in IκB and increase in NF-κB. MG132 treatment significantly inhibited proteasomal activity, companied by the upregulation of IκB and downregulation of NF-κB. It is widely accepted that inflammation contributes to the pathogenesis and progression of DN. NF-κB is a protein complex that controls many genes involved in inflammation. Several studies showed that MG132 inhibited the expression of inflammatory cytokines [33, 34], but its mechanism was not fully known. Under physiological conditions, NF-κB is sequestered in the cytoplasm by its inhibitor, called IκB [35–37]. When activated by signals, IκB is phosphorylated and ubiquitinated, which then leads them to be degraded by the proteasome [38, 39]. With the degradation of IκB, NF-κB complex is freed to enter the nucleus where it promotes the expression of specific genes that encodes proinflammatory cytokines. In the present study, MG132, the proteasome inhibitor, increased IκB and decreased NF-κB. Thus, it is reasonable to assume that MG132 inhibited proteasomal activity, resulting in the decrease in IκB degradation. Consequently, NF-κB was retained in the cytoplasm, which prevented NF-κB activation. Finally, MG132 suppressed renal inflammation. The possible mechanisms by which MG132 ameliorated DN were shown in Figure 7.

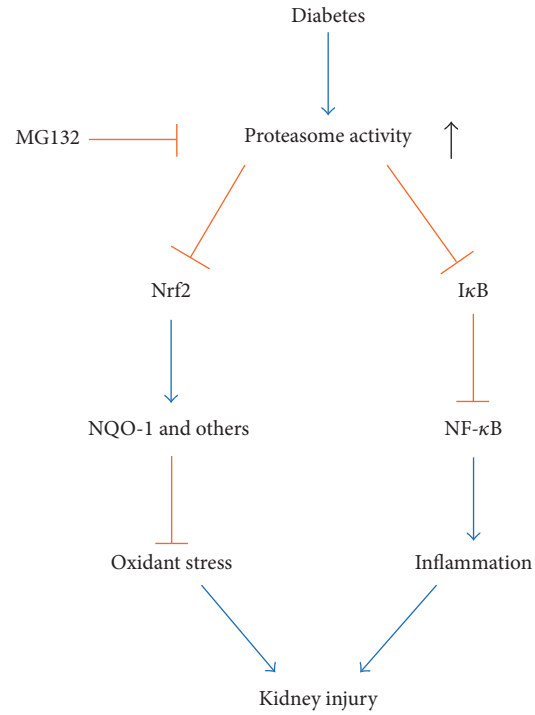

Figure 7: Sketch map of possible mechanisms under which MG132 attenuates DN. MG132 inhibits proteasome activity, leading to the upregulation of Nrf2 and IκB. For one thing, antioxidant genes, such as *NQO-1*, are activated due to the upregulation of Nrf2; therefore, renal oxidative damage is reduced. On the other hand, NF-κB is downregulated secondary to the upregulation of IκB, resulting in the reduction of inflammation. Consequently, MG132 alleviates diabetic nephropathy.

Current study showed that MG132 decreased TGF-β expression in diabetic mice. It is widely accepted that both oxidative stress and inflammation lead to TGF-β activation and fibrosis. In addition, in current study, we hypothesized that MG132 suppressed both oxidative stress via Nrf2 upregulation and inflammation via NF-κB downregulation (Figure 7). Therefore, MG132 mediated oxidative stress and inflammation inhibition may explain the phenomenon of TGF-β reduction. In a recent study, Huang et al. suggested that MG132 alleviated DN by inhibiting TGF-β signaling and this effect was associated with the ability of MG132 to reduce the degradation of SnoN protein [40]. This might be another mechanism by which MG132 decreased TGF-β.

In summary, the present study demonstrates for the first time that proteasome inhibitor MG132 at low dose ameliorates DN by both induction of Nrf2 and inhibiting NF-κB via

upregulation of IκB. As we reported before [6], the dosage of MG132 in current study (10 μg/kg/day) was the lowest dosage reported in the literature in vivo. Since proteasome activity increased in diabetic kidney, whether increasing MG132 dosage (nontoxic) can enhance its effectiveness needs to be further investigated in DN models.

Competing Interests

The authors declare no conflict of interests.

Authors' Contributions

Wenpeng Cui and Lining Miao conceived and designed the experiments; Lili Kong, Yangwei Wang, and Manyu Luo performed the experiments; Yi Tan analyzed the data; Lili Kong wrote the paper.

Acknowledgments

This work was supported by Natural Science Foundation of China (no. 81200525), Jilin Province Science and Technology Development Program Funded Project (no. 20150520034JH and no. 20160414014GH), Jilin Province Scientific Research Program Funded Project (no. 2016446), and Norman Bethune Program of Jilin University (no. 2015214). The authors would like to express their gratitude to the doctors participating in this study.

References

[1] Y. Aso, "Cardiovascular disease in patients with diabetic nephropathy," *Current Molecular Medicine*, vol. 8, no. 6, pp. 533–543, 2008.

[2] F. C. Sasso, P. Chiodini, O. Carbonara et al., "High cardiovascular risk in patients with Type 2 diabetic nephropathy: the predictive role of albuminuria and glomerular filtration rate. The NID-2 Prospective Cohort Study," *Nephrology Dialysis Transplantation*, vol. 27, no. 6, pp. 2269–2274, 2012.

[3] D. Kawanami, K. Matoba, and K. Utsunomiya, "Signaling pathways in diabetic nephropathy," *Histology and Histopathology*, vol. 31, no. 10, pp. 1059–1067, 2016.

[4] A. Mima, "Inflammation and oxidative stress in diabetic nephropathy: new insights on its inhibition as new therapeutic targets," *Journal of Diabetes Research*, vol. 2013, Article ID 248563, 8 pages, 2013.

[5] J. Mori, V. B. Patel, T. Ramprasath et al., "Angiotensin 1-7 mediates renoprotection against diabetic nephropathy by reducing oxidative stress, inflammation, and lipotoxicity," *American Journal of Physiology—Renal Physiology*, vol. 306, no. 8, pp. F812–F821, 2014.

[6] W. Cui, B. Li, Y. Bai et al., "Potential role for Nrf2 activation in the therapeutic effect of MG132 on diabetic nephropathy in OVE26 diabetic mice," *American Journal of Physiology—Endocrinology and Metabolism*, vol. 304, no. 1, pp. E87–E99, 2013.

[7] Y. Wang, W. Sun, B. Du et al., "Therapeutic effect of MG-132 on diabetic cardiomyopathy is associated with its suppression of proteasomal activities: roles of Nrf2 and NF-κB," *American Journal of Physiology—Heart and Circulatory Physiology*, vol. 304, no. 4, pp. H567–H578, 2013.

[8] L. Cai, J. Wang, Y. Li et al., "Inhibition of superoxide generation and associated nitrosative damage is involved in metallothionein prevention of diabetic cardiomyopathy," *Diabetes*, vol. 54, no. 6, pp. 1829–1837, 2005.

[9] Q. Zhang, Y. Li, T. Liang et al., "Loss of FGF21 in diabetic mouse during hepatocellular carcinogenetic transformation," *American Journal of Cancer Research*, vol. 5, no. 5, pp. 1762–1774, 2015.

[10] W. Cui, Y. Bai, X. Miao et al., "Prevention of diabetic nephropathy by sulforaphane: possible role of Nrf2 upregulation and activation," *Oxidative Medicine and Cellular Longevity*, vol. 2012, Article ID 821936, 12 pages, 2012.

[11] O. Coux, K. Tanaka, and A. L. Goldberg, "Structure and functions of the 20S and 26S proteasomes," *Annual Review of Biochemistry*, vol. 65, pp. 801–847, 1996.

[12] H. Dreger, K. Westphal, A. Weller et al., "Nrf2-dependent upregulation of antioxidative enzymes: a novel pathway for proteasome inhibitor-mediated cardioprotection," *Cardiovascular Research*, vol. 83, no. 2, pp. 354–361, 2009.

[13] S. Meiners, A. Ludwig, M. Lorenz et al., "Nontoxic proteasome inhibition activates a protective antioxidant defense response in endothelial cells," *Free Radical Biology & Medicine*, vol. 40, no. 12, pp. 2232–2241, 2006.

[14] B. H. Kim, E. S. Lee, R. Choi et al., "Protective effects of curcumin on renal oxidative stress and lipid metabolism in a rat model of type 2 diabetic nephropathy," *Yonsei Medical Journal*, vol. 57, no. 3, pp. 664–673, 2016.

[15] T. Jiang, Q. Chang, J. Cai, J. Fan, X. Zhang, and G. Xu, "Protective effects of melatonin on retinal inflammation and oxidative stress in experimental diabetic retinopathy," *Oxidative Medicine and Cellular Longevity*, vol. 2016, Article ID 3528274, 13 pages, 2016.

[16] N. Zhang, Z. Yang, S.-Z. Xiang et al., "Nobiletin attenuates cardiac dysfunction, oxidative stress, and inflammatory in streptozotocin: induced diabetic cardiomyopathy," *Molecular and Cellular Biochemistry*, vol. 417, no. 1-2, pp. 87–96, 2016.

[17] K. Itoh, N. Wakabayashi, Y. Katoh et al., "Keap1 represses nuclear activation of antioxidant responsive elements by Nrf2 through binding to the amino-terminal Neh2 domain," *Genes & Development*, vol. 13, no. 1, pp. 76–86, 1999.

[18] K. Itoh, T. Chiba, S. Takahashi et al., "An Nrf2/small Maf heterodimer mediates the induction of phase II detoxifying enzyme genes through antioxidant response elements," *Biochemical and Biophysical Research Communications*, vol. 236, no. 2, pp. 313–322, 1997.

[19] Y. Yang, G. Chen, X. Cheng et al., "Therapeutic potential of digitoflavone on diabetic nephropathy: nuclear factor erythroid 2-related factor 2-dependent anti-oxidant and anti-inflammatory effect," *Scientific Reports*, vol. 5, Article ID 12377, 2015.

[20] H. Zheng, S. A. Whitman, W. Wu et al., "Therapeutic potential of Nrf2 activators in streptozotocin-induced diabetic nephropathy," *Diabetes*, vol. 60, no. 11, pp. 3055–3066, 2011.

[21] T. Nguyen, P. J. Sherratt, H.-C. Huang, C. S. Yang, and C. B. Pickett, "Increased protein stability as a mechanism that enhances Nrf2-mediated transcriptional activation of the antioxidant response element: degradation of Nrf2 by the 26 S proteasome," *Journal of Biological Chemistry*, vol. 278, no. 7, pp. 4536–4541, 2003.

[22] K. R. Sekhar, S. R. Soltaninassab, M. J. Borrelli et al., "Inhibition of the 26S proteasome induces expression of GLCLC, the catalytic subunit for γ-glutamylcysteine synthetase," *Biochemical and Biophysical Research Communications*, vol. 270, no. 1, pp. 311–317, 2000.

[23] K. R. Sekhar, X. X. Yan, and M. L. Freeman, "Nrf2 degradation by the ubiquitin proteasome pathway is inhibited by KIAA0132, the human homolog to INrf2," *Oncogene*, vol. 21, no. 44, pp. 6829–6834, 2002.

[24] D. Stewart, E. Killeen, R. Naquin, S. Alam, and J. Alam, "Degradation of transcription factor Nrf2 via the ubiquitin-proteasome pathway and stabilization by cadmium," *Journal of Biological Chemistry*, vol. 278, no. 4, pp. 2396–2402, 2003.

[25] B. Cvek, "Proteasome inhibitors," *Progress in Molecular Biology and Translational Science*, vol. 109, pp. 161–226, 2012.

[26] J. Chen and R. F. Regan, "Increasing expression of heme oxygenase-1 by proteasome inhibition protects astrocytes from heme-mediated oxidative injury," *Current Neurovascular Research*, vol. 2, no. 3, pp. 189–196, 2005.

[27] S. K. Sahni, E. Rydkina, and A. Sahni, "The proteasome inhibitor MG132 induces nuclear translocation of erythroid transcription factor Nrf2 and cyclooxygenase-2 expression in human vascular endothelial cells," *Thrombosis Research*, vol. 122, no. 6, pp. 820–825, 2008.

[28] J. Xu, Y. Wu, P. Song, M. Zhang, S. Wang, and M.-H. Zou, "Proteasome-dependent degradation of guanosine 5$\prime$-triphosphate cyclohydrolase I causes tetrahydrobiopterin deficiency in diabetes mellitus," *Circulation*, vol. 116, no. 8, pp. 944–953, 2007.

[29] J. Hu, J. D. Klein, J. Du, and X. H. Wang, "Cardiac muscle protein catabolism in diabetes mellitus: activation of the ubiquitin-proteasome system by insulin deficiency," *Endocrinology*, vol. 149, no. 11, pp. 5384–5390, 2008.

[30] R. Marfella, C. D. Filippo, M. Portoghese et al., "The ubiquitin-proteasome system contributes to the inflammatory injury in ischemic diabetic myocardium: the role of glycemic control," *Cardiovascular Pathology*, vol. 18, no. 6, pp. 332–345, 2009.

[31] X. Wang, Z. Hu, J. Hu, J. Du, and W. E. Mitch, "Insulin resistance accelerates muscle protein degradation: activation of the ubiquitin-proteasome pathway by defects in muscle cell signaling," *Endocrinology*, vol. 147, no. 9, pp. 4160–4168, 2006.

[32] Z.-F. Luo, W. Qi, B. Feng et al., "Prevention of diabetic nephropathy in rats through enhanced renal antioxidative capacity by inhibition of the proteasome," *Life Sciences*, vol. 88, no. 11-12, pp. 512–520, 2011.

[33] A. S. Ahmed, M. Ahmed, J. Li et al., "Proteasome inhibitor MG132 modulates inflammatory pain by central mechanisms in adjuvant arthritis," *International Journal of Rheumatic Diseases*, 2014.

[34] Y. Quan, C.-T. Jiang, B. Xue, S.-G. Zhu, and X. Wang, "High glucose stimulates TNFα and MCP-1 expression in rat microglia via ROS and NF-κB pathways," *Acta Pharmacologica Sinica*, vol. 32, no. 2, pp. 188–193, 2011.

[35] K. Brown, S. Park, T. Kanno, G. Franzoso, and U. Siebenlist, "Mutual regulation of the transcriptional activator NF-kappa B and its inhibitor, I kappa B-alpha," *Proceedings of the National Academy of Sciences of the United States of America*, vol. 90, no. 6, pp. 2532–2536, 1993.

[36] P. A. Ganchi, S.-C. Sun, W. C. Greene, and D. W. Ballard, "IκB/MAD-3 masks the nuclear localization signal of NF-κB p65 and requires the transactivation domain to inhibit NF-κB p65 DNA binding," *Molecular Biology of the Cell*, vol. 3, no. 12, pp. 1339–1352, 1992.

[37] T. Léveillard and I. M. Verma, "Diverse molecular mechanisms of inhibition of NF-kappa B/DNA binding complexes by I kappa B proteins," *Gene Expression*, vol. 3, no. 2, pp. 135–150, 1993.

[38] Z. Chen, J. Hagler, V. J. Palombella et al., "Signal-induced site-specific phosphorylation targets IκBα to the ubiquitin-proteasome pathway," *Genes & Development*, vol. 9, no. 13, pp. 1586–1597, 1995.

[39] V. J. Palombella, O. J. Rando, A. L. Goldberg, and T. Maniatis, "The ubiquitinproteasome pathway is required for processing the NF-κB1 precursor protein and the activation of NF-κB," *Cell*, vol. 78, no. 5, pp. 773–785, 1994.

[40] W. Huang, C. Yang, Q. Nan et al., "The proteasome inhibitor, MG132, attenuates diabetic nephropathy by inhibiting SnoN degradation in vivo and in vitro," *BioMed Research International*, vol. 2014, Article ID 684765, 11 pages, 2014.

Hindawi
Oxidative Medicine and Cellular Longevity
Volume 2017, Article ID 5750897, 13 pages
https://doi.org/10.1155/2017/5750897

Research Article

Small Interfering RNA Targeting Mitochondrial Calcium Uniporter Improves Cardiomyocyte Cell Viability in Hypoxia/Reoxygenation Injury by Reducing Calcium Overload

Yuriana Oropeza-Almazán,[1] Eduardo Vázquez-Garza,[1] Héctor Chapoy-Villanueva,[1] Guillermo Torre-Amione,[1,2,3] and Gerardo García-Rivas[1,2]

[1]*Cátedra de Cardiología y Medicina Vascular, Escuela de Medicina, Tecnológico de Monterrey, Monterrey, NL, Mexico*
[2]*Centro de Investigación Biomédica, Hospital Zambrano-Hellion, San Pedro Garza-García, NL, Mexico*
[3]*Methodist DeBakey Heart and Vascular Center, The Methodist Hospital, Houston, TX, USA*

Correspondence should be addressed to Gerardo García-Rivas; gdejesus@itesm.mx

Received 6 October 2016; Revised 24 December 2016; Accepted 5 January 2017; Published 27 February 2017

Academic Editor: Leopoldo Aguilera-Aguirre

Intracellular Ca^{2+} mishandling is an underlying mechanism in hypoxia/reoxygenation (H/R) injury that results in mitochondrial dysfunction and cardiomyocytes death. These events are mediated by mitochondrial Ca^{2+} (mCa^{2+}) overload that is facilitated by the mitochondrial calcium uniporter (MCU) channel. Along this line, we evaluated the effect of siRNA-targeting MCU in cardiomyocytes subjected to H/R injury. First, cardiomyocytes treated with siRNA demonstrated a reduction of MCU expression by 67%, which resulted in significant decrease in mitochondrial Ca^{2+} transport. siRNA treated cardiomyocytes showed decreased mitochondrial permeability pore opening and oxidative stress trigger by Ca^{2+} overload. Furthermore, after H/R injury MCU silencing decreased necrosis and apoptosis levels by 30% and 50%, respectively, and resulted in reduction in caspases 3/7, 9, and 8 activity. Our findings are consistent with previous conclusions that demonstrate that MCU activity is partly responsible for cellular injury induced by H/R and support the concept of utilizing siRNA-targeting MCU as a potential therapeutic strategy.

1. Introduction

Coronary heart disease (CHD) is the leading cause of death in industrialized and third-world countries [1]. The effects of CHD are associated with the negative effects of ischemia-reperfusion. Ischemia-reperfusion injury normally arises in patients presenting myocardial infarction with acute ST-segment elevation in which timely and effective myocardial reperfusion is limiting the infarct size and death. However, several events that appear during myocardial reperfusion can induce further cell damage in a phenomenon known as reperfusion injury [2].

Numerous experimental studies have identified some critical factors that act in concert to mediate the unfavorable effects of reperfusion injury. First, intracellular and mitochondrial Ca^{2+} (mCa^{2+}) overload are exacerbated during reperfusion due to oxidative stress-induced disruption of the sarcolemma and sarcoplasmic reticulum membranes [3]. Second, mitochondrial reenergization during reoxygenation allows the recovery of the membrane potential that drives the Ca^{2+} uptake into the mitochondria through the mitochondrial Ca^{2+} uniporter (MCU) channel and subsequently induces mCa^{2+} overload [4]. These events result in mitochondrial dysfunction, leading to cardiomyocyte death by the opening of the mitochondrial transition pore ($_m$PTP) [5]. Accordingly, targeting oxidative stress and/or modulating the activity of MCU by a selective blocker such as Ru_{360} [6, 7] or the inhibition of $_m$PTP opening by cyclosporine A (CsA) provide specific targets for intervention [8].

The role of MCU in the regulation of mCa^{2+} overload is supported by the observations that, in a model of cardiac

ischemia-reperfusion, treatment with Ru_{360} decreased the $[Ca^{2+}]_m$ and maintained mitochondrial ATP synthesis [6]. Ru_{360}-treated hearts following in vivo reperfusion were less prone to undergo mitochondrial permeability transition ($_m$PTP) and apoptosis [9, 10]. The recent description of the molecular identity of the MCU channel [11, 12] and several subunits that are crucial for mCa^{2+} uptake allowed for the development of adult heart-specific transgenic models [13]. In this regard, conditional cardiac-specific MCU$^{-/-}$ mice subjected to reperfusion resulted in significant reduction of mCa^{2+} overload that disabled the activation of $_m$PTP and inhibited cardiomyocytes apoptosis and necrosis [14, 15]. These data together provide experimental rationale to develop strategies to target MCU activity with the purpose of preventing ischemic-reoxygenation injury.

On the other hand, small interfering RNA- (siRNA-) based treatments provide a potential therapeutic strategy to block MCU activity. Of interest, several phases I and II clinical studies involving patients with hepatitis, hypercholesterolemia, macular degeneration, and solid tumors have been completed [16] and appear to be safe strategy for gene therapy in humans [17].

Therefore, the purpose of this study was to explore the potential use of siRNA-targeting MCU in an in vitro model of hypoxia/reoxygenation (H/R) injury. Our results confirm previous observations that define the MCU as an essential modulator of the detrimental effects of reperfusion injury and suggest that MCU silencing using siRNA has the therapeutic potential to be used as a cardioprotective strategy.

2. Materials and Methods

2.1. Reagents. All chemical reagents, cell culture media and supplements, siRNA, and fluorescent probes were purchased from Sigma-Aldrich (St. Louis, MO, USA), unless otherwise stated.

2.2. MCU siRNA Sequence. To silence MCU, specific siRNA sequence was designed using RNAi siDirect v2.0 with the lowest predicted off-target potentials and 100% homology with the rat gene (NCBI Reference Sequence NM_001106398.1). Then, we used siRNA-MCU Calcium1, nt 761–779 of the corresponding mRNA, sense strand sequence: 5′-CGGCUUACCUGGUGGGAAU-3′. siRNA duplex was synthesized by Sigma-Aldrich (St. Louis, MO, USA). The nontargeting siRNA sequence is the MISSION® siRNA Universal Negative Control #1 (SIC001) named as siRNA-Neg.

2.3. Cell Culture and siRNA Transfection. Rat ventricular myocardial H9c2 cell line (CRL-1446™) was obtained from ATCC® (Manassas, VA, USA). Cells were grown in Dulbecco's modified Eagle's medium (DMEM) (D7777) and supplemented with 10% fetal bovine serum (FBS) Invitrogen (Carlsbad, CA, USA) and 1x penicillin-streptomycin (P4333) in a humidified incubator at 37°C with 5% CO_2 and 95% air. For MCU silencing, H9c2 cells were seeded at 2.5×10^4 cells per well in 12-well plates and 24 h later were transfected with 18.8, 112.5, or 225 nM of siRNA-MCU designed or siRNA-Neg using the HiPerFect™ Transfection Reagent (Qiagen®, Venlo, Netherlands), according to the manufacturer's protocols.

2.4. RNA Extraction, Reverse Transcription, and Gene Expression Analysis by Quantitative PCR. For the gene expression analysis of MCU silencing, after 96 h of transfection, total RNA was isolated from H9c2 cells by homogenization in TriReagent™ following manufacturer's instructions. The RNA quantification and purity assessment was performed with a Take3™ Micro-Volume plate used in the microplate spectrophotometer Synergy™ HT (BioTek® Instruments, Winooski, VT, USA). From one microgram of total RNA of each sample, cDNA was synthesized with the ImProm-II™ Reverse Transcription System (Promega®, Madison, WI, USA) and 5 ng was analyzed by qRT-PCR SensiFast™ SYBR® Lo-Rox Kit (Bioline®, London, UK). The housekeeping gene β-actin was used to normalize all data. Real-time PCR primer sequences to amplify a fragment of 158 bp of CCDC109A (MCU) gene are the following: fw, 5′-CACACAGTTTGGCATTTTGG-3′, and rv, 5′-TGTCTCTGGCTTCAGGATAA-3′. The primer sequences to amplify a fragment of 110 bp of β-actin are fw, 5′-GAAAAGATGACCCAGATCATG-3′, and rv, 5′-ATCACAATGCCAGTGGTAC-3′. Comparing expression analysis in siRNA-MCU cells to siRNA-Neg cells was performed using $2^{-\Delta\Delta Ct}$ method.

2.5. Western Blot Assay. Cell proteins were extracted after 96 h of H9c2 transfection, as previously described [18]. Briefly, after being washed with cold PBS, cell cultures were scraped, harvested, and resuspended in RIPA buffer. The samples were vortexed and sonicated on rounds of 10 sec sonication/10 sec rest and centrifuged at 15000 ×g 10 min. The protein concentration of the lysate was determined by Lowry protein assay. Protein lysates (30 μg/lane) were resolved on SDS-PAGE gel 10%, transferred onto PVDF membrane at 150 mA, 50 min, and incubated with anti-MCU antibody ab121499 (Abcam, Cambridge, MA, USA) 1 : 500 and washed three times for 10 min with PBS-Tw 0.5% and subsequently probed with secondary antibody anti-rabbit IgG conjugated with HRP (Millipore, Billerica, MA, USA) 1 : 5000 for 2 h at room temperature (RT). After washing three times for 10 min, protein-antibody blots were developed with Clarity™ Western ECL (Bio-Rad, Hercules, CA) and quantified by using a BioSpectrum 415 Image Acquisition System (UVP®, Upland, CA, USA). Anti-β-actin antibody (ab8229) 1 : 500 or anti-GAPDH antibody (ab9484) 1 : 500 (both of them from Abcam, Cambridge, MA, USA) was used as a loading control. The level of MCU expression was the ratio of intensities of the MCU-signal/β-actin signal normalized versus siRNA-Neg signal.

2.6. Measurement of the Mitochondrial Ca^{2+} Uptake. Cytosolic-free Ca^{2+} was monitored in digitonin-permeabilized H9c2 transfected cells. Briefly, 5×10^4 cells were washed three times in Tyrode solution (in mM: 128 NaCl, 0.4 NaH_2PO_4, 5 glucose, 5.4 KCl, 0.5 MgCl-6H_2O, and 25 HEPES, pH 7.4) without Ca^{2+} and resuspended in 50 μL of respiration

buffer containing in mM the following: 150 sucrose, 50 KCl, 2 KH_2PO_4, 20 Tris-HCl pH 7.3, 5 succinate, 2 μg/mL rotenone, 40 μM digitonin, 0.5 μM thapsigargin (TG), 1 μM CsA, 0.3 μM Calcium Green-5N (CG-5N) salt-free (Thermo Fisher Scientific, Waltham, MA, USA). CG-5N fluorescence (λ_{ex}485 nm/λ_{em}528 nm) was monitored at 25°C at basal conditions and after 15 μM Ca^{2+} addition with constant agitation using a microplate fluorescence spectrophotometer Synergy HT (BioTek Instruments, Winooski, VT, USA).

2.7. Mitochondrial Membrane Potential ($\Delta\psi_m$) and $_m$PTP Measurements. Safranin was used to assess $\Delta\psi_m$ in digitonin-permeabilized transfected cardiomyocytes as previously described by Oliveira et al. [19], with some modifications. Briefly, 5×10^4 H9c2 transfected cells were washed and resuspended as already stated in 50 μL of respiration media with 2 μM safranin. Safranin fluorescence was recorded at λ_{ex}485 nm and λ_{em}590 nm using a microplate fluorescence reader. After 5 min, 10 mM succinate was added as substrate until steady state was reached. A Ca^{2+} pulse of 7.5 or 15 μM was added to induce permeability transition, and 1 μM cyclosporin A (CsA) or 0.5 μM Ru_{360} was used as pharmacological inhibitors of $_m$PTP opening and MCU, respectively. Cyanide *m*-chlorophenyl hydrazone (CCCP, 20 μM) was added when indicated to dissipate $\Delta\psi_m$. Depolarization was measured after 13 min of Ca^{2+} addition. Experimental data were normalized to the maximum safranin fluorescence (100% $\Delta\psi$), calculated as the difference between the steady state fluorescence and after addition of CCCP.

To support that Ca^{2+} induces $_m$PTP opening, with 5×10^4 H9c2 permeabilized transfected cardiomyocytes in respiration media, we carried out a Ca^{2+} retention experiment with a single 50 μM Ca^{2+} bolus using CG-5N as a Ca^{2+} indicator. The experiment was performed with (1 μM) or without CsA.

2.8. Flow Cytometry Measurements. Transfected cardiomyocytes were stained and analyzed in a FACSCanto II™ Flow Cytometer (BD Bioscience, San Jose, CA), and each time point analysis consisted of 5,000 recorded events. Cell morphology was assessed by analyzing the Forward Scatter (FSC) and Side Scatter (SSC) parameter and we excluded doublets by FSC-A/FSC-W gating. Debris was discarded by its distinct low Forward and Side Scatter. Samples were run uncompensated and the FMI analysis was performed using the FlowJo™ vX.07 (Tree Star, Ashland, OR, USA).

2.8.1. Measurements of ROS Production. To assess mitochondrial ROS (superoxide) production, transfected cardiomyocytes were stained with MitoSOX Red (Thermo Fisher Scientific), as previously reported by Mukhopadhyay et al. [20]. Briefly, cells were allowed to load MitoSOX for 30 min at 37°C. After staining, the cells were washed with Tyrode solution. Finally, each sample was stimulated with TG at a concentration of 5 μM. Before TG addition, siRNA-Neg cardiomyocytes were incubated with or without 5 μM Ru_{360} for 30 min or 1 μM CsA during 10 min as pharmacological inhibitors of superoxide production. Serial analysis of the samples was performed at different time points (0.5, 15, 30, 60, and 120 min). The data of the MitoSOX are presented as the fold increase of median intensity fluorescence against the siRNA-Neg controls.

2.8.2. Cytotoxicity Assay. Cell viability and apoptotic and necrotic cell death were measured by Annexin V/PI staining followed by flow cytometry analysis. Briefly, after normoxy (Nxy), hypoxia, and 1.5 and 3 h reoxygenation conditions, H9c2 transfected cells were washed, resuspended in 195 μL Tyrode + 2.5 mM $CaCl_2$ solution, and stained with 5 μL of Annexin V Apoptosis Detection Set PE-Cy7 88-8103 (eBioscience, San Diego, CA, USA) for 10 min. Later, cells were washed and resuspended in 195 μL Tyrode + 2.5 mM $CaCl_2$ solution and incubated with 100 ng of PI (P4170) to discard necrotic cells. Stained cells were immediately analyzed by flow cytometry. The assay was performed with a two-color-analysis of PE-Cy7-labeled Annexin V binding and PI dye excited with 488 nm laser. To evaluate the proportions of viable, apoptotic, and necrotic cells, we performed fluorescence compensation. After discarding doublets, the living cells (Annexin V^-/PI^-, Q4), early apoptotic cells (Annexin V^+/PI^-, Q3), late apoptotic cells (Annexin V^+/PI^+, Q2), and necrotic cells (Annexin V^-/PI^+, Q1) were distinguished.

2.9. Measurement of ATP Content. Intracellular ATP content was measured in 96 h transfected cardiomyocytes, using the CellTiter-Glo® Luminescent Assay (Promega, Madison, USA), according to the manufacturer's protocol. The ATP content is expressed as luminescence relative units (LRU).

2.10. In Vitro Hypoxia/Reoxygenation Model. For hypoxic challenges, H9c2 transfected cells were trypsinized, washed with Tyrode without glucose, and incubated with a modified Tyrode solution simulating ischemic conditions (IT) (in mM: 135 NaCl, 8 KCl, 0.5 $MgCl_2$, 0.33 NaH_2PO_4, 5 HEPES, 1.8 $CaCl_2$, and 20 Na^+-lactate, pH 6.8) [21] and transferred into an anaerobic chamber with an oxygen level <1% at 37°C. After 3 h hypoxia, cells were washed and incubated with Tyrode (plus 5 mM glucose, 1.8 mM $CaCl_2$) and transferred into an incubator in normoxic conditions (37°C with 5% CO_2 and 95% air) for 1.5 and 3 h for reoxygenation and analyzed for apoptosis and necrosis at each time. During hypoxia, an experimental group remained in normoxic conditions. A schematic representation of hypoxia/reoxygenation model is shown in Figure 1.

2.11. Caspase Activity Measurements. For caspase activity measurements, H9c2 were seeded at 1.5×10^3 cells per well in 96-well plates and 24 h later were transfected as described previously. After 96 h of transfection, the cells were washed with Tyrode, incubated with IT solution, and transferred into an anaerobic chamber with an oxygen level <1% at 37°C. After 3 h hypoxia, IT solution was removed and cells were incubated with DMEM at normoxic conditions (37°C with 5% CO_2 and 95% air) for 0, 1.5, and 3 h reoxygenation and analyzed for caspases 3 and 7 and caspases 8 and 9 activity at each time. During hypoxia, an experimental group remained in normoxic conditions. The activity of caspases 3 and 7 and caspase 9 and caspase 8 was measured using Caspase-Glo 3/7,

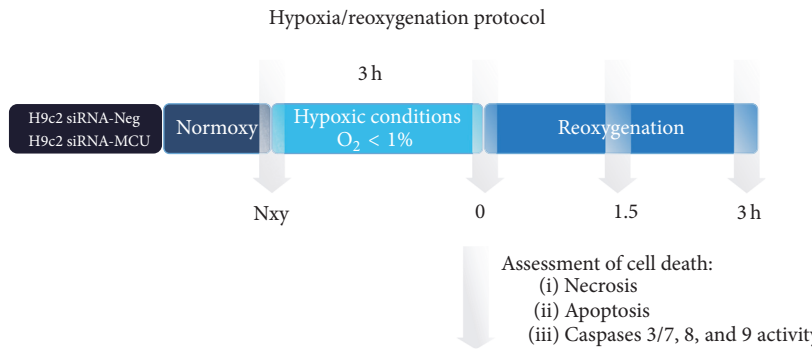

Figure 1: Schematic representation showing the hypoxia/reoxygenation (H/R) protocol applied to each experimental group. At normoxic conditions, siRNA-Neg (control group) and siRNA-MCU cardiomyocytes were subjected to 3 h of normothermic hypoxia (H) with an ischemic Tyrode solution (IT) followed by 3 h of reoxygenation (R). Transfected cardiomyocytes were harvested when indicated by arrows: measurements of necrosis and apoptosis by flow cytometry were performed and caspases 3 and 7 and caspases 9 and 8 activity were determined as described in Materials and Methods. Nxy, normoxy.

9, and 8 assay (Promega, Madison, WI, USA), respectively, according to the manufacturer's protocols.

2.12. Statistical Analysis. Statistical data are presented as mean ± SEM. Comparisons between means were made by unpaired Student's t-test or one-way ANOVA followed by Dunnett's, Tukey's, or Bonferroni's post hoc tests when appropriate to compare experimental groups. Differences were considered significant when $P < 0.05$. Data processing, graphs, and statistical analysis were performed with GraphPad Prism (V.5.01, La Jolla, CA, USA) and OriginPro 8.1 SR3 v8.1 (OriginLab Corporation, Northampton, MA, USA).

3. Results

3.1. siRNA-Targeting MCU Efficiently Decreases Mitochondrial Ca^{2+} Transport in Cardiomyocytes. Rat cardiomyocytes were transfected with specific MCU-targeted siRNA (siRNA-MCU) or nonsilencing siRNA (siRNA-Neg) to investigate the role of MCU in cell death. Using qPCR assays, we determined that there was a 70% ± 5 ($P < 0.001$) reduction in MCU mRNA expression levels up to 96 h after transfection (Figure 2(a)). Next, our silencing effects were verified using western blot assays. In cardiomyocytes transfected with the siRNA-MCU, MCU expression was lower than that in those transfected with siRNA-Neg cells. This effect showed a time-dependent response with a ~50% silencing at 48 and 72 h (Figure 2(b)). Moreover, at 96 h of transfection, we found significantly lower MCU protein levels by 67% ± 8 ($P < 0.001$). In addition, under this condition the concentration of MCU siRNAs used (225 nM) did not adversely affect the number of viable cells or the cardiomyocyte morphology and ATP production (Suppl. Figure 1A–E, Supplementary Material available online at https://doi.org/10.1155/2017/5750897). Based on these results, we used siRNAs at 225 nM for 96 hrs in the remainder of our experiments, in which we obtained the maximal silencing of MCU mRNA and protein expression (Figures 3(a) and 3(b)). In addition, siRNA-MCU did not modify the relative expression of other uniplex components, such as MICU1, MICU2, EMRE, and MCUR1 (Figure 2(c)).

Figure 3(c) shows representative $m\mathrm{Ca}^{2+}$ uptake traces for the control and MCU-silenced cardiomyocytes. Permeabilized transfected cardiomyocytes were challenged with a 15 μM Ca^{2+} addition in the presence of 1 μM CsA to determine the maximum MCU activity [9]. In control cells, a rapid $m\mathrm{Ca}^{2+}$ entry was observed (completely abolished by Ru_{360}, data not shown); however, in siRNA-MCU treated cells, the Ca^{2+} transport was drastically reduced. Mitochondrial Ca^{2+} uptake time to its 50% ($T_{50\%}$) provides a quantitative index of MCU activity. For the control cardiomyocytes, $T_{50\%}$ was 1.08 ± 0.22 min, while, in MCU-silenced cells, it was 2.02 ± 0.4 min ($P < 0.05$) (Figure 3(d)). These results indicate a significant reduction in the rate of mitochondrial transport in our MCU-silenced cardiomyocytes.

3.2. MCU Silencing Reduces Mitochondrial Ca^{2+} Overload, Permeability Transition Pore, and Oxidative Stress in Cardiomyocytes. Since excessive Ca^{2+} accumulation in the mitochondrial matrix leads to the collapse of the mitochondrial potential, transfected cardiomyocytes were challenged with Ca^{2+} overload following their effects on the membrane potential. At a steady state, the membrane potential did not show a difference in $\Delta\psi_m$ between the control and MCU-silenced cardiomyocytes (Suppl. Figure 1C-D). Nevertheless, after a Ca^{2+} pulse, the control cardiomyocytes showed a significant Ca^{2+}-dependent depolarization compared with MCU-silenced cardiomyocytes (Figure 4(a)). At the same time, MCU-silenced cells were able to maintain $\Delta\psi_m$ in ~75% ($P < 0.05$) (Figure 4(b)). Ru_{360} and CsA treatment protected against Ca^{2+}-induced membrane depolarization by ~95% (Figures 4(c) and 4(d) and Suppl. Figure 2A).

Moreover, in Ca^{2+} retention experiments with a 50 μM Ca^{2+} bolus, we observed an early and dramatic release of Ca^{2+} from control cardiomyocytes compared with the MCU-silenced cells (Suppl. Figure 2B). Ca^{2+} release was inhibited

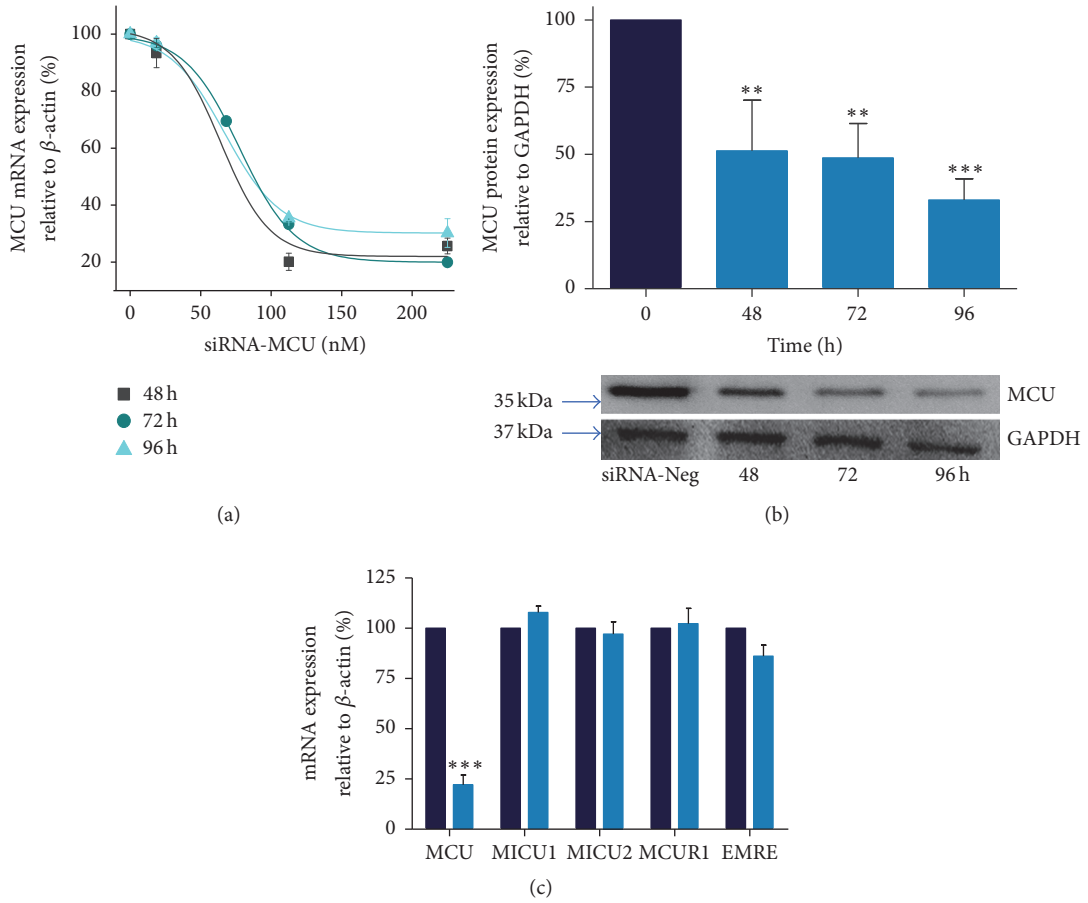

Figure 2: Dose-response analysis of MCU expression in cardiomyocytes transfected with a specific siRNA designed targeting MCU (siRNA-MCU). (a) MCU mRNA expression by qRT-PCR normalized versus β-actin using 18.7, 112.5, or 225 nM of siRNA at 0, 48, 72, and 96 h of transfection. We obtained EC50 ~67.2 nM at 96 h of transfection, mean ± SEM, $n = 3$. (b) Representative protein expression analysis of MCU in cardiomyocytes silenced with 225 nM of siRNA-MCU at 48 h ($^{**}P < 0.01$); at 72 h ($^{**}P < 0.01$); and at 96 h of transfection. GAPDH served as a loading control ($^{***}P < 0.001$), mean ± SEM, $n = 3$–6. (c) Relative mRNA abundance of associated regulatory genes in MCU-silenced cardiomyocytes using 225 nM of siRNA-MCU at 96 h of transfection, mean ± SEM, $n = 4$. MICU1, mitochondrial calcium uptake 1; MICU2, mitochondrial calcium uptake 2; MCUR1, mitochondrial calcium uniporter regulator 1; EMRE, essential mitochondrial calcium uniporter regulator.

by CsA, indicating the involvement of $_m$PTP as a trigger of membrane potential collapse.

Oxidative stress and Ca^{2+} overload are known to have detrimental effects on mitochondrial membrane integrity since both are inducers of $_m$PTP opening [22]. Figure 5(a) shows the time-course analysis of superoxide production in response to TG-induced Ca^{2+} overload. At basal conditions, the control and MCU-silenced cardiomyocytes showed a similar fluorescence intensity of MitoSOX. After 60 and 120 min of TG treatment, MitoSOX intensity was significantly higher in siRNA-Neg transfected cells than in MCU-deficient cardiomyocytes (Figure 5(a)). Therefore, MCU-deficient cardiomyocytes showed a 51% ($P < 0.001$) reduction in Ca^{2+} overload-induced superoxide production (Figure 5(b)). Under these conditions, the Ru_{360} and CsA treatment also decreases ROS production by 22% (ns) and 49% ($P < 0.001$), respectively (Figure 5(c)). In accordance with these findings, MCU silencing might exert protective effects by reducing oxidative stress induced by Ca^{2+} overload.

3.3. MCU Silencing Reduces Cardiomyocyte Cell Death in Hypoxia/Reoxygenation Injury. Transfected cardiomyocytes were incubated for 3 h in a hypoxic chamber for O_2 (1%) in combination with glucose-deprivation, serum-free, and acidosis (pH 6.8) conditions to induce hypoxia. A schematic model of hypoxia/reoxygenation is shown in Figure 1. Cell viability and apoptosis were determined by Annexin V/PI staining and analyzed by flow cytometry at specific time points during Nxy and during reoxygenation: at the beginning (0 h), after 1.5 h, and after 3 h. Representative flow cytometry dot plots showing the populations of viable (Annexin V^-, IP^-) and apoptotic cells (Annexin V^+/IP^- and Annexin V^+/IP^+) are shown in Figures 6(a) and 6(b) at Nxy and 1.5 h of reoxygenation. Cell viability was

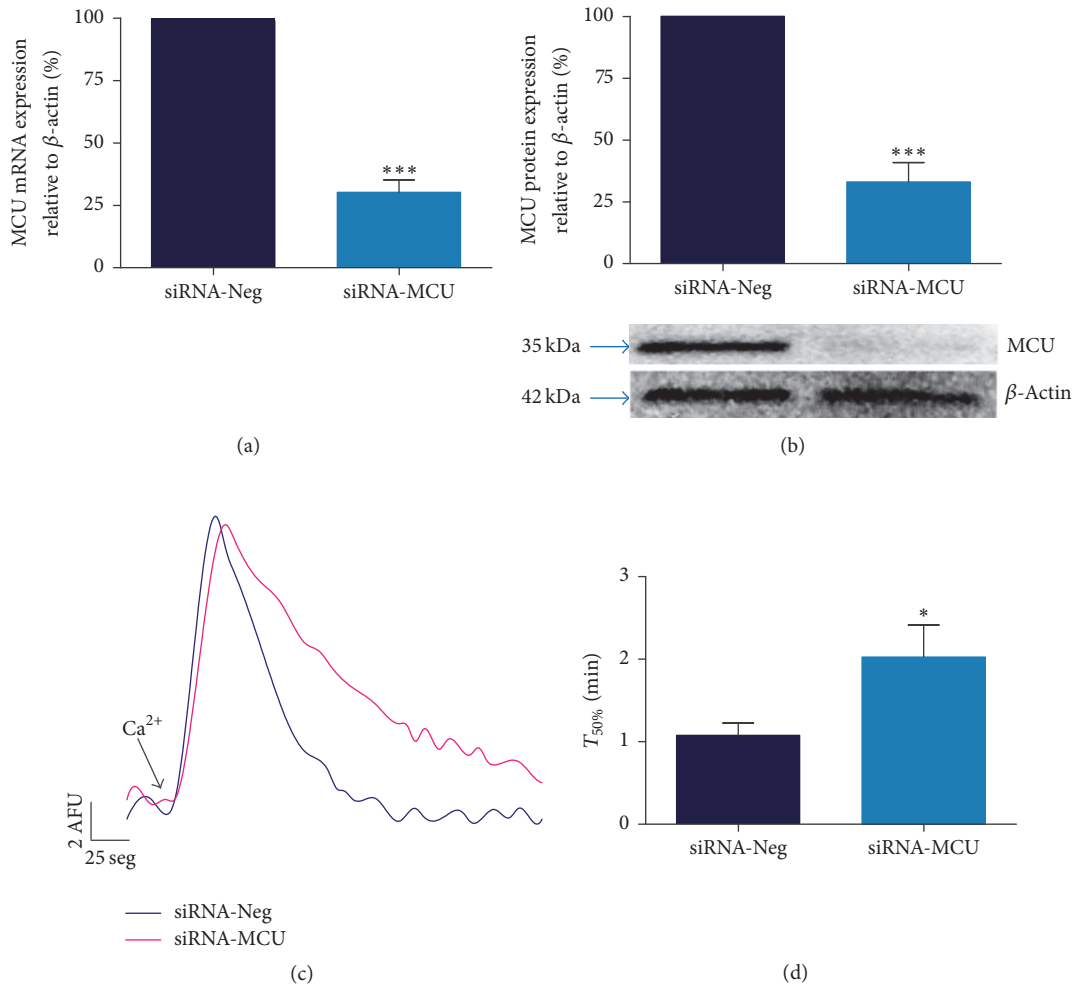

FIGURE 3: MCU silencing reduces mitochondrial Ca^{2+} transport. (a) MCU mRNA expression by semiquantitative qRT-PCR in silenced cardiomyocytes, $^{***}P < 0.001$ versus siRNA-Neg, mean ± SEM, $n = 7$. (b) MCU protein expression, with β-actin used as a loading control. $^{***}P < 0.001$ versus siRNA-Neg, mean ± SEM, $n = 6$. (c) Representative traces of mitochondrial Ca^{2+} uptake in permeabilized MCU-silenced cardiomyocytes using CG-5N Ca^{2+} indicator after 15 μM Ca^{2+} addition. The experiment was performed in the presence of 1 μM CsA. AFU, arbitrary fluorescence units. (d) Time to 50% decay analysis ($T_{50\%}$) of mitochondrial Ca^{2+} transport. $^{*}P < 0.05$ versus siRNA-Neg, mean ± SEM, $n = 6$. MCU silencing conditions were using 225 nM of siRNA-MCU at 96 h of transfection.

~90% (Suppl. Figure 1A) and apoptosis was ~3–5% in both transfected cardiomyocytes at normoxic conditions. At the onset of reoxygenation, we did not find any changes in cell death between the controls (12.6%) and the MCU-silenced cardiomyocytes (8.2%), as shown in Figure 6(c). However, after 1.5 h of reoxygenation, necrosis increased by 46% in the control cardiomyocytes compared to the MCU-silenced cardiomyocytes (16.7%, $P < 0.05$). After 3 h of reoxygenation, the viable cells were preserved in MCU-silenced cardiomyocytes in 60.3 ± 8% and then dropped by 30.5 ± 3.6% ($P < 0.01$) in the control cardiomyocytes. Apoptotic cell death measurements showed similar results; no significant changes were observed in the level of apoptosis at Nxy or the beginning of reoxygenation between the experimental groups. Nevertheless, we found a twofold decrease in MCU-deficient (4.3 ± 1.1) versus siRNA-Neg cardiomyocytes (8.4 ± 0.67) after 1.5 h of reoxygenation ($P < 0.01$). In the same way, after 3 h of reoxygenation, the apoptosis level increased 1.5-fold in siRNA-Neg cardiomyocytes (9.12 ± 0.94 versus 6.04 ± 0.5, $P < 0.05$). Accordingly, caspases 3 and 7 activities increased by 2-fold at the onset of reoxygenation in the control cardiomyocytes (6.86 ± 0.18) compared to the MCU-deficient cardiomyocytes (3.38 ± 0.7, $P < 0.001$). At the same time, caspase 9 activity increased significantly ($P < 0.001$) in both experimental groups, but, after 1.5 h of reoxygenation, the activation levels of caspase 9 dropped 1.5-fold in the MCU-deficient cardiomyocytes ($P < 0.01$). In fact, the activation of caspase 9 and caspases 3 and 7 persisted until 3 h after reoxygenation in siRNA-Neg cells compared to the MCU-silenced cardiomyocytes. Additionally, we observed an 18-fold increase in activation of caspase 8 at the onset of reoxygenation in control cells. Nevertheless, we observed a 40% reduction in caspase 8 activity in MCU-silenced cells compared with control cells (4.95 ± 0.7 versus 8.36 ± 1.6, RLU·mg^{-1}). Overall, these results demonstrate that MCU silencing in cardiomyocytes

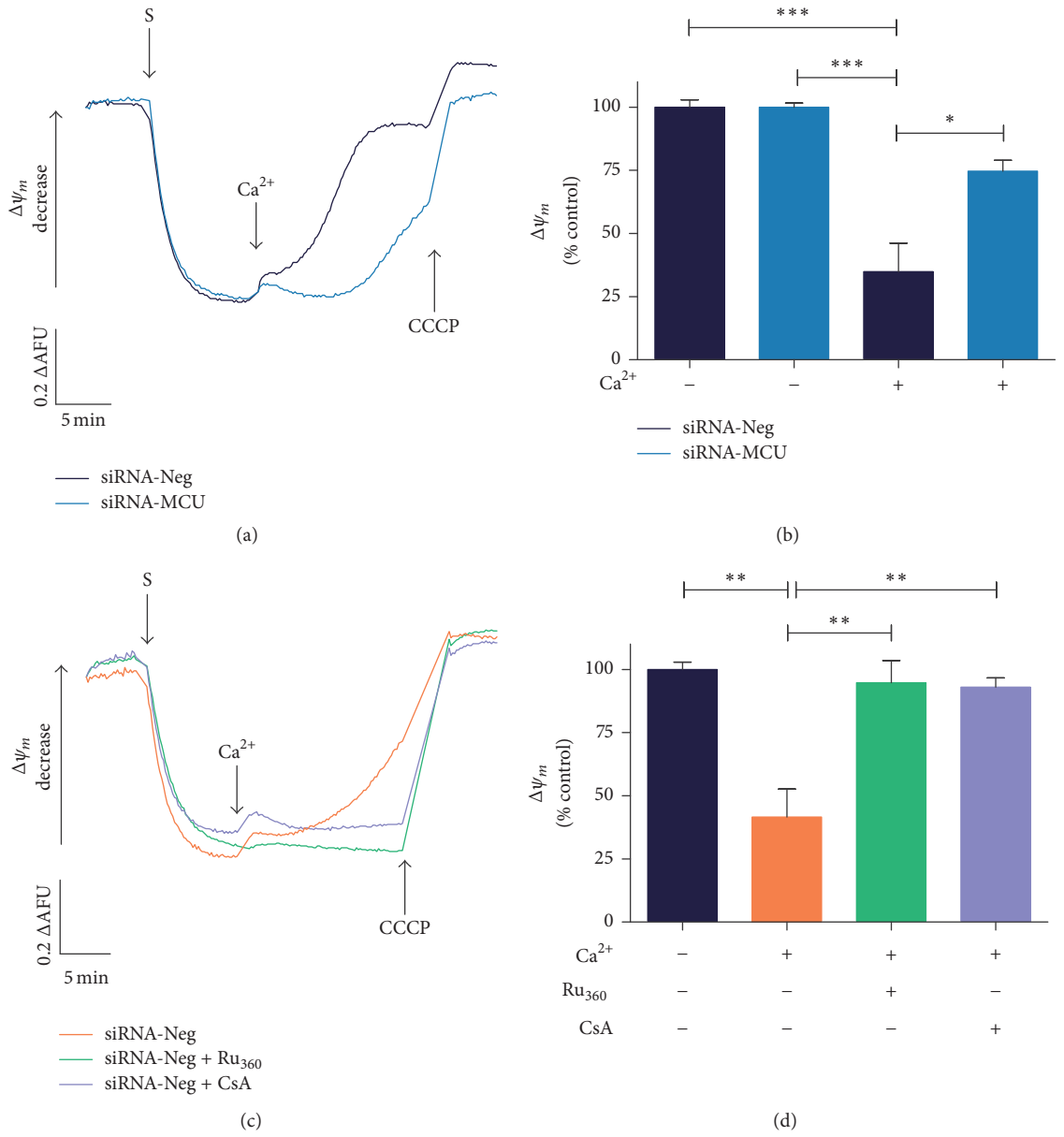

FIGURE 4: MCU silencing reduces significantly mitochondrial permeability transition by calcium overload. (a) Representative mitochondrial $\Delta\psi_m$ traces in permeabilized MCU-silenced cardiomyocytes using 2 μM safranin, after 7.5 μM Ca^{2+} addition. siRNA-Neg cardiomyocytes show no difference in $\Delta\psi_m$ compared to MCU-silenced cells at baseline. MCU-silenced cardiomyocytes were able to maintain significantly $\Delta\psi_m$ after 7.5 μM Ca^{2+} addition. Upon completion of the traces, 20 μM CCCP was added as uncoupling. (b) Semiquantitative analysis of $\Delta\psi_m$ after Ca^{2+} addition in transfected cardiomyocytes. $^{*}P < 0.05$ versus siRNA-Neg, mean ± SEM, $n = 3$. (c) Representative mitochondrial safranin $\Delta\psi$ recordings in siRNA-Neg cardiomyocytes treated with 5 μM Ru_{360} or 1 μM CsA before 7.5 μM Ca^{2+} pulse. (d) Semiquantitative analysis of $\Delta\psi_m$ in siRNA-Neg cardiomyocytes treated with Ru_{360} or CsA. $^{**}P < 0.01$ versus siRNA-Neg, mean ± SEM, $n = 5$-4. Upon completion of the registers, 20 μM CCCP was added as uncoupling. All semiquantitative data is normalized to 100% of untreated siRNA-Neg cardiomyocytes at basal conditions. AFU, arbitrary fluorescence units. $^{***}P < 0.001$ versus siRNA-Neg.

reduces necrosis and apoptosis of the hypoxia/reoxygenation injury.

4. Discussion

In the heart, $m$$Ca^{2+}$ uptake can shape cytosolic calcium signals to regulate some physiological processes, principally matching workload and energy production [23]. Nevertheless, an excessive uptake of Ca^{2+} triggers mitochondrial dysfunction through $_m$PTP opening, leading to cell injury by apoptosis and necrosis [5]. In this regard, several studies have suggested that dysregulation of cytosolic Ca^{2+} which leads to $m$$Ca^{2+}$ overload is present in the physiopathology of ischemia/reperfusion (I/R) injury and heart failure (HF) [24]. The MCU channel, the principal $m$$Ca^{2+}$ transport system,

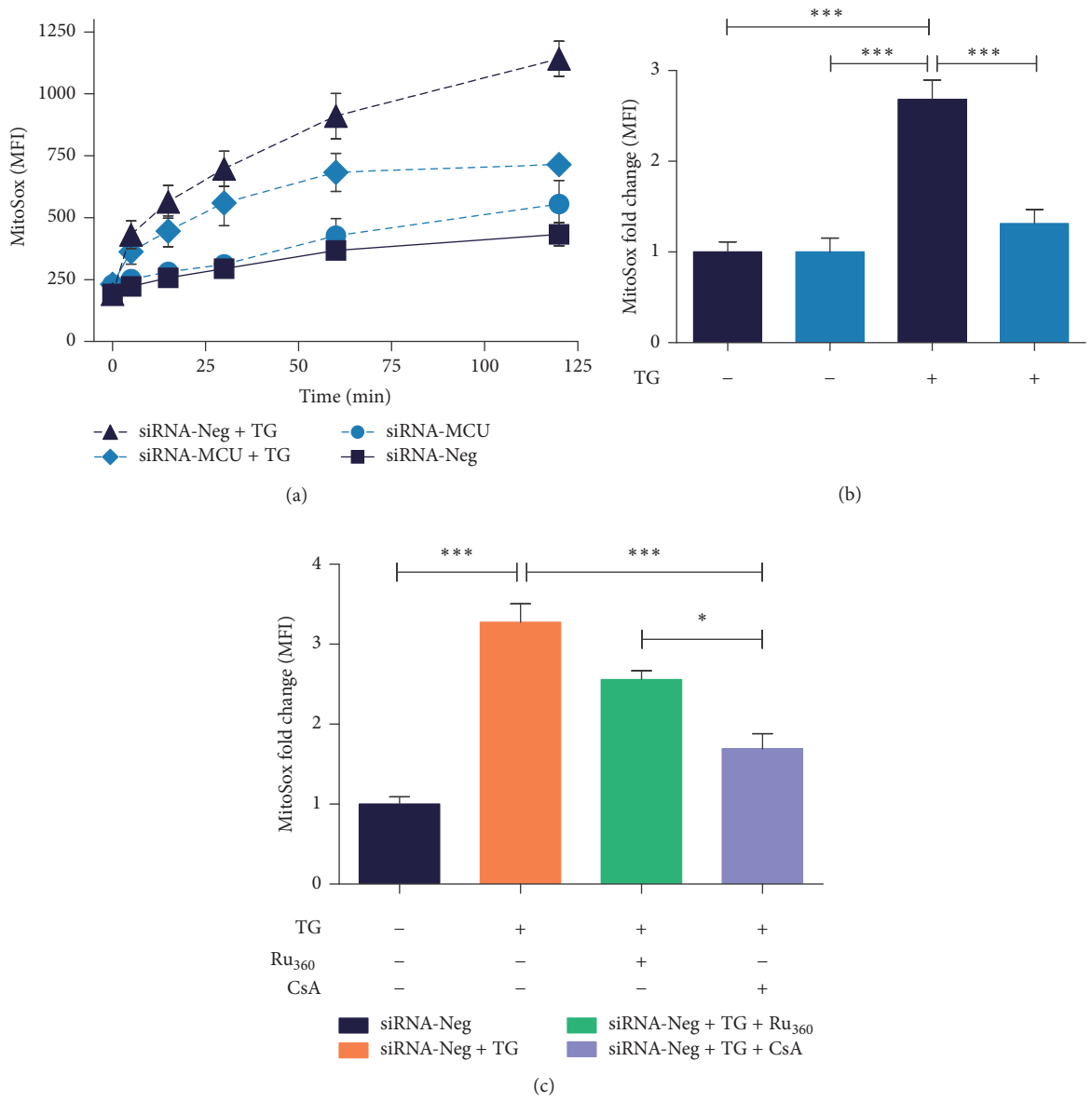

FIGURE 5: MCU silencing reduces mitochondrial oxidative stress. (a) Time-response curve of mitochondrial ROS (superoxide) production evoked by cytosolic Ca^{2+} overload with 5 μM TG in transfected cardiomyocytes. Measurements were realized over 120 min of TG treatment and ROS was detected with MitoSOX Red by flow cytometry. (b) ROS levels at 120 min of TG addition is presented as FMI fold change with respect to TG untreated cardiomyocytes. ROS production in siRNA-Neg cardiomyocytes was twofold greater than that in MCU-silenced cardiomyocytes after TG addition, $^{***}P < 0.001$, mean ± SEM, $n = 5$. (c) ROS production in siRNA-Neg cardiomyocytes pretreated with 5 μM Ru_{360} or 1 μM CsA, measured after 120 min of 5 μM TG addition. Data are presented as described previously. $^{*}P < 0.05$ and $^{***}P < 0.001$; mean ± SEM and $n = 6$–8.

carries out this mechanism. However, the precise role in the regulation of Ca^{2+} handling and its consequences on heart disease remain controversial [25]. Not until recently has the molecular characterization of the MCU been made possible [11, 12], allowing for the study of its univocal role in the physiopathology of myocardial diseases. This finding led us to explore the possibility of modulating MCU expression in knockout mice or using a siRNA technology. In this regard, we tested a specific siRNA design to knock down MCU expression in the cardiomyocyte line for an in vitro MCU target validation. After being challenged to a mCa^{2+} overload, MCU-deficient cells were able to largely sustain $\Delta\psi_m$ and retain Ca^{2+} similarly to those pharmacologically treated with CsA, as expected. Altogether, these findings indicate that MCU silencing confers resistance to $_m$PTP opening [6, 14]. Furthermore, MCU-silenced cardiomyocytes treated with TG (a SR-Ca^{2+}/ATPase (SERCA) inhibitor), which promotes a burst of cytosolic Ca^{2+} and later ROS, failed to increase

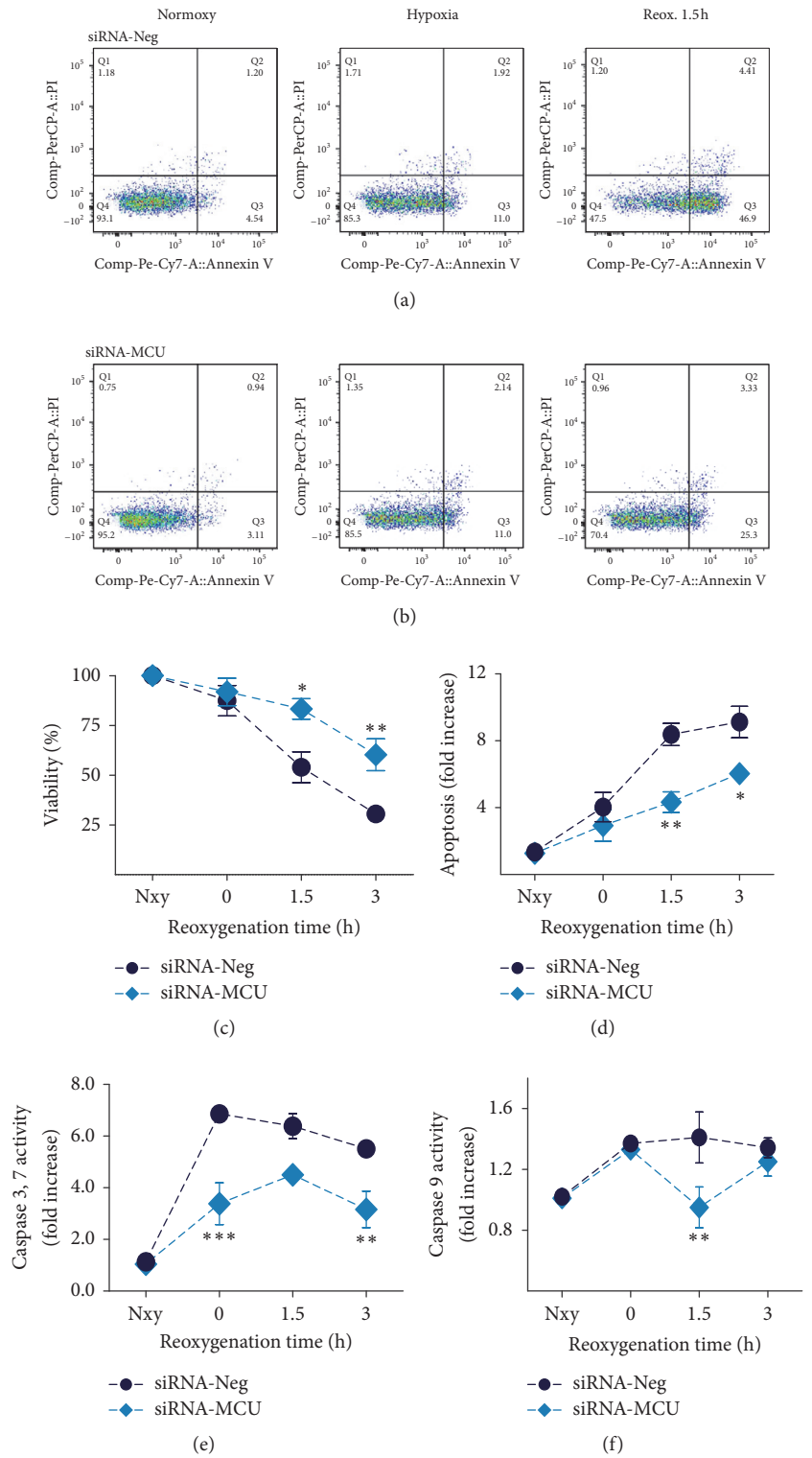

Figure 6: MCU silencing markedly reduced cardiomyocyte cell death in hypoxia/reoxygenation injury. (a and b) Representative dot-plot diagrams of flow cytometry viability/apoptosis analysis of siRNA-Neg and MCU-silenced cardiomyocytes in Nxy, after hypoxia and 1.5 h reoxygenation time. Viability and apoptosis were determined by PI and Annexin V PE-Cy7 conjugated staining, respectively. Q4 quadrant represents the viable cells, Q2 and Q3 represent the apoptotic cells, while Q1 and Q2 are the necrotic population. (c and d) Reoxygenation-time dependent cardiomyocyte viability and apoptosis at 0, 1.5, and 3 h reoxygenation, respectively. $^{**}P < 0.01$; mean ± SEM; $n = 7$. Data is presented as percentage of Nxy conditions. (d) Apoptosis was ~twofold and 1.5-fold increase in siRNA-Neg cardiomyocytes with respect to MCU-silenced cells at 1.5 and 3 h reoxygenation, respectively. Apoptosis is normalized to Nxy and expressed as fold change. $^{*}P < 0.05$, $^{**}P < 0.01$, versus siRNA-Neg cardiomyocytes, mean ± SEM, $n = 7$. (e) Time-dependent activation of caspases 3 and 7 and (f) caspase 9 during reoxygenation. $^{**}P < 0.01$, $^{***}P < 0.001$, versus siRNA-Neg cells, mean ± SEM, and $n = 7$; Nxy, normoxic conditions.

superoxide radical production. Also, after H/R protocol, siRNA-MCU-silenced cardiomyocytes reduced $_m$PTP opening and activation of caspases 8 and 9. In accordance with our results, caspase 8 might initiate the execution phase of cell apoptosis, after which mitochondrial dysfunction induces activation of caspase 9. One potential explanation for this finding is that caspase 8 activation cleaves Bid [26], and then the cleaved Bid activates mitochondrial Bax/Bak and contributes to multiple mitochondrial dysfunction, including the release of the intramembrane space proteins, and activation of apaf-1, which in turn cleaves the proenzyme of caspase 9 into the active form. These observations are similar to those reported when Ru_{360}-MCU was inhibited in in vivo and ex vivo models of I/R [9, 10], confirming that partial or acute MCU inhibition could be a therapeutic strategy to reduce cell death [27]. Moreover, this cardioprotective effect has been linked to MCU as an ischemic preconditioning (IPC) mediator [6, 28]. The mechanisms implicated in IPC are not fully understood; however, low levels of mCa^{2+}-generated ROS are involved as a trigger of IPC by activation of survival kinases [29]. Since a large production of ROS during reperfusion contributes importantly to $_m$PTP opening inducing cardiomyocyte death, the controlled ROS production by MCU silencing mimics the IPC cardioprotective effects. Therefore, our findings are in accordance with the observed protection in conditional cardiac-specific MCU$^{-/-}$ mice [14, 15]. In this transgenic model, deletion of MCU in adult cardiomyocytes leads to protection from cell death induced by acute damage such as ischemia-reperfusion injury. However, the results in MCU-knockout constitutive animals are still controversial. For instance, during reperfusion injury, MCU-knockout hearts were similar to control hearts, and CsA did not exert a protective effect. This suggests that Ca^{2+}-independent death pathways take place in the absence of MCU and that alternative mechanisms exist for Ca^{2+} entry [30]. Of note, inbred MCU-knockout mice are not viable because they are embryonically lethal; only mixed-strain MCU-knockout mice are viable [31]. In addition to this controversy, recent results in MCU overexpressing mice are more resistant to reperfusion injury in part due to an enhanced activity of survival kinases [32].

In addition to defining the contribution of MCU activity in pathologies, the discovery of therapeutic strategies that modulate MCU activity will be extremely important for the future development of putative MCU-targeting therapies. Here, using siRNA or several pharmacological strategies (such as Ru_{360} or CsA), we attempted to diminish $_m$PTP opening or reduce mCa^{2+} overload in order to decrease the likelihood of arrhythmias and postmyocardial infarction cardiac dysfunction [2]. In this regard, in vitro and ex vivo studies of cytosolic Ca^{2+} overload and IR injury have shown that CsA is a potent inhibitor of $_m$PTP, protecting against reperfusion cardiomyocyte death [8, 33]. Indeed, CsA application in small animal models at the onset of reperfusion has demonstrated a reduction of the myocardial infarct area by ~45% [34] by suppressing $\Delta\psi_m$ loss, NADH oxidation, Ca^{2+} release, and mitochondrial swelling [35]. Accordingly, some clinical trials have been performed to determine its protective effect from reperfusion injury in patients with myocardial infarction [36]. Nevertheless, a recent meta-analysis of randomized controlled trials reveals that CsA could not have protective effects towards reperfusion injury in clinical patients [37]. The cause of these effects is not yet clear, but it could be because CsA is an immunosuppressive agent that has multiple targets such as cyclophilins and calcineurin [38]. Additionally, CsA only increases the threshold of $_m$PTP inducers, so it would be desirable to explore another strategy to prevent the formation of $_m$PTP and reperfusion injury. On the other hand, the use of Ru_{360} as a specific inhibitor of the MCU has been used in intact cardiac cells [7], isolated hearts [6, 10], and murine models [9] which provided protection against reperfusion injury, improving mechanical parameters, and decreasing infarct size and intracellular enzymes release [9, 39]. However, their pharmacokinetic parameters, bioavailability, and side effects have not been completely described.

Moreover, these therapeutic strategies that reduce ischemic injury could be beneficial to slow the progression of HF. In this regard, Santulli et al. [40] recently demonstrated that an intracellular Ca^{2+} leak could cause mitochondrial Ca^{2+} overload and dysfunction in HF murine models. In particular, a sarcoplasmic reticulum Ca^{2+} leak can establish a pathological feedback with mitochondria in which mitochondrial dysfunction increases ROS production, which consequently leads to oxidation/nitrosylation of some important sarcoplasmic reticulum channels such as RyR2, enhancing the diastolic Ca^{2+} leak and affecting cell contractility. Moreover, we found that selective MCU inhibition has the therapeutic potential to prevent catecholamine-induced toxicity as observed in HF [41]. In this regard, Anderson's group using MCU dominant-negative transgenic mice confirmed our findings of MCU's role on catecholamine response, because their mice were incapable of reaching catecholamine response [14, 27]. These novel data provide experimental rationale to explore the role of MCU during HF development.

At present, knockdown of gene expression by siRNA technologies offers a potent therapeutic approach to specific modulation of gene targeting [42]. siRNA therapeutics is suitable for drug use because it does not require genome integration and can be inexpensive and easily synthesized. Since a rational design of siRNA can specifically inhibit endogenous gene expression, it can modulate any disease-related gene expression [43]. Because of their great therapeutic potential, at least 20 siRNA-based drugs have now entered clinical trials in humans [43]. However, siRNA molecules are unstable in the serum and have shown poor cellular uptake and immunogenicity [44]. In this regard, the successful application of siRNA for therapy requires the development of effective drug delivery systems, in particular, nanovectors [45]. Recently, endothelial dysfunction present in HF has been explored as a novel avenue for the delivery of nanovectors, and the resulting endothelial permeability opens the field to nanotechnology-based therapies that could reach the myocardium through dysfunctional permeable endothelium [46]. In a murine model of HF, a

passive intracardiac accumulation of high concentrations of nanocarriers occurred after a single application. Compared to the normal heart tissues, the accumulation of nanovectors was 12 times higher in HF animals [47]. This approach should be used as a potential avenue for siRNA-MCU therapy in reperfusion injury or HF, potentially translating towards novel therapies that might improve patient outcomes.

5. Conclusion

In summary, as the first proof of concept, we have shown that MCU silencing by specific siRNA reduces in vitro H/R injury as seen by cardiomyocyte death abatement. Therefore, this knowledge will allow for the development of a suitable delivery system to test the therapeutic potential of this siRNA in an in vivo model of mitochondrial calcium overload and dysfunction as those present in HF. In this context, the novel MCU druggability should be a fertile area of research in the future.

Abbreviations

AFU: Arbitrary fluorescence units
CG-5N: Calcium Green-5N
CCCP: Cyanide *m*-chlorophenyl hydrazone
CsA: Cyclosporin A
ETC: Electron transport chain
HR: Hypoxia/reoxygenation
MFI: Median fluorescence intensity
$m\mathrm{Ca}^{2+}$: Mitochondrial calcium
MCU: Mitochondrial calcium uniporter
$_m$PTP: Mitochondrial permeability transition pore
$\Delta\psi_m$: Mitochondrial membrane potential
MVO_2: Myocardial oxygen consumption
Nxy: Normoxy
PI: Propidium iodide
RLU: Relative luminescence units
ROS: Reactive oxygen species
SERCA: Sarco/endoplasmic reticulum calcium-ATPase
TG: Thapsigargin
TI: Tyrode ischemic solution
Uniplex: Mitochondrial calcium uniporter holocomplex.

Disclosure

This work was submitted in partial fulfillment of the requirements for the Ph.D. degree of Yuriana Oropeza-Almazán for the Doctorate in Biotechnology of Tecnológico de Monterrey.

Competing Interests

The authors declare that they have no competing interests.

Authors' Contributions

Conception and design of research were done by Gerardo García-Rivas and Yuriana Oropeza-Almazán. Yuriana Oropeza-Almazán, Eduardo Vázquez-Garza, and Héctor Chapoy-Villanueva performed experiments; Yuriana Oropeza-Almazán, Eduardo Vázquez-Garza, and Héctor Chapoy-Villanueva analyzed data; Yuriana Oropeza-Almazán and Gerardo García-Rivas drafted manuscript; Yuriana Oropeza-Almazán, Eduardo Vázquez-Garza, Héctor Chapoy-Villanueva, Guillermo Torre-Amione, and Gerardo García-Rivas interpreted results of experiments; Yuriana Oropeza-Almazán prepared figures; Gerardo García-Rivas and Guillermo Torre-Amione edited and revised manuscript. Eduardo Vázquez-Garza and Héctor Chapoy-Villanueva contribute equally.

Acknowledgments

The authors thank Dr. Arturo Chávez-Reyes for their support with siRNA design and critical review of experimental results, Silvia Cárdenas Rodríguez, M.D., and Miguel A. Flores, B.S., for exceptional technical assistance. They also thank Valeria Oropeza for editing the figures. This work was partially supported by Endowed Chair in Cardiology (Tecnológico de Monterrey, 0020CAT131) as well as CONACYT Grants 151136, 133591, and 269399 and Fronteras de la Ciencia grant (0682) and Xignus Research Fund. Postdoctoral fellowship (CONACYT to Eduardo Vázquez-Garza and Héctor Chapoy-Villanueva) is also acknowledged.

References

[1] D. J. Hausenloy, E. A. Boston-Griffiths, and D. M. Yellon, "Cyclosporin A and cardioprotection: from investigative tool to therapeutic agent," *British Journal of Pharmacology*, vol. 165, no. 5, pp. 1235–1245, 2012.

[2] D. M. Yellon and D. J. Hausenloy, "Myocardial reperfusion injury," *The New England Journal of Medicine*, vol. 357, no. 11, pp. 1121–1135, 2007.

[3] S.-M. Kang, S. Lim, H. Song et al., "Allopurinol modulates reactive oxygen species generation and Ca 2+ overload in ischemia-reperfused heart and hypoxia-reoxygenated cardiomyocytes," *European Journal of Pharmacology*, vol. 535, no. 1-3, pp. 212–219, 2006.

[4] A. P. Halestrap, "Mitochondria and reperfusion injury of the heart—a holey death but not beyond salvation," *Journal of Bioenergetics and Biomembranes*, vol. 41, no. 2, pp. 113–121, 2009.

[5] A. P. Halestrap, "What is the mitochondrial permeability transition pore?" *Journal of Molecular and Cellular Cardiology*, vol. 46, no. 6, pp. 821–831, 2009.

[6] G. D. J. García-Rivas, A. Guerrero-Hernández, G. Guerrero-Serna, J. S. Rodríguez-Zavala, and C. Zazueta, "Inhibition of the mitochondrial calcium uniporter by the oxo-bridged dinuclear ruthenium amine complex (Ru_{360}) prevents from irreversible injury in postischemic rat heart," *FEBS Journal*, vol. 272, no. 13, pp. 3477–3488, 2005.

[7] M. A. Matlib, Z. Zhou, S. Knight et al., "Oxygen-bridged dinuclear ruthenium amine complex specifically inhibits Ca^{2+} uptake into mitochondria in vitro and in situ in single cardiac myocytes," *Journal of Biological Chemistry*, vol. 273, no. 17, pp. 10223–10231, 1998.

[8] E. J. Griffiths, C. J. Ocampo, J. S. Savage, M. D. Stern, and H. S. Silverman, "Protective effects of low and high doses of cyclosporin A against reoxygenation injury in isolated rat cardiomyocytes are associated with differential effects on mitochondrial calcium levels," *Cell Calcium*, vol. 27, no. 2, pp. 87–95, 2000.

[9] G. J. García-Rivas, K. Carvajal, F. Correa, and C. Zazueta, "Ru_{360}, a specific mitochondrial calcium uptake inhibitor, improves cardiac post-ischaemic functional recovery in rats *in vivo*," *British Journal of Pharmacology*, vol. 149, no. 7, pp. 829–837, 2006.

[10] F. Correa, V. Soto, and C. Zazueta, "Mitochondrial permeability transition relevance for apoptotic triggering in the post-ischemic heart," *The International Journal of Biochemistry & Cell Biology*, vol. 39, no. 4, pp. 787–798, 2007.

[11] J. M. Baughman, F. Perocchi, H. S. Girgis et al., "Integrative genomics identifies MCU as an essential component of the mitochondrial calcium uniporter," *Nature*, vol. 476, no. 7360, pp. 341–345, 2011.

[12] D. De Stefani, A. Raffaello, E. Teardo, I. Szabó, and R. Rizzuto, "A forty-kilodalton protein of the inner membrane is the mitochondrial calcium uniporter," *Nature*, vol. 476, no. 7360, pp. 336–340, 2011.

[13] D. De Stefani, R. Rizzuto, and T. Pozzan, "Enjoy the trip: calcium in mitochondria back and forth," *Annual Review of Biochemistry*, vol. 85, pp. 161–192, 2016.

[14] J. Q. Kwong, X. Lu, R. N. Correll et al., "The mitochondrial calcium uniporter selectively matches metabolic output to acute contractile stress in the heart," *Cell Reports*, vol. 12, no. 1, pp. 15–22, 2015.

[15] T. S. Luongo, J. P. Lambert, A. Yuan et al., "The mitochondrial calcium uniporter matches energetic supply with cardiac workload during stress and modulates permeability transition," *Cell Reports*, vol. 12, no. 1, pp. 23–34, 2015.

[16] C.-F. Xu and J. Wang, "Delivery systems for siRNA drug development in cancer therapy," *Asian Journal of Pharmaceutical Sciences*, vol. 10, no. 1, pp. 1–12, 2015.

[17] J. E. Zuckerman and M. E. Davis, "Clinical experiences with systemically administered siRNA-based therapeutics in cancer," *Nature Reviews Drug Discovery*, vol. 14, no. 12, pp. 843–856, 2015.

[18] M. Patron, V. Checchetto, A. Raffaello et al., "MICU1 and MICU2 finely tune the mitochondrial Ca^{2+} uniporter by exerting opposite effects on MCU activity," *Molecular Cell*, vol. 53, no. 5, pp. 726–737, 2014.

[19] K. A. P. Oliveira, K. G. Zecchin, L. C. Alberici, R. F. Castilho, and A. E. Vercesi, "Simvastatin inducing PC3 prostate cancer cell necrosis mediated by calcineurin and mitochondrial dysfunction," *Journal of Bioenergetics and Biomembranes*, vol. 40, no. 4, pp. 307–314, 2008.

[20] P. Mukhopadhyay, M. Rajesh, K. Yoshihiro, G. Haskó, and P. Pacher, "Simple quantitative detection of mitochondrial superoxide production in live cells," *Biochemical and Biophysical Research Communications*, vol. 358, no. 1, pp. 203–208, 2007.

[21] M. Zhao, L. Sun, X.-J. Yu et al., "Acetylcholine mediates AMPK-dependent autophagic cytoprotection in H9c2 cells during hypoxia/reoxygenation injury," *Cellular Physiology and Biochemistry*, vol. 32, no. 3, pp. 601–613, 2013.

[22] P. Bernardi, F. Di Lisa, F. Fogolari, and G. Lippe, "From ATP to PTP and back: a dual function for The mitochondrial ATP synthase," *Circulation Research*, vol. 116, no. 11, pp. 1850–1862, 2015.

[23] C. Mammucari, A. Raffaello, D. V. Reane, and R. Rizzuto, "Molecular structure and pathophysiological roles of the Mitochondrial Calcium Uniporter," *Biochimica et Biophysica Acta—Molecular Cell Research*, vol. 1863, no. 10, pp. 2457–2464, 2016.

[24] M. Luo and M. E. Anderson, "Mechanisms of altered Ca^{2+} handling in heart failure," *Circulation Research*, vol. 113, no. 6, pp. 690–708, 2013.

[25] B. S. Jhun, J. Mishra, S. Monaco et al., "The mitochondrial Ca^{2+} uniporter: regulation by auxiliary subunits and signal transduction pathways," *American Journal of Physiology—Cell Physiology*, vol. 311, no. 1, pp. C67–C80, 2016.

[26] X. Luo, I. Budihardjo, H. Zou, C. Slaughter, and X. Wang, "Bid, a Bcl2 interacting protein, mediates cytochrome c release from mitochondria in response to activation of cell surface death receptors," *Cell*, vol. 94, no. 4, pp. 481–490, 1998.

[27] T. P. Rasmussen, Y. Wu, M.-L. A. Joiner et al., "Inhibition of MCU forces extramitochondrial adaptations governing physiological and pathological stress responses in heart," *Proceedings of the National Academy of Sciences of the United States of America*, vol. 112, no. 29, pp. 9129–9134, 2015.

[28] S.-Z. Zhang, Q. Gao, C.-M. Cao, I. C. Bruce, and Q. Xia, "Involvement of the mitochondrial calcium uniporter in cardioprotection by ischemic preconditioning," *Life Sciences*, vol. 78, no. 7, pp. 738–745, 2006.

[29] D. J. Hausenloy and D. M. Yellon, "Survival kinases in ischemic preconditioning and postconditioning," *Cardiovascular Research*, vol. 70, no. 2, pp. 240–253, 2006.

[30] X. Pan, J. Liu, T. Nguyen et al., "The physiological role of mitochondrial calcium revealed by mice lacking the mitochondrial calcium uniporter," *Nature Cell Biology*, vol. 15, no. 12, pp. 1464–1472, 2013.

[31] E. Murphy, X. Pan, T. Nguyen, J. Liu, K. M. Holmström, and T. Finkel, "Unresolved questions from the analysis of mice lacking MCU expression," *Biochemical and Biophysical Research Communications*, vol. 449, no. 4, pp. 384–385, 2014.

[32] F. Di Lisa, M. Campesan, T. Zaglia, D. De Stefani, M. Mongillo, and R. Rizzuto, "Mitochondrial Ca^{2+} and ROS formation in cardiac injury and protection," *Biochimica et Biophysica Acta (BBA)—Bioenergetics*, vol. 1857, p. e11, 2016.

[33] D. J. Hausenloy, H. L. Maddock, G. F. Baxter, and D. M. Yellon, "Inhibiting mitochondrial permeability transition pore opening: a new paradigm for myocardial preconditioning?" *Cardiovascular Research*, vol. 55, no. 3, pp. 534–543, 2002.

[34] S. Y. Lim, D. J. Hausenloy, S. Arjun et al., "Mitochondrial cyclophilin-D as a potential therapeutic target for post-myocardial infarction heart failure," *Journal of Cellular and Molecular Medicine*, vol. 15, no. 11, pp. 2443–2451, 2011.

[35] A.-C. Wei, T. Liu, S. Cortassa, R. L. Winslow, and B. O'Rourke, "Mitochondrial Ca^{2+} influx and efflux rates in guinea pig cardiac mitochondria: low and high affinity effects of cyclosporine A," *Biochimica et Biophysica Acta—Molecular Cell Research*, vol. 1813, no. 7, pp. 1373–1381, 2011.

[36] P. Z. Gerczuk and R. A. Kloner, "An update on cardioprotection: a review of the latest adjunctive therapies to limit myocardial infarction size in clinical trials," *Journal of the American College of Cardiology*, vol. 59, no. 11, pp. 969–978, 2012.

[37] K. Song, S. Wang, and D. Qi, "Effects of cyclosporine on reperfusion injury in patients: a meta-analysis of randomized controlled trials," *Oxidative Medicine and Cellular Longevity*, vol. 2015, Article ID 287058, 6 pages, 2015.

[38] A. P. Halestrap and P. Pasdois, "The role of the mitochondrial permeability transition pore in heart disease," *Biochimica et Biophysica Acta—Bioenergetics*, vol. 1787, no. 11, pp. 1402–1415, 2009.

[39] K. Shintani-Ishida, M. Inui, and K.-I. Yoshida, "Ischemia-reperfusion induces myocardial infarction through mitochondrial Ca^{2+} overload," *Journal of Molecular and Cellular Cardiology*, vol. 53, no. 2, pp. 233–239, 2012.

[40] G. Santulli, W. Xie, S. R. Reiken, and A. R. Marks, "Mitochondrial calcium overload is a key determinant in heart failure," *Proceedings of the National Academy of Sciences of the United States of America*, vol. 112, no. 36, pp. 11389–11394, 2015.

[41] E. Fernández-Sada, C. Silva-Platas, C. A. Villegas et al., "Cardiac responses to β-adrenoceptor stimulation is partly dependent on mitochondrial calcium uniporter activity," *British Journal of Pharmacology*, vol. 171, no. 18, pp. 4207–4221, 2014.

[42] D. Kim and J. Rossi, "RNA mechanisms and applications," *Biotechniques*, vol. 44, pp. 613–616, 2009.

[43] B. A. Sullenger and S. Nair, "From the RNA world to the clinic," *Science*, vol. 352, no. 6292, pp. 1417–1420, 2016.

[44] F. Alexis, E. Pridgen, L. K. Molnar, and O. C. Farokhzad, "Factors affecting the clearance and biodistribution of polymeric nanoparticles," *Molecular Pharmaceutics*, vol. 5, no. 4, pp. 505–515, 2008.

[45] K. Whitehead, R. Langer, and D. Anderson, "Knocking down barriers: advances in siRNA delivery," *Nature Reviews Drug Discovery*, vol. 8, pp. 129–138, 2009.

[46] W. G. Roberts and G. E. Palade, "Increased microvascular permeability and endothelial fenestration induced by vascular endothelial growth factor," *Journal of Cell Science*, vol. 108, no. 6, pp. 2369–2379, 1995.

[47] G. U. Ruiz-Esparza, V. Segura-Ibarra, A. M. Cordero-Reyes et al., "A specifically designed nanoconstruct associates, internalizes, traffics in cardiovascular cells, and accumulates in failing myocardium: a new strategy for heart failure diagnostics and therapeutics," *European Journal of Heart Failure*, vol. 18, no. 2, pp. 169–178, 2016.

Hindawi
Oxidative Medicine and Cellular Longevity
Volume 2017, Article ID 6838921, 6 pages
https://doi.org/10.1155/2017/6838921

Research Article

Identification of Patients Affected by Mitral Valve Prolapse with Severe Regurgitation: A Multivariable Regression Model

Paola Songia,[1,2] Benedetta Porro,[1] Mattia Chiesa,[1] Veronika Myasoedova,[1] Francesco Alamanni,[1,3] Elena Tremoli,[1] and Paolo Poggio[1]

[1]*Centro Cardiologico Monzino IRCCS, Milan, Italy*
[2]*Dipartimento di Scienze Farmacologiche e Biomolecolari, Università degli Studi di Milano, Milan, Italy*
[3]*Dipartimento di Scienze Cliniche e di Comunità, Università degli Studi di Milano, Milan, Italy*

Correspondence should be addressed to Paolo Poggio; paolo.poggio@ccfm.it

Received 8 September 2016; Revised 30 December 2016; Accepted 11 January 2017; Published 2 February 2017

Academic Editor: Cecilia Zazueta

Background. Mitral valve prolapse (MVP) is the most common cause of severe mitral regurgitation. Besides echocardiography, up to now there are no reliable biomarkers available for the identification of this pathology. We aim to generate a predictive model, based on circulating biomarkers, able to identify MVP patients with the highest accuracy. *Methods*. We analysed 43 patients who underwent mitral valve repair due to MVP and compared to 29 matched controls. We assessed the oxidative stress status measuring the oxidized and the reduced form of glutathione by liquid chromatography-tandem mass spectrometry method. Osteoprotegerin (OPG) plasma levels were measured by an enzyme-linked immunosorbent assay. The combination of these biochemical variables was used to implement several logistic regression models. *Results*. Oxidative stress levels and OPG concentrations were significantly higher in patients compared to control subjects (0.116 ± 0.007 versus 0.053 ± 0.013 and 1748 ± 100.2 versus 1109 ± 45.3 pg/mL, respectively; $p < 0.0001$). The best regression model was able to correctly classify 62 samples out of 72 with accuracy in terms of area under the curve of 0.92. *Conclusions*. To the best of our knowledge, this is the first study to show a strong association between OPG and oxidative stress status in patients affected by MVP with severe regurgitation.

1. Introduction

Myxomatous mitral valve prolapse (MVP) is the most common indication for mitral valve surgery due to severe mitral regurgitation (MR). The prevalence of MVP is estimated at 2-3% with approximately 144 million people affected worldwide [1]. Echocardiographically, MVP is defined as a single or bileaflet prolapse, at least 2 mm beyond the long-axis annular plane, while the assessment of valve regurgitation takes into account the effective regurgitant orifice area (EROA) [2]. Interestingly, the pathology is equally distributed between men and women [3] and patients with prolapse have significantly lower body-mass index (BMI) and waist-to-hip ratio than those without prolapse [1].

Despite the pathology was first described in the late 1800s [3], no major risk factor has been identified yet [4] and the triggering mechanisms of MVP are not fully understood. In this context, a very recent study by Deroyer et al. [5] showed a negative association between severity of MR and high-density lipoproteins (HDL) levels. Interestingly, HDL concentrations and levels of Apo-A1, the major protein component of HDL, which participates in the reverse cholesterol transport, decreased according to the severity of MR. In addition, MVP patients showed an alteration in the antioxidant defence systems and an increase in lipid peroxidation markers [6].

Given the background, we investigated Osteoprotegerin (OPG), a well-known protein linked to oxidative stress status [7] and to endothelial mesenchymal transition on endothelial cells isolated from MVP patients [8]. OPG is a secretory glycoprotein of the tumour necrosis factor receptor superfamily involved in calcification, apoptosis, proliferation, and migration processes [9]. It possesses high affinity to receptor activator of nuclear factor-kb (RANKL), to tumour necrosis factor-related apoptosis-inducing ligand (TRAIL),

Table 1: Patient demographics.

	Control ($N = 29$)	MVP ($N = 43$)	p value
Variable			
Age (years)	57.3 [53.2, 61.4]	60.1 [56.8, 63.5]	0.291
Sex (male)	19 (65.5%)	29 (67.4%)	0.865
Diabetes	3 (10.3%)	3 (7.0%)	0.685
Hypertension	14 (48.3%)	16 (37.2%)	0.660
Hypercholesterolemia	14 (48.3%)	25 (58.1%)	0.688
Smokers	6 (20.7%)	5 (11.6%)	0.514
BMI	27.4 ± 0.76	24.8 ± 0.43	**0.005**
Total cholesterol (mg/dL)	216.1 ± 7.4	215.2 ± 6.6	0.973
Triglycerides (mg/dL)	111.2 ± 9.0	110.3 ± 6.7	0.690
HDL (mg/dL)	55.8 ± 3.2	51.3 ± 1.9	0.249
LDL (mg/dL)	138.0 ± 7.1	132.4 ± 6.5	0.658
NYHA class			**0.001**
I	29 (100%)	19 (44.2%)	
II	—	17 (39.5%)	
III	—	7 (16.3)	
IV	—	—	
Drug therapies			
Antiplatelets (%)	1 (3%)	2 (5%)	1.00
Angiotensin receptor blockers (%)	4 (14%)	3 (7%)	0.429
Converting enzyme inhibitors (%)	5 (17%)	14 (32%)	0.295
Calcium channel blockers (%)	3 (10%)	3 (7%)	0.679
Beta-blockers (%)	1 (3%)	16 (37%)	**0.007**
Nitrates (%)	0 (0%)	1 (2%)	1.00
Statins (%)	6 (21%)	6 (14%)	0.527

BMI: body mass index; HDL: high-density lipoprotein; LDL: low-density lipoprotein; NYHA: New York Heart Association. [minimum, maximum]; (percentage); mean ± standard error.

and to syndecan family receptors (SDC). This molecule has been associated with cardiometabolic disorders [9], as well as increased cardiovascular and overall mortality [10, 11]. In addition, it has been shown that transforming growth factor beta (TGF-β), a well-known player in myxomatous MVP pathogenesis [12], increases oxidative stress status [13] as well as OPG production and secretion directly stimulating OPG promoter activity [14].

In this study, we aim to generate a predictive model able to identify MVP patients with the highest accuracy with the combination of biochemical parameters easily quantifiable.

2. Patients and Methods

2.1. Patient Demographics. This observational study was approved by the Institutional Review Board and by the Ethical Committee of Centro Cardiologico Monzino (CCM), IRCCS. The investigation conformed to the principles outlined in the Declaration of Helsinki (1964).

A total of 51 consecutive patients that underwent mitral valve repair, at CCM, due to MVP were enrolled. Based on exclusion criteria (presence of bicuspid aortic valve, premature menopause, and/or osteoporosis, prior aortic or mitral valve surgery, rheumatic heart disease, endocarditis, active malignancy, chronic liver failure, calcium regulation disorders, and chronic or acute inflammatory states), we selected and analysed 43 patients matched by age, sex, diabetes, hypertension, hypercholesterolemia, and smoking habits with 29 control subjects from those attending the clinic for global control of cardiovascular risk at CCM. The demographic and clinical features of the two study groups are listed in Table 1. The subjects were assessed with detailed medical history, physical examination, and echocardiography. In all patients, blood collection was performed before coronary angiography and surgery, with the exception of controls, which underwent samples collection at a scheduled visit.

2.2. Blood Sampling and Biochemical Measurements

Whole Blood. Peripheral blood sample was drawn from patients and controls while fasting into tubes containing EDTA (9.3 mM; Vacutainer Systems, Becton Dickinson, Franklin Lakes, NJ, USA) kept on ice and immediately precipitated with 10% trichloroacetic acid (Sigma-Aldrich, St. Louis, MO, USA) in 1 mM EDTA solution. After centrifugation at 10,000g for 10 min at 4°C, the supernatant was stored at −80°C until analysis.

Plasma. EDTA anticoagulated blood was centrifuged at 3,000g for 10 min at 4°C within 30 min after being drawn.

Plasma was separated and aliquots were stored at −80°C until analysis.

2.3. Oxidative Stress Measurement. For oxidative stress evaluation whole blood concentrations of the oxidized (GSSG) and reduced (GSH) form of glutathione, whose ratio (GSSG/GSH) is a well-recognized index, were assessed by a previously developed and validated LC-MS/MS method [15].

2.4. Osteoprotegerin Evaluation. Plasma levels of soluble OPG were measured with an enzyme-linked immunosorbent assay (ELISA) kit (DuoSet, R&D) following manufacturer instructions. The standard of this particular kit is similar to full-length OPG, making this ELISA kit more representative of circulating OPG molecule [9].

2.5. Statistical Analysis. Continuous variables are summarized as mean ± standard error, except for age, which is represented as mean [minimum, maximum], while categorical variables are summarized as frequency and percentage.

For data analysis, Mann–Whitney test has been performed between MVP and control classes on continuous variables, while Fisher's exact test has been performed on discrete ones.

Finally, taking into account OPG measurement and GSSG/GSH ratio, we have implemented several logistic regression procedures in order to identify a classification rule, able to predict outcomes with the highest accuracy.

The logistic model is

$$p\left(Y_i = \text{“MVP”}\right) = \frac{1}{1 + e^{-(\beta_0 + \beta_1 x_1 + \beta_2 x_2)}}, \quad (1)$$

where p is probability to have MVP, x_1 is OPG measurement (in pg/mL), and x_2 is GSSG/GSH ratio.

A receiver operating characteristic (ROC) curve has been plotted for each model and performances have been evaluated by comparing areas under the ROC Curve (AUC).

3. Results

3.1. Patient Characteristics. In this study we analysed 43 patients and 29 controls matched by age, sex, diabetes, hypertension, hypercholesterolemia, and smoking habits. The two groups were comparable for all the clinical and demographic features considered, except for BMI, which was significantly lower in MVP patients than in controls ($p = 0.005$), and as expected, New York Heart Association (NYHA) class that was significantly higher in MVP patients ($p < 0.001$, Table 1). Drug therapies were not significantly different between MVP and controls, apart from beta-blockers, mostly taken by patients. However, up to now, no data are available about any influence of this drug class on oxidative stress levels. In Table 2 the qualitative and quantitative echocardiographic characteristics of mitral valves are reported. As expected the peak E velocity and the ratio between peak E and peak A velocity (E/A ratio) were significantly different between the two groups ($p < 0.001$).

Table 2: Echocardiography evaluation.

Echocardiography parameters	Control ($N = 29$)	MVP ($N = 43$)	p value
LVEF (%)	65.9 ± 1.6	63 ± 1.6	0.416
Peak E velocity (cm/s)	72.8 ± 3.8	103 ± 4.2	**<0.001**
Deceleration E (ms)	229 ± 13.4	199 ± 7.7	0.094
Peak A velocity (cm/s)	79.1 ± 4.8	68.9 ± 2.8	0.111
E/A ratio	0.96 ± 0.07	1.6 ± 0.1	**<0.001**
EROA (cm^2)	—	0.6 ± 0.04	

LVEF: left ventricular ejection fraction; EROA: effective regurgitant orifice area. Mean ± standard error.

3.2. Osteoprotegerin Levels and Oxidative Stress Status. The assessment of OPG levels revealed that this protein was significantly higher in MVP patients when compared to controls (1748 ± 100.2 versus 1109 ± 45.3 pg/mL, respectively; $p < 0.0001$, Figure 1(a)). Since it has already been shown that OPG concentration increases with age [9], we implemented an adjusted model for this variable and the difference between the groups maintains its significance ($p < 0.0001$). In addition, we adjusted for NYHA class as well as BMI and the difference in OPG levels remained significant between the two groups ($p < 0.01$). Finally, we confirmed that the oxidative stress status, represented by GSSG/GSH ratio, was higher in MVP patients compared to control subjects (0.116 ± 0.007 versus 0.053 ± 0.013, respectively; $p < 0.0001$, Figure 1(b)) and remained significant even after NYHA class and BMI adjustment ($p < 0.01$). Notice that no correlation has been found between NYHA class and OPG levels or GSSG/GSH ratio.

3.3. Binary Logistic Regression Model. To assess if OPG or GSSG/GSH ratio could be used as potential circulating markers of MVP, we implemented a step-wise binary logistic regression model. To further improve the specificity and sensibility, we took OPG and GSSG/GSH ratio alone and then together. We also evaluated their possible interaction; however, it was not statistically significant ($p = 0.243$) and therefore we did not include it in the regression model. The regression parameters obtained from estimation procedure were $\beta_0 = -7.590$, $\beta_1 = 0.005$, and $\beta_2 = 24.493$. The logistic model implemented is described in Section 2.5. This model was able to correctly classify 62 samples out of 72 (Figure 2). In addition, the logistic regression model pointed out an odds ratio of 38.5 (95% CI: 9.9–150.6; $p < 0.0001$) to have MVP for subjects with $p(Y_i = \text{“MVP”}) > 0.5$.

3.4. Combination of Osteoprotegerin and Oxidative Stress as Potential Circulating Marker of MVP. Receiver operator characteristic curve (ROC) was performed to determine if OPG or GSSG/GSH ratio alone or together could be used to identify MVP patients. As shown in Figure 3, OPG and GSSG/GSH ratio had an area under ROC curve (AUC) of 0.83 and 0.79, respectively ($p < 0.0001$). However, if we considered OPG combined with GSSG/GSH we observed

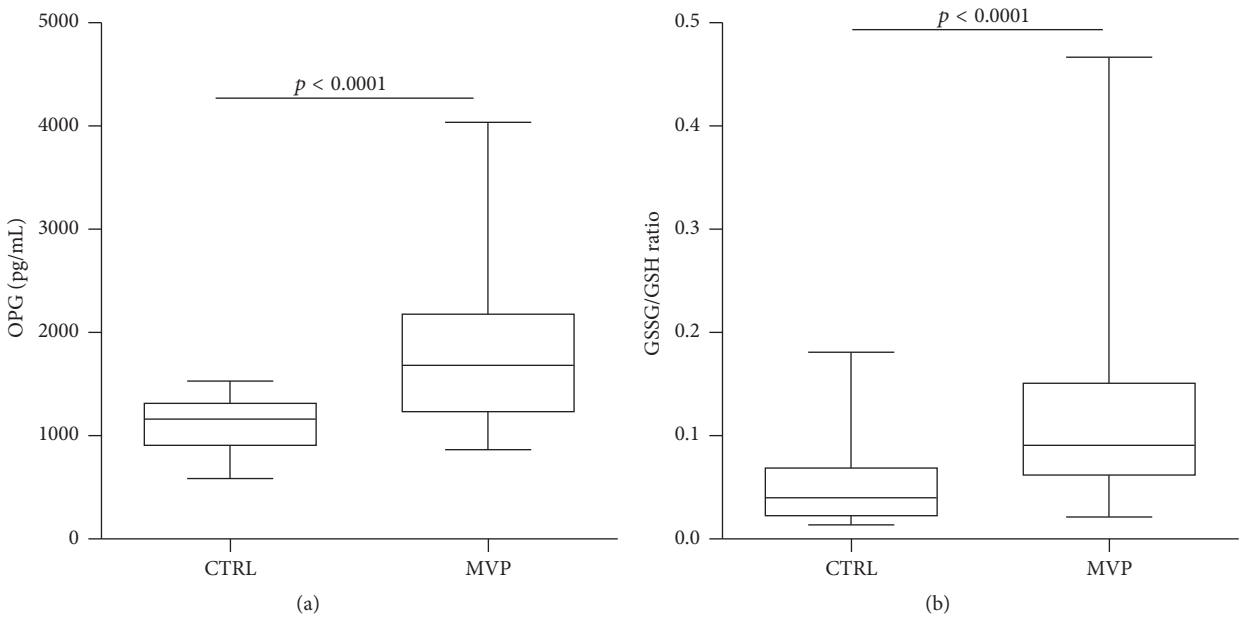

Figure 1: Osteoprotegerin and oxidative stress levels. (a) Osteoprotegerin (OPG) enzyme-linked immunosorbent assay (ELISA) on plasma samples from control subjects (CTRL) and mitral valve prolapse (MVP) patients. (b) Ratio between oxidized (GSSG) and reduced (GSH) form of glutathione as oxidative stress status index.

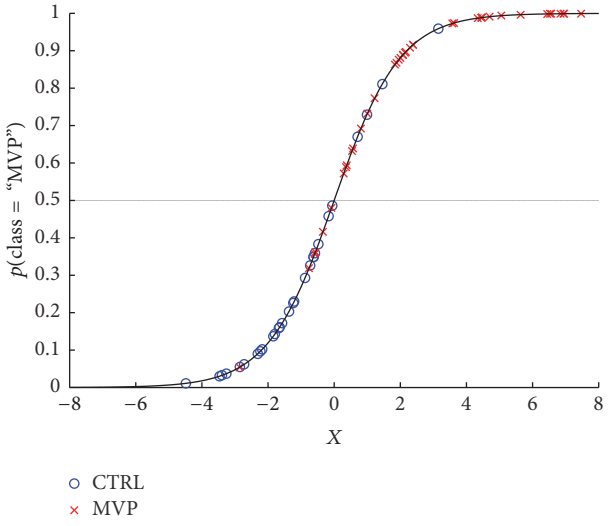

Figure 2: Binary logistic regression model. Graph representing the prediction of the best binary logistic regression model.

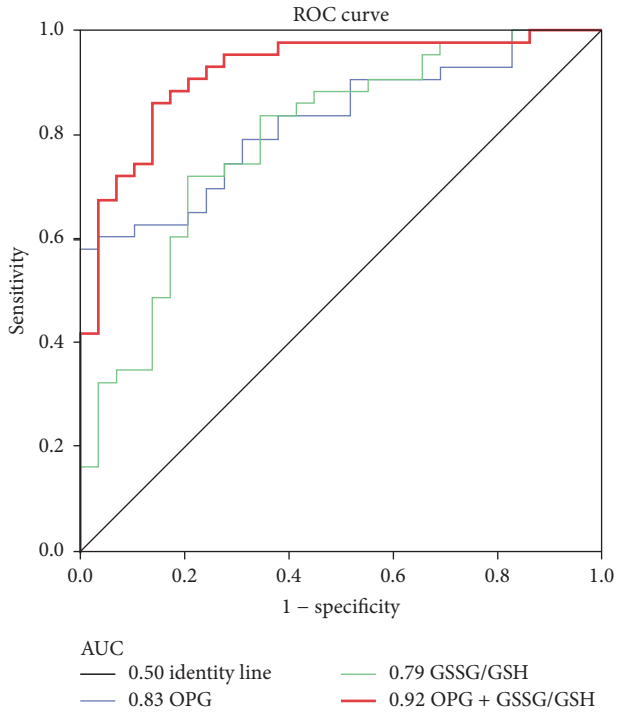

Figure 3: Osteoprotegerin combined with oxidative stress, as potential circulating marker of MVP. Receiver operating characteristic (ROC) curves and area under the curve (AUC) of Osteoprotegerin (OPG), ratio between oxidized (GSSG) and reduced (GSH) form of glutathione (GSSG/GSH) and their combination (OPG + GSSG/GSH). (Control subjects $n = 29$, Mitral Valve Prolapse patients $n = 43$; $p < 0.0001$).

accuracy in terms of AUC of 0.92 with 95% CI: 0.86–0.98 and $p < 0.0001$ (red thick line; Figure 3).

4. Discussion

Myxomatous mitral valve prolapse (MVP) with severe regurgitation (MR) is the most common cause for mitral valve surgery. The MVP diagnosis is some of the most challenging

aspects in clinical cardiology and, up to now, echocardiography is the only clinical reliable tool. No biomarkers are available for this pathology and, to the best of our knowledge, only a comparative proteomic study on plasma samples from 24 pooled MVP patients with moderate to severe MR revealed reduced levels of haptoglobin, platelet basic protein, and complement component C4b in the MVP/MR patients as compared to the 24 pooled matched control cases [16]. However, the clinical applicability is unclear, in part because most of the identified biomarkers had low AUC. In addition, Thalji et al. [12] and Sainger et al. [17] identified novel players that could be involved in myxomatous mitral valve degeneration and their data offer novel insights into the pathogenesis of MVP but no circulating biomarkers have been evaluated.

Results of the present work show that circulating OPG and oxidative stress status are positively associated with severe MR due to MVP. Based on these premises, we developed a multivariable logistic regression model with OPG and GSSG/GSH levels. This model is able to correctly identify 86% of MVP patients and 86% of control subjects.

Since all patients, in the MVP group, were the ones who underwent surgery due to symptoms, we evaluated and excluded that left ventricular ejection fraction (LVEF) and heart failure (NYHA classes) were the causes that increased OPG plasma levels and oxidative stress status. Therefore, our data supports that severe MR caused by myxomatous MVP could be identify through a multivariable binary logistic regression model.

The analyses of OPG as well as oxidative stress alone are not disease specific; indeed OPG has already been linked to coronary artery syndromes [18], aortic valve stenosis [19], myocardial infarction [20], and cardiovascular postoperative outcome [21]. However, the combination of these biochemical parameters allowed us to identify these patients with high accuracy.

Recently, we showed that OPG was involved in mitral valve endothelial to mesenchymal transition and plasma OPG levels permitted to identify MVP patients with an AUC of 0.92 [8]. However, all the selected MVP patients had only posterior MVP. It is known that two-thirds of MVP patients present the posterior prolapse, while the remaining third show anterior or bileaflet prolapse [22, 23]. Considering this, to obtain a model able to discriminate MVP from healthy subjects, in primary screening, we must use a population with not only posterior but also anterior and bileaflet prolapse. Thus, in the present study we enrolled 43 MVP patients: 28 with posterior MVP (65%) and 15 with anterior or bileaflet MVP (35%). In this population, OPG had an AUC of 0.83 that was brought back to 0.92 when OPG was combined with GSSG/GSH ratio; meaning that OPG alone is not sufficient to discriminate with high accuracy the MVP mixed population (posterior, anterior, and bileaflet) from healthy subjects.

The present study has some limitations: first, the exiguous number of patients enrolled and the lack of strong disease-specificity of OPG and oxidative stress with MVP. In addition, in our cohorts we had only two cases with mitral annulus calcification (MAC). Since OPG is involved in many cellular processes, in particular calcification, further studies need to address also the possible implication of this molecule not only in patients with MAC but also in those who have mitral valve stenosis. Lastly, patients with severe regurgitation compose the MVP cohort and further studies are needed to evaluate if this model is able to discriminate mild or moderate mitral valve regurgitation in the presence or absence of prolapse.

5. Conclusion

In conclusion, considering the prevalence of this disease (over 6% ≥65 years old [1]), the aging population, and the price of the echocardiographic evaluation, the health system costs may rise if no pharmacological treatment or cheaper diagnosis tools will be identified. In particular, circulating molecular signatures could be used in primary screening to identify possible MVP patients and then a confirmatory echocardiography could be performed only in these subjects. Thus, the study of new circulating markers and the combination of already known ones involved in MVP progression could lead to novel insights and possibly new therapeutic targets. To the best of our knowledge, this is the first study to show a strong association between OPG and oxidative stress status. In addition, these molecules could be measured in the clinical setting by the implementation and validation of diagnostic enzyme-linked immunosorbent assay (ELISA) for OPG and colorimetric assay for GSH and GSSG. Finally, since it is quite hard to believe that one single protein could discriminate two populations with high specificity and sensitivity, we believe that this approach could improve the identification of several signatures not only in mitral valve disease. However, the mechanisms explaining these correlations are still unclear; further molecular studies along with clinical validations will be necessary to confirm our findings.

Abbreviations

AUC: Area under the curve
BMI: Body-mass index
GSH: Reduced glutathione
GSSG: Oxidized glutathione
HDL: High-density lipoproteins
MAC: Mitral annulus calcification
MVP: Mitral valve prolapse
OPG: Osteoprotegerin.

Competing Interests

The authors declare that they have no competing interests.

Authors' Contributions

Paola Songia and Benedetta Porro equally contributed to this work.

Acknowledgments

The authors thank the entire Cardiac Surgery Unit at Centro Cardiologico Monzino for clinical data and blood collection.

This work was supported by the Fondazione Gigi e Pupa Ferrari ONLUS and the Italian Ministry of Health [RC2015-BIO30-2613051 to Centro Cardiologico Monzino].

References

[1] L. A. Freed, D. Levy, R. A. Levine et al., "Prevalence and clinical outcome of mitral-valve prolapse," *New England Journal of Medicine*, vol. 341, no. 1, pp. 1–7, 1999.

[2] S. Vahanian A, O. Alfieri, F. Andreotti et al., "Guidelines on the management of valvular heart disease (version 2012)," *European Heart Journal*, vol. 33, no. 19, pp. 2451–2496, 2012.

[3] F. N. Delling and R. S. Vasan, "Epidemiology and pathophysiology of mitral valve prolapse: new insights into disease progression, genetics, and molecular basis," *Circulation*, vol. 129, no. 21, pp. 2158–2170, 2014.

[4] R. G. Singh, R. Cappucci, R. Kramer-Fox et al., "Severe mitral regurgitation due to mitral valve prolapse: risk factors for development, progression, and need for mitral valve surgery," *American Journal of Cardiology*, vol. 85, no. 2, pp. 193–198, 2000.

[5] C. Deroyer, J. Magne, M. Moonen et al., "New biomarkers for primary mitral regurgitation," *Clinical Proteomics*, vol. 12, article 25, 2015.

[6] V. Cavalca, E. Tremoli, B. Porro et al., "Oxidative stress and nitric oxide pathway in adult patients who are candidates for cardiac surgery: patterns and differences," *Interactive Cardiovascular and Thoracic Surgery*, vol. 17, no. 6, pp. 923–930, 2013.

[7] J.-Y. Kim, Y.-J. Park, K.-J. Kim, J.-J. Choi, W.-U. Kim, and C.-S. Cho, "Osteoprotegerin causes apoptosis of endothelial progenitor cells by induction of oxidative stress," *Arthritis and Rheumatism*, vol. 65, no. 8, pp. 2172–2182, 2013.

[8] P. Songia, E. Branchetti, A. Parolari et al., "Mitral valve endothelial cells secrete osteoprotegerin during endothelial mesenchymal transition," *Journal of Molecular and Cellular Cardiology*, vol. 98, pp. 48–57, 2016.

[9] C. Pérez De Ciriza, A. Lawrie, and N. Varo, "Osteoprotegerin in cardiometabolic disorders," *International Journal of Endocrinology*, vol. 2015, Article ID 564934, 15 pages, 2015.

[10] A. Avignon, A. Sultan, C. Piot et al., "Osteoprotegerin: a novel independent marker for silent myocardial ischemia in asymptomatic diabetic patients," *Diabetes Care*, vol. 30, no. 11, pp. 2934–2939, 2007.

[11] D. Gordin, A. Soro-Paavonen, M. C. Thomas et al., "Osteoprotegerin is an independent predictor of vascular events in finnish adults with type 1 diabetes," *Diabetes Care*, vol. 36, no. 7, pp. 1827–1833, 2013.

[12] N. M. Thalji, M. A. Hagler, H. Zhang et al., "Nonbiased molecular screening identifies novel molecular regulators of fibrogenic and proliferative signaling in myxomatous mitral valve disease," *Circulation: Cardiovascular Genetics*, vol. 8, no. 3, pp. 516–528, 2015.

[13] M. A. Hagler, T. M. Hadley, H. Zhang et al., "TGF-β signalling and reactive oxygen species drive fibrosis and matrix remodelling in myxomatous mitral valves," *Cardiovascular Research*, vol. 99, no. 1, pp. 175–184, 2013.

[14] K. Thirunavukkarasu, R. R. Miles, D. L. Halladay et al., "Stimulation of osteoprotegerin (OPG) gene expression by transforming growth factor-β (TGF-β). Mapping of the OPG promoter region that mediates TGF-β effects," *Journal of Biological Chemistry*, vol. 276, no. 39, pp. 36241–36250, 2001.

[15] I. Squellerio, D. Caruso, B. Porro, F. Veglia, E. Tremoli, and V. Cavalca, "Direct glutathione quantification in human blood by LC-MS/MS: comparison with HPLC with electrochemical detection," *Journal of Pharmaceutical and Biomedical Analysis*, vol. 71, pp. 111–118, 2012.

[16] H. T. Tan, L. H. Ling, M. C. Dolor-Torres, J. W.-L. Yip, A. M. Richards, and M. C. M. Chung, "Proteomics discovery of biomarkers for mitral regurgitation caused by mitral valve prolapse," *Journal of Proteomics*, vol. 94, pp. 337–345, 2013.

[17] R. Sainger, J. B. Grau, E. Branchetti et al., "Human myxomatous mitral valve prolapse: role of bone morphogenetic protein 4 in valvular interstitial cell activation," *Journal of Cellular Physiology*, vol. 227, no. 6, pp. 2595–2604, 2012.

[18] D. Tousoulis, G. Siasos, K. Maniatis et al., "Serum osteoprotegerin and osteopontin levels are associated with arterial stiffness and the presence and severity of coronary artery disease," *International Journal of Cardiology*, vol. 167, no. 5, pp. 1924–1928, 2013.

[19] A. Borowiec, R. Dąbrowski, I. Kowalik et al., "Osteoprotegerin in patients with degenerative aortic stenosis and preserved left-ventricular ejection fraction," *Journal of Cardiovascular Medicine*, vol. 16, no. 6, pp. 444–450, 2015.

[20] A. Margonato, R. Gorla, A. Macchi et al., "Role of plaque calcification regulators osteoprotegerin and matrix Gla-proteins in stable angina and acute myocardial infarction," *Journal of Cardiovascular Medicine*, vol. 16, no. 3, pp. 156–162, 2015.

[21] S. M. Venuraju, A. Yerramasu, R. Corder, and A. Lahiri, "Osteoprotegerin as a predictor of coronary artery disease and cardiovascular mortality and morbidity," *Journal of the American College of Cardiology*, vol. 55, no. 19, pp. 2049–2061, 2010.

[22] D. R. Johnston, A. M. Gillinov, E. H. Blackstone et al., "Surgical repair of posterior mitral valve prolapse: implications for guidelines and percutaneous repair," *The Annals of Thoracic Surgery*, vol. 89, no. 5, pp. 1385–1394, 2010.

[23] A. E. Weyman and M. Scherrer-Crosbie, "Marfan syndrome and mitral valve prolapse," *The Journal of Clinical Investigation*, vol. 114, no. 11, pp. 1543–1546, 2004.

Hindawi Publishing Corporation
Oxidative Medicine and Cellular Longevity
Volume 2016, Article ID 9045736, 10 pages
http://dx.doi.org/10.1155/2016/9045736

Research Article

Demethoxycurcumin Preserves Renovascular Function by Downregulating COX-2 Expression in Hypertension

Yingjuan Li,[1] Danyang Tian,[2] Chunhua Zhu,[3] and Liqun Ren[1]

[1]*Department of Geriatrics, Zhongda Hospital, Medical School, Southeast University, 87# Ding Jiaqiao, Nanjing 210009, China*
[2]*Department of Physiology, Hebei Medical University, Shi Jiazhuang 050017, China*
[3]*Department of Neurology, Second Hospital of Hebei Medical University, Shi Jiazhuang 050017, China*

Correspondence should be addressed to Chunhua Zhu; zhuchunhua@hebmu.edu.cn and Liqun Ren; rlq6345@126.com

Received 30 September 2016; Accepted 9 November 2016

Academic Editor: Noemí García

Hypertension-associated endothelial dysfunction is largely due to the exaggerated vasoconstrictor generation by cyclooxygenase-2 (COX-2). COX-2 is induced under inflammatory condition. Demethoxycurcumin (DMC) is a major component of *Curcuma longa* L, which possesses anti-inflammatory action. This study aimed to examine whether DMC protects endothelial function in hypertension by modulating COX-2. Changes in isometric tension showed that in vivo and ex vivo treatment with DMC rescued the attenuated endothelium-dependent relaxations (EDRs) and elevated endothelium-dependent contractions (EDCs) in the renal arteries of SHR, which were also corrected by acute usage of the COX-2 inhibitor celecoxib. The restoration of renovascular activity by DMC was accompanied by the normalization of COX-2 expression. The enhanced COX-2 expression observed in the renal arteries of hypertensive patients was suppressed by incubation of excised arteries with DMC for 12 hrs. In the renal arteries of Wistar-Kyoto rats (WKY), DMC prevented the endothelial dysfunction caused by angiotensin II. The reduction in the generation of nitric oxide (NO) and expression of eNOS phosphorylation (Ser1177) in human umbilical vein endothelial cells caused by angiotensin II (Ang II) were restored by DMC or celecoxib. Our findings suggest that DMC may decrease COX-2 expression and improve endothelial function in hypertension.

1. Introduction

Healthy endothelium is essential to maintain normal vascular tone by releasing vasodilators and vasoconstrictors [1, 2]. Endothelial dysfunction, owing to the imbalance between dilating and constricting factors, is often encountered in the common setting of cardiovascular risk factors such as hypertension [3].

Disturbed COX-2 metabolism contributes largely to the development of hypertension-associated endothelial dysfunction through overgeneration of vasoconstrictors [4]. Under physiological conditions, a minimal amount of COX-2 is expressed in the vascular wall. A striking upregulation of COX-2 is observed in the inflamed vascular tissue, which was also documented extensively in hypertension [5]. Experimental and clinical findings have implicated the striking generation of COX-dependent endothelium-derived contracting factors in the initiation and development of endothelial dysfunction in hypertension. Vasoconstrictors and reactive oxygen species (ROS) produced by COX-2 result in disturbed endothelial dysfunction [6].

Animal studies have provided solid evidence that COX-2 inhibitors can prevent cardiovascular disease [3]. The growing recognition of the critical role of COX-2 in the pathogenesis of endothelial function, and the reported serious side effects of COX-2 inhibitors make the development of a new anti-inflammatory drug urgent.

Plants are the main sources of naturally occurring anti-inflammatory agents. The rich source and potential safety make plant-derived inflammatory agents advantageous over synthetic compounds. Many extracts from plants possess anti-inflammatory activity either directly or indirectly. Demethoxycurcumin (DMC) is a natural derivative of curcumin, a major component of *Curcuma longa L* [7]. The anti-inflammatory and anticancer effects of curcumin have been widely demonstrated, but its medical utility has been limited

because of rapid plasma clearance. The growing evidence of the stronger effectiveness and higher stability of DMC compared with curcumin indicates DMC as an attractive and promising replacement for curcumin in the treatment of cancer and inflammation-associated diseases [8]. Several studies have also suggested the anti-inflammatory action of DMC [9]. In addition, a recent study showed the beneficial action of DMC in pulmonary hypertension by inhibiting the PDE5 [10]. However, it remains uncertain whether DMC can provide benefits against endothelial dysfunction in hypertension, depending on its anti-inflammatory action. The aim of the present study was to test whether DMC protects renovascular function, and if so, whether COX-2 serves as a downstream effector.

2. Methods

2.1. Animals and Treatment Protocols. The animal experimental protocols in the present study were approved by the animal care and use committees of the Southeast University and were conducted according to the US National Institutes of Health Guide for the Care and Use of Laboratory Animals. Thirty-week-old male Wistar-Kyoto rats (WKY) and spontaneous hypertensive rats (SHR) were supplied by the Laboratory Animal Services Centre, Southeast University. All the animals were housed in a temperature-controlled room (22–24°C) with a 12-h light/dark cycle and supplied with standard diet and water. The rats were assigned to one of the following three groups: (1) WKY control, (2) SHR treated with vehicle dimethylsulfoxide (DMSO; SHR + vehicle), and (3) SHR treated with DMC at 10 mg/kg per day (SHR + DMC) by intraperitoneal injection for 3 weeks.

2.2. Blood Pressure Measurement. Blood pressure was measured using the tail-cuff electrosphygmomanometer system (AD Instruments, Sydney, Australia). Blood pressure measurement was performed after the rats remained stable and quiescent. The average of 3 readings was considered the systolic blood pressure of each animal.

2.3. Preparation of Human Arteries. The use of human renal arteries in the present study was approved by the Clinical Research Ethics Committee of the Southeast University. The arteries were obtained from normotensive and hypertensive patients undergoing radical nephrectomy with their consent. The patients received radical nephrectomy for renal carcinoma. Hypertension was defined as systolic pressure above 140 mmHg and diastolic pressure above 90 mmHg. The mean age of the six hypertensive patients was 52 years (ranging between 51 and 69 years) and that of the six normotensive patients was 55 years (ranging between 48 and 70 years). Renal arteries from hypertensive patients were cultured for 12 hrs in the presence or absence of DMC (10 μmol/L) in Dulbecco's Modified Eagle Medium (DMEM, GIBCO, Gaithersburg, MD, USA) with the addition of 10% fetal bovine serum (FBS, GIBCO) and 1% penicillin/streptomycin (GIBCO) at 37°C.

2.4. Preparation of Animal Renal Arteries. Normotensive WKY rats and SHR were sacrificed by carbon dioxide inhalation. After careful dissection, intralobal renal arteries were placed in Krebs solution of the following composition: (mmol/L) 119 NaCl, 4.7 KCl, 2.5 $CaCl_2$, 1 $MgCl_2$, 25 $NaHCO_3$, 1.2 KH_2PO_4, and 11 D-glucose. After removal of the surrounding connective tissue, the arteries were cut into 4–6 ring segments of ~1.6 mm length for functional assessment of endothelial function in a Multi Myograph System (610M, Danish Myo Technology A/S, Aarhus N, Denmark). Briefly, the artery was fixed to the jaws of the myograph by two stainless steel wires, which passed through the arterial lumen. The myograph chamber was filled with 5 mL Krebs solution that was continually supplied with 95% O_2 and 5% CO_2 and kept at a pH level of ~7.4 at 37°C. After being subjected to an optimal resting tension of 2.5 mN, the arteries were equilibrated for 60 min for the following experiments.

2.5. Isometric Tension Assessment. After the contraction evoked by 1 μmol/L phenylephrine was stable, concentration-dependent relaxations induced by increasing concentrations of acetylcholine (ACh 0.003–10 μmol/L) were recorded. Endothelium-dependent relaxation (EDR) was described as the percentage reduction in phenylephrine-induced contraction. When endothelium-dependent contraction (EDC) was tested, the arteries were preincubated with N^G-nitro-L-arginine methyl ester (L-NAME, 100 μmol/L) to block the vasodilating effect of nitric oxide (NO). Cumulative concentrations of ACh (0.03–100 μM) were added to trigger contractions. ACh-induced tension changes in the renal arteries were expressed as the tension recorded divided by the tension evoked by 60 mmol/L KCl. COX-2 inhibitor celecoxib (3 μmol/L), when used, was added for 30 min prior to the addition of ACh.

2.6. Western Blot Assay. After treatment, renal arteries or human umbilical vein endothelial cells (HUVECs) were homogenized in RIPA lysis buffer (1 μg/mL leupeptin, 5 μg/mL aprotinin, 100 μg/mL PMSF, 1 mmol/L sodium orthovanadate, 1 mmol/L EGTA, 1 mmol/L EDTA, 1 mmol/L NaF, and 2 mg/mL β-glycerophosphate). The homogenates were then centrifuged at 20000g for 20 min at 4°C after incubation on ice. The supernatants were harvested and stored at −80°C. Before western blot assay, the protein concentration was determined using the Lowry method (Bio-Rad Laboratories, Hercules, CA, USA). Equal amounts of protein samples were electrophoresed on a 10% SDS-polyacrylamide gel and then transferred onto an immobilon-P polyvinylidene difluoride (PVDF) membrane (Millipore, Billerica, MA, USA). Nonspecific binding sites were blocked by 5% nonfat milk or 1% bovine serum albumin (BSA) in 0.05% Tween-20 phosphate-buffered saline (PBST) for 1 h and then probed overnight at 4°C with primary antibodies against COX-2, P-eNOS (Ser1177) or eNOS (Abcam, Cambridge, MA, USA) at a dilution of 1 : 500. The membranes were washed three times in PBST before incubation with the appropriate secondary antibodies at a 1 : 3000 dilution for 1 h at room temperature. Finally, the membranes were washed and developed with

an enhanced chemiluminescence detection system (ECL reagents, Millipore, Billerica, MA, USA) and exposed to X-ray films. Equal protein loading was confirmed using a housekeeping anti-GAPDH antibody (Ambion, Austin, TX, USA).

2.7. Immunofluorescence Microscopy. Changes in the expression of COX-2 in the renal arteries from hypertensive patients after DMC administration for 12 hrs were visualized using immunofluorescence microscopy. The arteries were embedded in OCT compound (Sakura Finetek, the Netherlands), snap frozen, and cut into 10-μm-thick cryostat sections, which were then fixed in 4% paraformaldehyde for 30 min, and treated with 0.05% Triton X in PBS for 1 min. The sections were blocked with 5% normal donkey serum for 1 h at room temperature and incubated with primary antibodies against COX-2 (Abcam, Cambridge, MA, USA) overnight at 4°C. After several washes in PBS, the sections were incubated with the appropriate Alexa Fluor 546 IgG (Invitrogen, Molecular Probes, California, USA) for 1 h at room temperature. After coverslipping, the sections were observed under an Olympus Fluoview FV1000 confocal microscope. Images were first acquired with the Olympus Fluoview software (version 1.5; FV10-ASW1.5) and then merged using the SPOT advanced software (Version 4.6, Diagnostic Instruments, Sterling Heights, MI, USA).

2.8. Confocal Microscopy for Real-Time NO Production in Endothelial Cells. HUVECs were cultured in the endothelial cell growth medium (Lonza, Basel, Switzerland), which was supplemented with 20% fetal bovine serum and 1% penicillin/streptomycin (GIBCO). Endothelial cells were plated on coverslips. Upon treatment with angiotensin II (Ang II; 1 μmol/L) with or without DMC for 12 hrs, cells were treated with 1 mmol/L DAF-FM diacetate (Molecular Probes, Invitrogen, Carlsbad, CA), a fluorescent probe used to detect intracellular changes in NO, for 10 min at room temperature. Then, the cells were excited at 495 nm with an emission wavelength of 515 nm, with the use of the Olympus confocal system (Tokyo, Japan). The A23187 (1 μmol/L) induced real time changes in NO generation were recorded at 1-min intervals for 20 min. A23187 serves as a calcium ionophore to stimulate the phosphorylation of eNOS. Results were expressed as a ratio of the fluorescence relative to the initial intensity (time 0 before the use of A23187).

2.9. Chemicals. ACh, phenylephrine, celecoxib, and DMSO were purchased from Sigma-Aldrich. Ang II, losartan, and A23187 were purchased from Tocris Bioscience (Avonmouth, UK), and DMC was purchased from Chengdu Mansite Pharmaceutical Company, China (>98% purity). ACh, phenylephrine, and Ang II were dissolved in distilled water, and others were prepared in DMSO.

2.10. Statistical Analysis. The data are expressed as mean ± SEM of four to six experiments. Data were analyzed using one-way ANOVA followed by Bonferroni post hoc tests whenever appropriate (GraphPad Software, San Diego, California). P values less than 0.05 were accepted to indicate statistically significant differences.

3. Results

3.1. In Vivo Treatment with DMC Reduces Blood Pressure of SHR and Improves the Deteriorated Renovascular Endothelial Function. The elevated blood pressure in SHR was reduced after 3-week treatment with DMC (10 mg/kg/day) via intraperitoneal injection (187.0 ± 2.5 mmHg before treatment versus 161.8 ± 1.8 mmHg after treatment, $P < 0.05$; Figure 1(a)). Blunted ACh-induced relaxation and pronounced ACh-induced contractions were observed in the renal arteries of the vehicle-treated SHR compared with the normotensive WKY controls (Figures 1(b) and 1(c)). Chronic treatment with DMC enhanced the relaxations and inhibited contractions. In contrast, sodium nitroprusside-induced relaxation was not changed in hypertension (Figure 1(d)).

3.2. In Vivo Treatment with DMC Corrects the Downregulation of P-eNOS (Ser1177) Expression and the Upregulation of COX-2 in the Renal Arteries Isolated from Vehicle-Treated SHR. Western blot assays revealed decreased P-eNOS (Ser1177) expression and elevated COX-2 expression in the renal arteries from vehicle-treated hypertensive animals. The observed changes in these proteins were normalized by chronic treatment with DMC (Figures 2(a) and 2(b)).

3.3. In Vitro Treatment with DMC Enhanced the Attenuated Endothelium-Dependent Relaxation and Inhibited the Augmented Endothelium-Dependent Contraction in the Renal Arteries of SHR, by Reducing the Elevated COX-2 Expression. Renal arteries from SHR exhibited attenuated EDR induced by ACh (Figure 3(a)). Furthermore, ACh induced contractions in the presence of the nitric oxide synthase (NOS) inhibitor L-NAME, whereas such contractions were small in the renal arteries of WKY rats (Figure 3(b)). In vitro exposure to 10 μmol/L DMC for 12 hrs corrected the attenuated relaxation and the elevated contractions, with similar effects afforded by the acute use of the COX-2 inhibitor celecoxib (Figures 3(a) and 3(b)). In addition, acute treatment with L-NAME abolished EDR. The improvement in endothelial function by treatment with DMC for 12 hrs was followed by the reduction in COX-2 expression (Figure 3(c)).

3.4. Ex Vivo Treatment with DMC Decreases the Elevated Expression of COX-2 in Renal Arteries from Hypertensive Patients. Western blot measurement (Figure 4(a)) and immunofluorescence assessment (Figure 4(b)) detected higher expression of COX-2 in the renal arteries from hypertensive patients compared to those of the normotensive patients. The enhanced COX-2 expression was depressed by treatment with DMC for 12 hrs (Figures 4(a) and 4(b)).

3.5. In Vitro DMC Preadministration in WKY Renal Arteries Prevents Ang II-Induced Renovascular Dysfunction, Normalizing the Increased COX-2 Expression. Incubation with

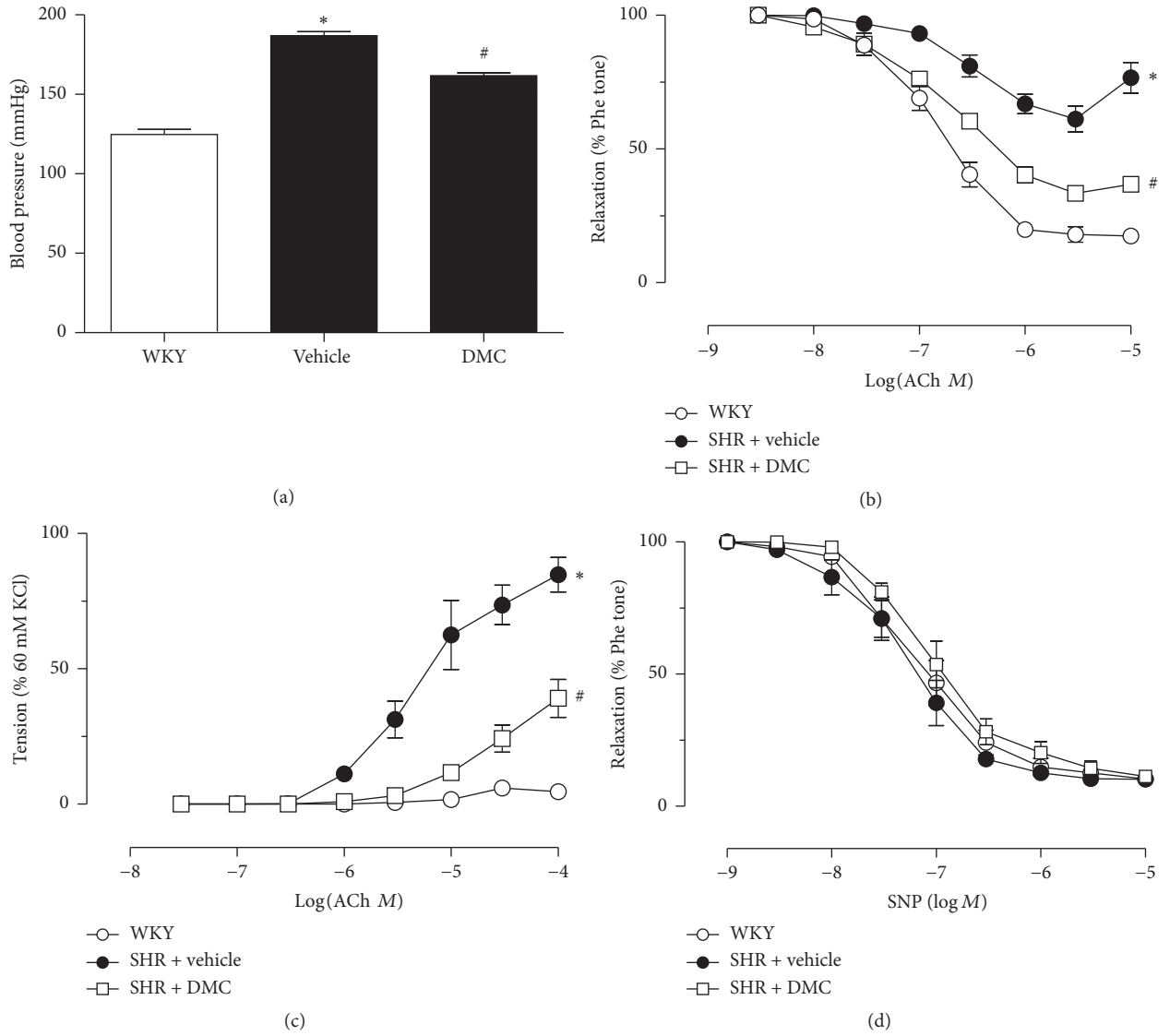

Figure 1: In vivo treatment with DMC reduces blood pressure in SHR and improves the deteriorated renovascular endothelial function. WKY rats exhibited blood pressure of 124.8 ± 1.8 mmHg. Higher blood pressure in SHR was reduced after 3-week treatment with DMC (downregulation of 13.48% after treatment, $P < 0.05$; (a)). Blunted ACh-induced relaxation and pronounced ACh-induced contractions were observed in the renal arteries of vehicle-treated SHR compared to the normotensive WKY controls ((b)-(c)). Chronic oral treatment with DMC (10 mg/kg/day for 3 weeks) enhanced the relaxations and inhibited contractions. Relaxation induced by SNP remained similar among the three groups. Data are means ± SEM of 7-8 experiments. $^{*}P < 0.05$ versus WKY; $^{\#}P < 0.05$ SHR + vehicle.

Ang II (100 nmol/L) for 12 hrs resulted in impaired ACh-induced relaxation and increased EDC (Figures 5(a) and 5(c)). Pretreatment with DMC and celecoxib prevented the impairment in EDR and abolished the contractions (Figures 5(b) and 5(d)). Ang II also promoted the overexpression of COX-2 and the elevated COX-2 expression was abrogated by preincubation with either DMC or Ang II type 1 receptor blocker losartan (3 μmol/L) (Figure 5(e)).

3.6. DMC Augments Nitric Oxide Generation in HUVECs. Treatment with Ang II (1 μmol/L) for 12 hrs led to a decrease in the A23187-stimulated NO production (Figure 6(a)). The presence of DMC, losartan (3 μmol/L) or celecoxib (3 μmol/L) restored the NO generation (Figures 6(b) and 6(c)). Similarly, the addition of DMC, losartan, or celecoxib reversed the downregulation of P-eNOS (Ser1177) expression in cells treated with Ang II for 12 hrs (Figure 6(d)).

4. Discussion

Although the anti-inflammatory and anticancer activities of DMC have been reported, its effect on vascular activity is unknown. Our present study provides evidence showing the beneficial effect of DMC on the renovascular function

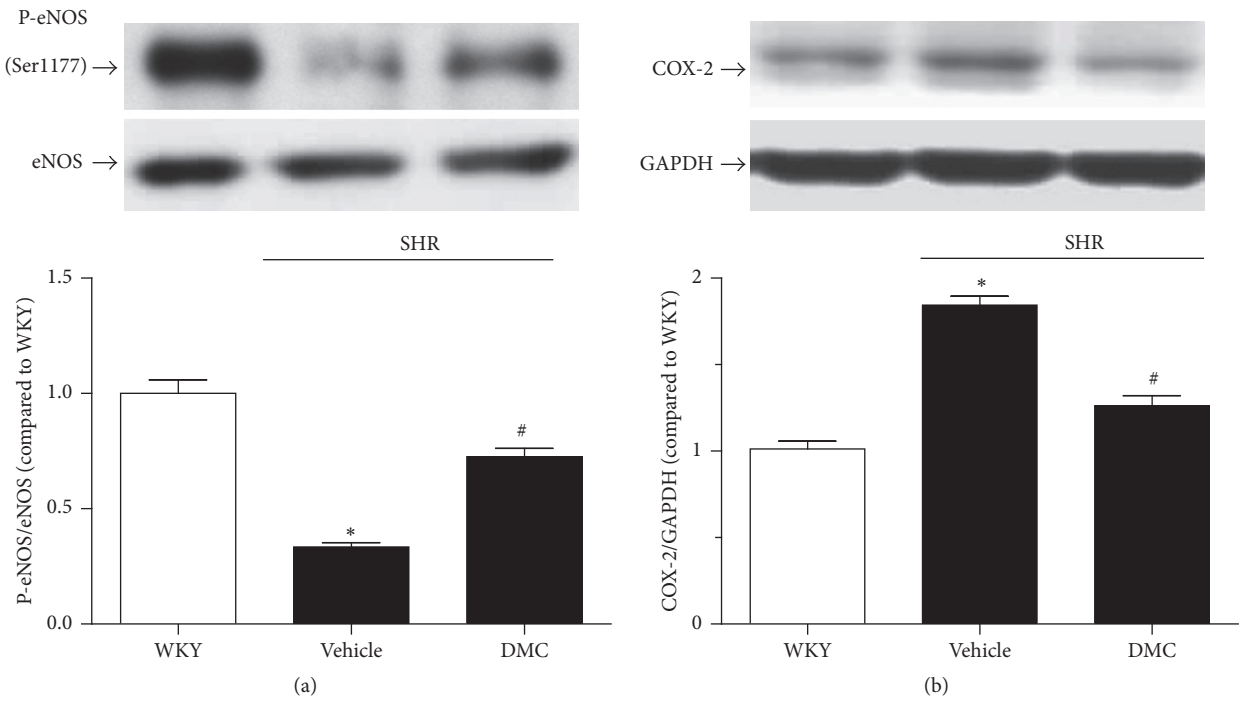

Figure 2: In vivo treatment with DMC corrects the downregulation of P-eNOS expression and the upregulation of COX-2 in the renal arteries isolated from vehicle-treated SHR. Western blot assay reveals decreased P-eNOS (Ser1177) expression and elevated COX-2 expression, which were corrected by DMC treatment for 3 weeks ((a)-(b)). Data are means ± SEM of 5-6 experiments. $^{*}P < 0.05$ versus WKY; $^{\#}P < 0.05$ SHR + vehicle.

in hypertension. Acting as an activating site, the phosphorylation sites 1177 on eNOS were used as a marker in endothelium dysfunction [11, 12]. Our major findings include (1) intraperitoneal injection of DMC in vivo for 3 weeks lowered blood pressure in the SHR. The attenuated EDR and elevated EDC in renal arteries from hypertensive animals were reversed by treatment with DMC for 3 weeks; (2) matched with the changes in vascular activity, reduced P-eNOS (Ser1177) expression in SHR renal arteries was increased by treatment with DMC in vivo for 3 weeks; (3) western blot assay and immunofluorescence measurement exhibited the upregulation of COX-2 in the renal arteries of hypertensive animals and patients, which was inhibited by DMC in vivo administration for 12 hrs; (4) in the renal arteries from normotensive patients, in vitro treatment with DMC prevented the Ang II-induced upregulation of COX-2 and the subsequent delayed renovascular function; (5) in vitro treatment with DMC reversed the reduction of NO production and P-eNOS (Ser1177) expression in HUVECs exposed to Ang II for 12 hrs.

The occurrence of endothelial dysfunction in hypertension has been well documented. COX-2 is positively responsible for the endothelial dysfunction under hypertensive conditions [6, 13]. This is related to the excessive production of vasoconstrictors and ROS derived from overactivation of COX-2 [14]. These agents disturb EDR and facilitate contraction. The pivotal role of COX-2 upregulation in the development of endothelial dysfunction in hypertension is being increasingly recognized. Here, we also demonstrated that it is likely that the proinflammatory enzyme COX-2 is a major contributor to endothelial dysfunction in hypertension, as evidenced by the protective action of COX-2 inhibitor and the upregulated COX-2 expression in SHR. Subsequent observations revealed the beneficial effect of DMC against endothelial dysfunction through downregulation of COX-2 expression.

COX-2 has been described as "inducible" owing to its upregulation under inflammatory conditions. Inhibition of COX-2 activity by celecoxib reverses the attenuation of vascular function [15, 16]. In addition to the functional studies, western blot assay and immunofluorescence measurement confirmed the positive involvement of COX-2 in the disordered renovascular function in hypertension, not only in animal but also in human specimen. In contrast, no change was detected in COX-1 expression (data not shown). The positive contribution of COX-2 to endothelial dysfunction lends credence to the concept that inhibition of COX-2 activity, or decreasing its abnormal over expression, could be a target to alleviate impaired vascular function. The serious side effects of these agents, owing to thorough depletion of COX-derived prostaglandins due to COX-2 activity inhibition [17], which led to the withdrawal of one of the widely used COX-2 inhibitors, Vioxx, from the market, suggest that remedies targeting the enhancement of COX-2 expression will be a more attractive and promising choice [18].

In this study, it was observed that in vitro treatment with DMC for 12 hrs normalized the blunted EDR and the

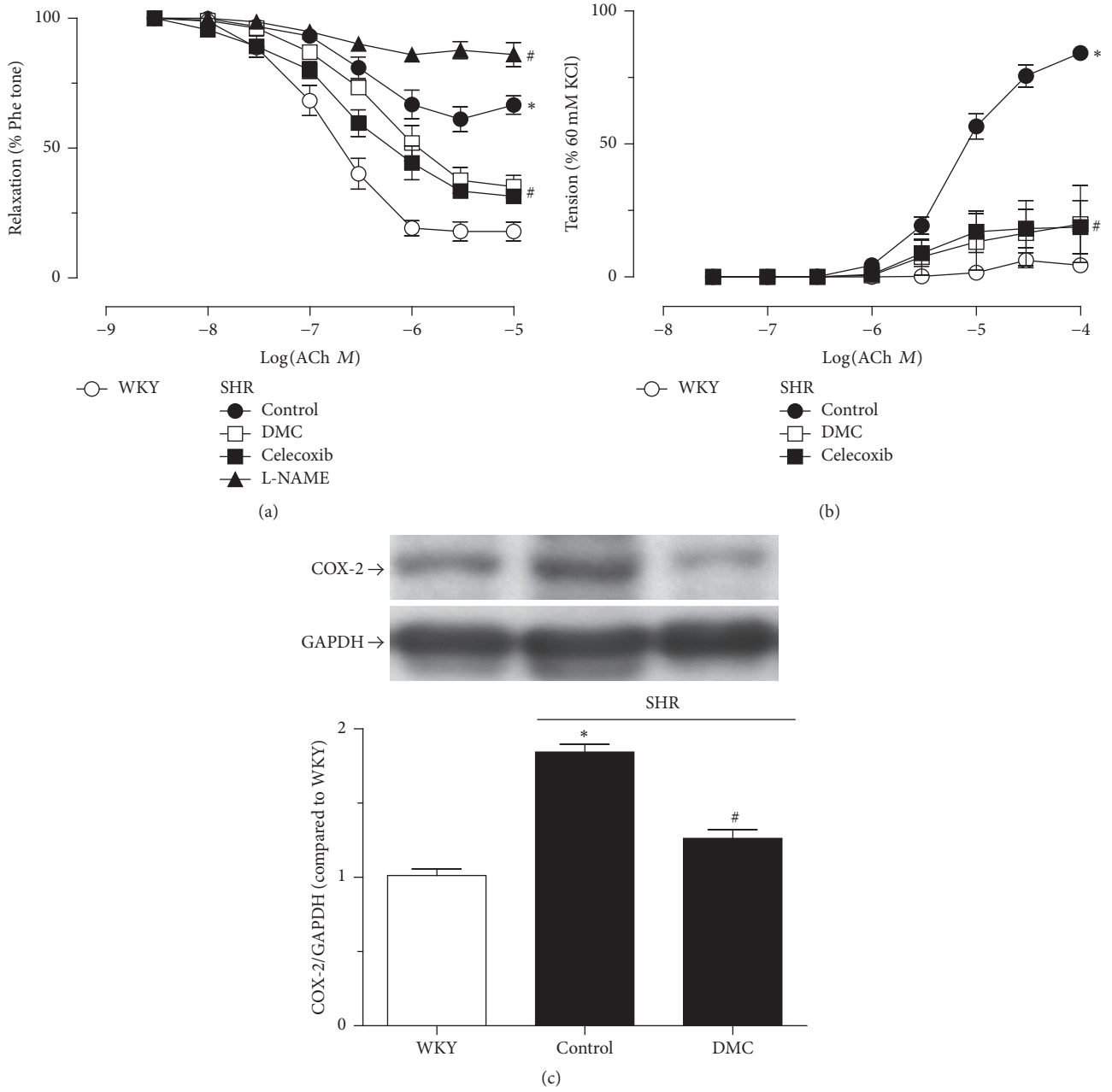

Figure 3: Ex vivo DMC treatment enhances the attenuated endothelium-dependent relaxation and decreases the elevated endothelium-dependent contractions in the renal arteries from SHR, reducing the upregulated COX-2 expression in the renal vascular wall. Renal arteries from WKY rats showed high relaxation and small contractions evoked by Ach, whereas renal arteries from SHR showed impaired relaxation and huge contractions ((a)-(b)). Treatment of cultured renal arteries from SHR with DMC (10 μmol/L) for 12 hrs was followed by improved relaxation and inhibited contractions ((a)-(b)). Compared to the renal arteries from WKY, the arteries from SHR exhibited elevated COX-2 expression and DMC (10 μmol/L) treatment for 12 hrs reversed the higher COX-2 expression (c). Data are means ± SEM of 5-6 experiments. $^{*}P < 0.05$ versus WKY; $^{\#}P < 0.05$ versus SHR control.

augmented EDC in hypertension, reducing the upregulated COX-2 expression. Furthermore, previous studies using cancer cells and N9 microglial cells validated the safety of DMC at 10 μmol/L [19, 20]. In vivo treatment with DMC had the effect to reduced IL-1β in the ischemic brain. Additionally, recent evidence indicated that DMC serves as a phosphodiesterase-5 inhibitor and delayed the development of pulmonary hypertension [10]. Our study showed the lower-blood pressure effect of DMC. In Kruangtip et al. findings, they exhibited the direct specifically dilating effect of DMC on pulmonary artery by inhibiting PDE5, which inactivate guanosine cyclic monophosphate (cGMP) via hydrolysis.

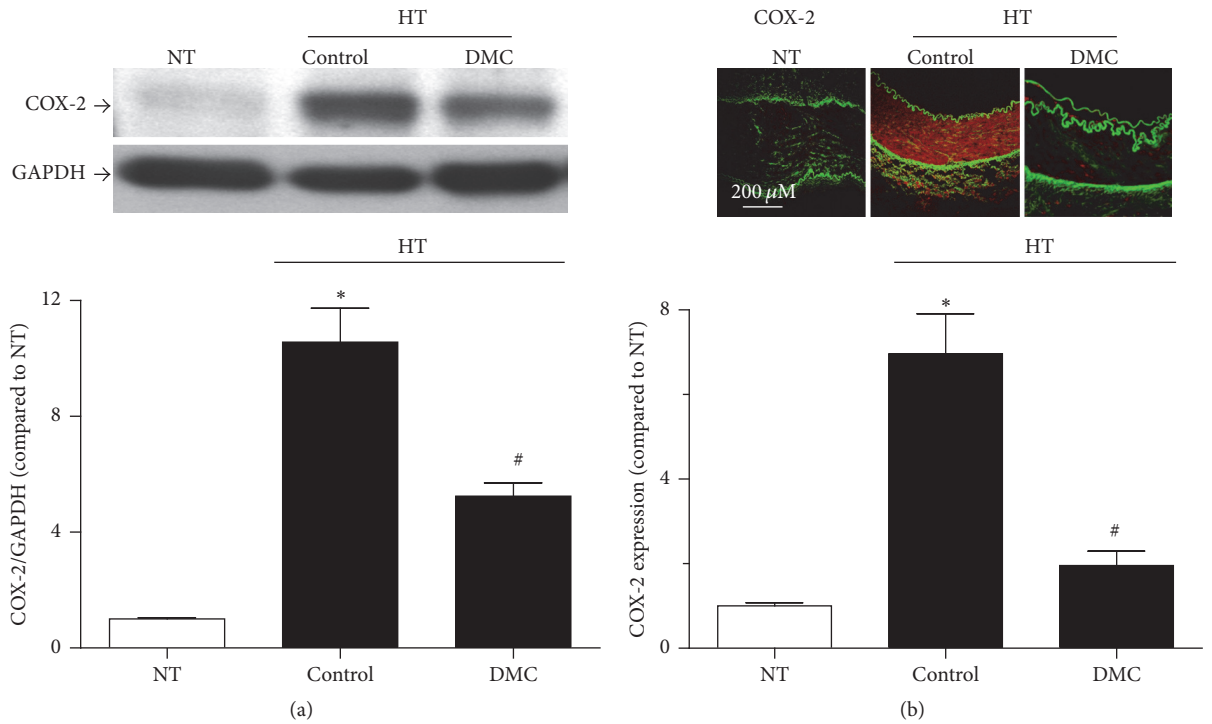

Figure 4: In renal arteries from hypertensive patients ex vivo treatment with DMC for 12 hrs normalizes the altered expression of COX-2 observed by western blot assay and immunofluorescence microscopy. The renal arteries from hypertensive patients exhibited altered COX-2 expression levels by western blot measurement (a) and immunofluorescence microscopy (b). The elevation of COX-2 expression was corrected with the addition of DMC for 12 hrs ((a)-(b)). Yellowish-green autofluorescence represents elastin in the internal and external elastic laminae (b). Higher level of arterial COX-2 expression, suggested by the intense reddish orange color, was reduced by DMC. Photomicrographs are representative images from experiments performed on samples from four to five different patients. The scale bar indicates length (200 μm). Data are means ± SEM of 5-6 experiments. $^{*}P < 0.05$ versus NT; $^{\#}P < 0.05$ versus HT control.

PDE accumulation has been proposed in the development of pulmonary artery hypertension (PAH), indicating the potentially anti-PAH effect of DMC.

As a key agent in the pathogenesis of hypertension, Ang II contributes largely to renovascular dysfunction and kidney dysfunction [21]. Mimicking hypertension in which circulating levels of Ang II were enhanced, renal arteries subjected to Ang II challenge showed augmented expression of COX-2. The impaired EDR, pronounced EDC, and excessive COX-2 expression were also normalized by cotreatment with DMC. Coupled with the upregulation of COX-2, lowered renovascular function was detected, which was restored when exposed to DMC. This result reinforced the beneficial action of DMC in vascular function in hypertension. Further experiments using HUVECs also showed that DMC normalized the reduction of NO and P-eNOS expression in Ang II–treated cells.

Endothelial dysfunction is recognized as an early feature in vascular disease. The assessment of endothelial function is essential in the evaluation of treatment effect in vascular disease [2, 22]. Notably, endothelial dysfunction is of significant use to predict the cardiovascular events due to its precedence of more serious cardiovascular attacks [23]. Hence, the present study offered solid evidence concerning the benefits of DMC against renovascular dysfunction. With regard to the inhibitory effect on COX-2 expression in the renal arteries of SHR, the effect of DMC may originate from the inhibition of NF-κB, which may secondarily downregulate COX-2 expression. A limitation of the present study is how DMC modulates COX-2 expression and whether the effect of DMC is dose-dependent.

5. Conclusion

In conclusion, the present study demonstrated for the first time that COX-2 is at least a downstream effector in the protection of DMC on renovascular function in hypertension. In addition, these findings provide constructive evidence for the development of DMC for therapeutic applications.

Competing Interests

The authors declare that no conflict of interests exist.

Acknowledgments

This work was supported by the Natural Science Foundation of Jiangsu Province [BK20141345].

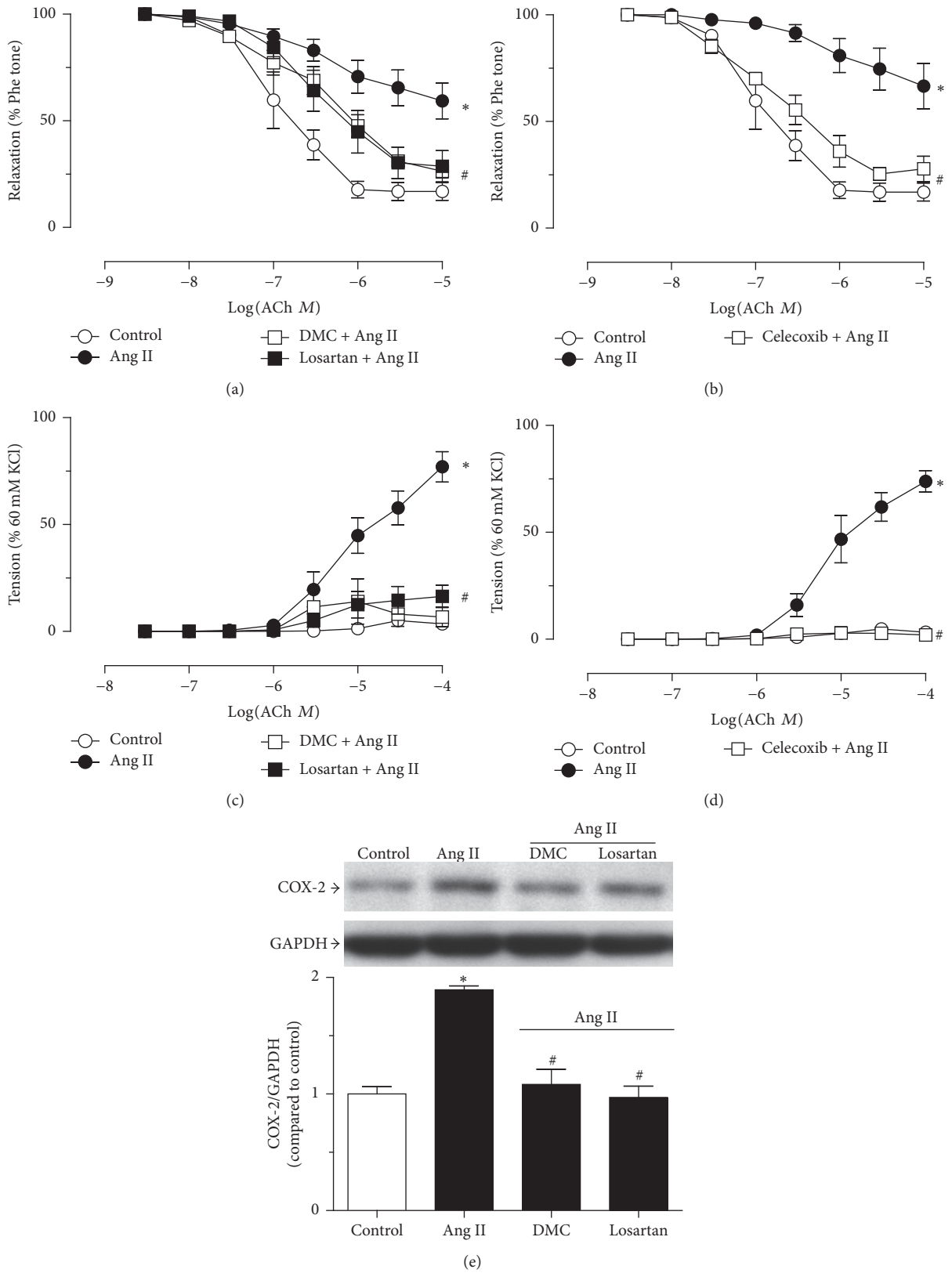

Figure 5: Combined exposure to DMC prevents Ang II-induced vascular dysfunction in the renal arteries from WKY, with normalization of increased COX-2 expression. Ang II (100 nmol/L, 12 hours) results in impaired relaxations to ACh and unmasked contractions to ACh in the renal arteries from WKY rats ((a) and (c)). Combined administration of DMC (10 μmol/L) rescued the impaired vascular function and COX-2 inhibitor celecoxib offered similar protection ((b) and (d)). The overexpression of COX-2 by Ang II was also reversed by coincubation with DMC (e). Data are means ± SEM of 5-6 experiments. $^{*}P < 0.05$ versus control; $^{\#}P < 0.05$ versus Ang II.

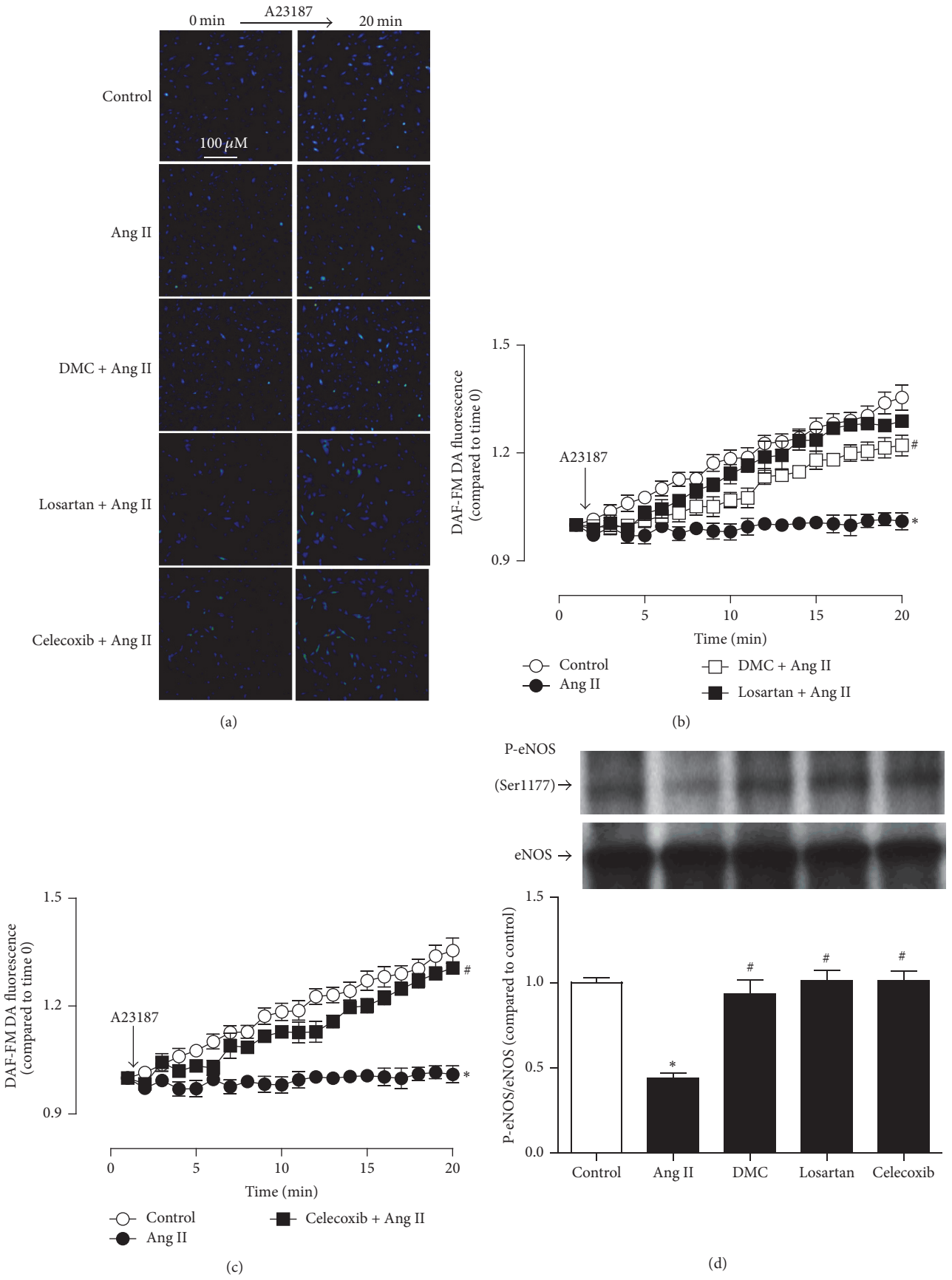

Figure 6: The effect of DMC treatment on nitric oxide generation in HUVECs Ang II (1 μmol/L) treatment for 12 hrs reduced the A23187-evoked NO production (a). Cotreatment with DMC, losartan or celecoxib restored the NO generation ((b)-(c)). Consistently, P-eNOS expression was downregulated in 12 hrs-Ang II-treated cells, which was reversed in the presence of DMC, losartan, or celecoxib (d). Data are means ± SEM of 5-6 experiments. $^{*}P < 0.05$ versus control; $^{\#}P < 0.05$ versus Ang II.

References

[1] D. H. Endemann and E. L. Schiffrin, "Endothelial dysfunction," *Journal of the American Society of Nephrology*, vol. 15, no. 8, pp. 1983–1992, 2004.

[2] D. C. Felmeden and G. Y. H. Lip, "Endothelial function and its assessment," *Expert Opinion on Investigational Drugs*, vol. 14, no. 11, pp. 1319–1336, 2005.

[3] S. Martínez-Revelles, M. S. Avendaño, A. B. García-Redondo et al., "Reciprocal relationship between reactive oxygen species and cyclooxygenase-2 and vascular dysfunction in hypertension," *Antioxidants and Redox Signaling*, vol. 18, no. 1, pp. 51–65, 2013.

[4] D. Versari, E. Daghini, A. Virdis, L. Ghiadoni, and S. Taddei, "Endothelium-dependent contractions and endothelial dysfunction in human hypertension," *British Journal of Pharmacology*, vol. 157, no. 4, pp. 527–536, 2009.

[5] A. Hartner, N. Cordasic, M. Goppelt-Struebe, R. Veelken, and K. F. Hilgers, "Role of macula densa cyclooxygenase-2 in renovascular hypertension," *American Journal of Physiology - Renal Physiology*, vol. 284, no. 3, pp. F498–F502, 2003.

[6] W. T. Wong, X. Y. Tian, Y. Chen et al., "Bone morphogenic protein-4 impairs endothelial function through oxidative stress-dependent cyclooxygenase-2 upregulation: implications on hypertension," *Circulation Research*, vol. 107, no. 8, pp. 984–991, 2010.

[7] A. Kunwar, A. Barik, S. K. Sandur, and K. I. Priyadarsini, "Differential antioxidant/pro-oxidant activity of dimethoxycurcumin, a synthetic analogue of curcumin," *Free Radical Research*, vol. 45, no. 8, pp. 959–965, 2011.

[8] H.-O. Pae, S.-O. Jeong, H. S. Kim et al., "Dimethoxycurcumin, a synthetic curcumin analogue with higher metabolic stability, inhibits NO production, inducible NO synthase expression and NF-κB activation in RAW264.7 macrophages activated with LPS," *Molecular Nutrition & Food Research*, vol. 52, no. 9, pp. 1082–1091, 2008.

[9] S. K. Sandur, M. K. Pandey, B. Sung et al., "Curcumin, demethoxycurcumin, bisdemethoxycurcumin, tetrahydrocurcumin and turmerones differentially regulate anti-inflammatory and anti-proliferative responses through a ROS-independent mechanism," *Carcinogenesis*, vol. 28, no. 8, pp. 1765–1773, 2007.

[10] O. Kruangtip, K. Chootip, P. Temkitthawon et al., "Curcumin analogues inhibit phosphodiesterase-5 and dilate rat pulmonary arteries," *Journal of Pharmacy and Pharmacology*, vol. 67, no. 1, pp. 87–95, 2015.

[11] I. M. Bird, "Endothelial nitric oxide synthase activation and nitric oxide function: new light through old windows," *Journal of Endocrinology*, vol. 210, no. 3, pp. 239–241, 2011.

[12] W. N. Durán, J. W. Breslin, and F. A. Sánchez, "The NO cascade, eNOS location, and microvascular permeability," *Cardiovascular Research*, vol. 87, no. 2, pp. 254–261, 2010.

[13] S. L. Wong, C. W. Lau, W. T. Wong et al., "Pivotal role of protein kinase Cδ in angiotensin II-induced endothelial cyclooxygenase-2 expression: a link to vascular inflammation," *Arteriosclerosis, Thrombosis, and Vascular Biology*, vol. 31, no. 5, pp. 1169–1176, 2011.

[14] A. Sirker, M. Zhang, and A. M. Shah, "NADPH oxidases in cardiovascular disease: insights from in vivo models and clinical studies," *Basic Research in Cardiology*, vol. 106, no. 5, pp. 735–747, 2011.

[15] M. E. Widlansky, D. T. Price, N. Gokce et al., "Short- and long-term COX-2 inhibition reverses endothelial dysfunction in patients with hypertension," *Hypertension*, vol. 42, no. 3, pp. 310–315, 2003.

[16] R. Chenevard, D. Hürlimann, M. Béchir et al., "Selective COX-2 inhibition improves endothelial function in coronary artery disease," *Circulation*, vol. 107, no. 3, pp. 405–409, 2003.

[17] R. C. Becker, "COX-2 inhibitors," *Texas Heart Institute Journal*, vol. 32, no. 3, pp. 380–383, 2005.

[18] L. J. Marnett, "The COXIB experience: a look in the rearview mirror," *Annual Review of Pharmacology and Toxicology*, vol. 49, pp. 265–290, 2009.

[19] L. Zhang, C. Wu, S. Zhao et al., "Demethoxycurcumin, a natural derivative of curcumin attenuates LPS-induced pro-inflammatory responses through down-regulation of intracellular ROS-related MAPK/NF-κB signaling pathways in N9 microglia induced by lipopolysaccharide," *International Immunopharmacology*, vol. 10, no. 3, pp. 331–338, 2010.

[20] X. Ni, A. Zhang, Z. Zhao, Y. Shen, and S. Wang, "Demethoxycurcumin inhibits cell proliferation, migration and invasion in prostate cancer cells," *Oncology Reports*, vol. 28, no. 1, pp. 85–90, 2012.

[21] P. K. Mehta and K. K. Griendling, "Angiotensin II cell signaling: physiological and pathological effects in the cardiovascular system," *American Journal of Physiology—Cell Physiology*, vol. 292, no. 1, pp. C82–C97, 2007.

[22] M. K. Reriani, L. O. Lerman, and A. Lerman, "Endothelial function as a functional expression of cardiovascular risk factors," *Biomarkers in Medicine*, vol. 4, no. 3, pp. 351–360, 2010.

[23] M. Mudau, A. Genis, A. Lochner, and H. Strijdom, "Endothelial dysfunction: the early predictor of atherosclerosis," *Cardiovascular Journal of Africa*, vol. 23, no. 4, pp. 222–231, 2012.

Hindawi Publishing Corporation
Oxidative Medicine and Cellular Longevity
Volume 2016, Article ID 5271251, 11 pages
http://dx.doi.org/10.1155/2016/5271251

Research Article

Pharmacological Inhibition of NLRP3 Inflammasome Attenuates Myocardial Ischemia/Reperfusion Injury by Activation of RISK and Mitochondrial Pathways

Raffaella Mastrocola,[1] Claudia Penna,[1] Francesca Tullio,[1] Saveria Femminò,[1] Debora Nigro,[1] Fausto Chiazza,[2] Loredana Serpe,[2] Debora Collotta,[2] Giuseppe Alloatti,[3] Mattia Cocco,[2] Massimo Bertinaria,[2] Pasquale Pagliaro,[1] Manuela Aragno,[1] and Massimo Collino[2]

[1]*Department of Clinical and Biological Sciences, University of Turin, Torino, Italy*
[2]*Department of Drug Science and Technology, University of Turin, Torino, Italy*
[3]*Department of Life Sciences and Systems Biology, University of Turin, Torino, Italy*

Correspondence should be addressed to Massimo Collino; massimo.collino@unito.it

Received 7 September 2016; Revised 12 October 2016; Accepted 23 October 2016

Academic Editor: Cecilia Zazueta

Although the nucleotide-binding oligomerization domain- (NOD-) like receptor pyrin domain containing 3 (NLRP3) inflammasome has been recently detected in the heart, its role in cardiac ischemia/reperfusion (IR) is still controversial. Here, we investigate whether a pharmacological modulation of NLRP3 inflammasome exerted protective effects in an *ex vivo* model of IR injury. Isolated hearts from male Wistar rats (5-6 months old) underwent ischemia (30 min) followed by reperfusion (20 or 60 min) with and without pretreatment with the recently synthetized NLRP3 inflammasome inhibitor INF4E (50 μM, 20 min before ischemia). INF4E exerted protection against myocardial IR, shown by a significant reduction in infarct size and lactate dehydrogenase release and improvement in postischemic left ventricular pressure. The formation of the NLRP3 inflammasome complex was induced by myocardial IR and attenuated by INF4E in a time-dependent way. Interestingly, the hearts of the INF4E-pretreated animals displayed a marked improvement of the protective RISK pathway and this effect was associated increase in expression of markers of mitochondrial oxidative phosphorylation. Our results demonstrate for the first time that INF4E protected against the IR-induced myocardial injury and dysfunction, by a mechanism that involves inhibition of the NLRP3 inflammasome, resulting in the activation of the prosurvival RISK pathway and improvement in mitochondrial function.

1. Introduction

Ischemic heart disease is one of the main culprits of illness and death [1, 2]. The main outcome of a transient cardiac ischemia is the progressive decline of the left ventricle contractile function, frequently paralleled by impairment of the mitochondrial energy metabolism [3, 4]. During the reperfusion phase the sudden mitochondrial oxygen overload induces oxidative stress and further worsens the metabolic derangement [4], thus paradoxically exacerbating myocardial injury and inducing pyroptosis [2, 5]. Pyroptosis is a caspase-1-dependent process leading to cell lysis, which has been demonstrated to be strongly regulated by the multiprotein platform complex nucleotide-binding oligomerization domain- (NOD-) like receptor pyrin domain containing 3 (NLRP3) inflammasome. The NLRP3 inflammasome comprises (a) NLRP3, (b) an apoptosis-associated speck-like protein containing a caspase activation recruitment domain (ASC), and (c) procaspase-1. In response to a wide range of danger signals, including oxygen-free radicals, K^+ efflux, or mitochondrial stress [6–8], NLRP3 recruits the adaptor protein ASC which in turn interacts with procaspase-1.

Inflammasome oligomerization promotes the autocatalytic activation of procaspase-1 and the processing of prointerleukin- (IL-) 1β [2]. More recently, a new protein has been identified as member of the NLRP3 inflammasome complex, the Gasdermin D (GSDMD), which is recruited with kinetics similar to those required for caspase-1 activation. The proteolytic cleavage of GSDMD by caspase-1 detaches its N-terminal fragment, which contributes to mediate IL-1β secretion and pyroptosis [9]. Since NLRP3 is detectable in many cardiac cell types, including cardiofibroblasts (the most important cell type in the heart in terms of number of cells) and cardiomyocytes (the most important cell type in terms of cell volumes), it is likely that it may play a pivotal role in acute myocardial infarction [10, 11]. Indeed, we and others have shown that NLRP3 is upregulated by ischemia/reperfusion (IR) injury and its myocardial activation is exacerbated by metabolic derangements [12, 13]. Interestingly, genetic modulation of NLRP3 has been reported to reduce myocardial infarct sizes upon IR [13]. However, a very recent study failed to find any role of NLRP3 in determining myocardial IR injury [14] and another investigation supported cardioprotective effects due to NLRP3 inflammasome activation, thus highlighting that the interpretation of NLRP3 inflammasome role in myocardial IR injury is far from clear. Nevertheless, a cross-talk between NLRP3 and mitochondria, the main player of IR injury, has been described, with NLRP3 being able to sense the presence of reactive oxygen species (ROS) produced by normal or dysfunctional mitochondria [15]. Thus, the present study aimed to investigate the effects of a newly synthesized NLRP3 inflammasome inhibitor, named INF4E [16], in an *ex vivo* model of myocardial IR injury. We deepened our investigation evaluating its ability, in the rat heart, (i) to interfere with the IR-induced NLRP3 inflammasome activation and pyroptotic cascade and (ii) to improve the mitochondrial metabolic response to IR insult.

2. Materials and Methods

2.1. INF4E Preparation. INF4E was dissolved at 200 mM concentration in DMSO. Stock solution was then diluted at a final concentration of 50 μM in the perfusion buffer (see below). The description of the synthesis and the specificity of the inhibitor is included in the Supplemental Material (available online at http://dx.doi.org/10.1155/2016/5271251), according to previous publications [16, 17].

2.2. Animals Protocol and Ex Vivo Ischemia/Reperfusion (IR) Injury. Male Wistar rats (Harlan Laboratories, Udine, Italy) 5-6 months old, reaching a body weight of 450–550 g, were cared in compliance with the European Directive 2010/63/EU on the protection of animals used for scientific purposes. The animal protocols followed in this study were approved by the local "Animal Use and Care Committee." After one week of quarantine, with drink and food *ad libitum*, rats were anesthetized and killed. The hearts were rapidly perfused. A constant flow was maintained to obtain a typical coronary perfusion pressure of about 80 mm Hg by the Langendorff technique with Krebs-Henseleit bicarbonate buffer containing (mM) NaCl 118, $NaHCO_3$ 25, KCl 4.7, KH_2PO_4 1.2, $MgSO_4$ 1.2, $CaCl_2$ 1.25, and Glucose 11. The buffer was gassed with 95% O_2 : 5% CO_2. The temperature of the perfusion system was maintained at 37°C. The hearts underwent 30 min stabilization and then were exposed to 30 min of global no-flow, normothermic ischemia followed by a period of 20 or 60 min of reperfusion. Hearts from a subgroup of rats (IR+INF4E) were pretreated with 50 μM INF4E in the perfusate for 20 min before ischemia (after the first 10 min of stabilization). Hearts from sham animals were exposed to 60 min perfusion only and served as reference group in Western blot analysis.

The hearts were electrically paced at 280–300 bpm and kept in a temperature-controlled chamber (37°C). Pacing was stopped at the beginning of the ischemia and restarted after the third min of reperfusion. Left ventricular pressure (LVP) and coronary perfusion pressure (CPP) were recorded and monitored with two electromanometers placed within the left ventricle and along the perfusion line, respectively. Coronary flow, CPP, and LVP were used as indices of preparation conditions. Moreover, end diastolic LVP was recorded as index of contracture development during I/R and developed ventricular pressure as index of contractile activity throughout the experiment using PowerLab data acquisition system and analyzed using Chart software (ADInstruments, Oxford, UK).

The perfusate flowing out of the heart was collected for measurement of lactate dehydrogenase (LDH) release 5 min immediately before ischemia and for the entire reperfusion period. To assess the conditions of experimental preparation the coronary flow rate was determined by the amount of perfusate measured in a specific time period. The heart was then cut in two parts by a coronal section (perpendicular to the long axis). The apical part (less than 1/3 of ventricular mass) was used for molecular analysis and, thus, frozen rapidly in liquid nitrogen and stored at −80°C. Infarct size assessment was performed by using the basal part of ventricle.

2.3. Measurement of the Infarct Size. Infarct mass was evaluated at the end of the reperfusion with the nitro-blue-tetrazolium (NBT) technique by using a gravimetric method [18]. The basal part of the ventricles was dissected by transverse sections into two/ three slices, which were incubated for 20 min with a solution of NBT (0.1%) in phosphate buffer. Two independent and blind observers carefully separated and then weighted both stained and unstained tissues. Total mass of necrosis was then calculated and expressed as percentage of ventricular mass. Since the ischemia was global and since we analyzed only the basal part of the ventricles the necrotic mass was expressed as a percentage of the analyzed ischemic tissue.

2.4. LDH Assay. Spectrophotometric analysis at 340 nm was performed on the collected perfusion effluent to measure LDH released from the heart.

2.5. Preparation of Tissue Extracts. Total proteins extracts were obtained from 10% (w/v) apex homogenates in RIPA

buffer (0.5% Nonidet P-40, 0.5% sodium deoxycholate, 0.1% SDS, 10 mmol/l EDTA, and protease inhibitors) as previously described [19]. Protein concentrations were measured by Bradford assay (BioRad, Hercules, CA, USA) and samples were then stored at −80°C for subsequent analysis.

2.6. Determination of IL-1β in Hearts Homogenates. Commercially available ELISA kit (R&D Systems, Abingdon, UK) was used to measure concentrations of IL-1β in tissue homogenates, according to the manufacturer's instructions.

2.7. Western Blot Analysis. Total proteins extracts were separated by SDS-PAGE and blotted to nitrocellulose membrane (GE-Healthcare Europe, Milano, Italy). Membranes were incubated with rabbit anti-NLRP3 (Abcam, Cambridge, UK), rabbit anti-caspase-1 (Santa Cruz Biotechnology, Dallas, TX, USA), mouse anti-GSDMDC1 (Santa Cruz Biotechnology), rabbit anti-IL-1β (Santa Cruz Biotechnology), rabbit anti-caspase-1 (Santa Cruz Biotechnology, Dallas, TX, USA), mouse anti-Tyr^{204} ERK1/2 (Cell Signaling Technology), rabbit anti-total ERK1/2 (Cell Signaling Technology), mouse anti-Ser^{473} Akt (Cell Signaling Technology), rabbit anti-total Akt (Cell Signaling Technology), rabbit anti-Ser^{9} GSK-3β (Abcam, Cambridge, UK), anti-total GSK-3β (Cell Signaling Technology), rabbit anti-mitochondrial transcription factor A (mtTFA) (Novus Biologicals, Cambridge, UK), mouse anti-nuclear respiratory factor-1 (NRF-1) (Santa Cruz Biotechnology), and mouse anti-sarcomeric mitochondrial creatine kinase (sMtCK) (Santa Cruz Biotechnology) and then probed with proper HRP-conjugated secondary antibodies (BioRad). Clarity Western ECL substrate (BioRad) was used for protein detection and quantification was performed by densitometric analysis (Quantity-One, Bio-Rad software). Data were normalized according to the related antitubulin densitometric values.

2.8. Real-Time PCR. Total RNA was extracted from heart samples using the AllPrep® DNA/RNA/protein kit (Qiagen, Hilden, Germany), according to the manufacture instructions. The total RNA concentration (μg/mL) was determined by the fluorometer Qubit and the Quant-iT™ RNA Assay Kit (Invitrogen, Milano, Italy). A total of 500 ng of RNA was reverse-transcribed using QuantiTect Reverse Transcription Kit (Qiagen). The synthesized cDNA was used for real-time polymerase chain reaction (RT-PCR). The cDNA was amplified by real-time PCR using SsoFast™ EvaGreen (Bio-Rad,) and primers specific for cytokine IL-1β (Mm_Il1b_2_SG, cat. number QT01048355, Qiagen). The PCR reaction was performed at 95°C for 30 s followed by 40 cycles of 95°C for 5 s, 55°C for 10 s. All samples were run in duplicate. At least two nontemplate controls were included in all PCR. The transcript of the reference gene ribosomal RNA 18S (Mm_Rn18s_3_SG, cat. number QT02448075, Qiagen) was used to normalize mRNA data, and the quantification data analyses were performed by using the Bio-Rad CFX Manager Software, version 1.6 (Bio-Rad) according to the manufacturer's instructions.

2.9. Materials. Compounds here used were obtained from the Sigma-Aldrich Company Ltd., unless otherwise stated.

2.10. Statistical Analysis. Data described in the text and figures are presented as means ± standard error of the mean (s.e.m.) of n observations, where n represents the number of animals studied. Statistical analysis was performed using ANOVA test followed by Bonferroni's posttest. A P value of less than 0.05 was considered to be statistically significant.

3. Results

3.1. INF4E Pretreatment Limits Infarct Size and Improves Contractility Recovery. Rat hearts exposed to a 30 min global ischemia and 60 min reperfusion developed a 60 ± 3% infarct size in the basal portion of ventricle evaluated by NBT staining. When hearts were pretreated (20 min prior to ischemia) with INF4E in the perfusate, the infarct size was significantly reduced compared to untreated hearts (IR) (Figure 1(a)). Importantly, LDH release in the perfusate was almost halved by drug treatment (Figure 1(b)). In addition, the INF4E pretreated hearts showed a twofold increase in contractile recovery after IR, as assessed by left ventricular pressure monitoring (Figure 1(c)).

Of note, IR caused an impairment of the mechanical performance, as evidenced by the dramatic reduction of developed LVP (DLVP) immediately after ischemia and the incomplete recovery during reperfusion. In fact, developed LVP fell from about 80 mmHg in the preischemic condition to about 25 mmHg after 10 min of reperfusion and then recovered to only 50 mmHg at 60 min reperfusion, thus reaching only less than 65% of the preischemic value (Figures 1(c) and 1(d)). The pretreatment with the NLRP3 inhibitor did not modify the recovery of DLVP at early reperfusion time (10 and 20 min), whereas an improvement starts to be detectable after 40 min, reaching values up to 85 mmHg at 60 min, corresponding to over 100% of the preischemic value at the end of reperfusion. The end diastolic LVP (EDLVP) was about 5 mmHg during stabilization; then, the 30 min global ischemia and the subsequent reperfusion caused a sustained increase of this parameter in both the IR and IR+INF4E groups (Figure 1(e)). Actually, an increase of EDLVP was appreciated immediately after the end of ischemia and continued during the first 20 min of reperfusion. Then EDLVP further increased in the IR group reaching values over 30 mm Hg, while in the group pretreated with the NLRP3 inhibitor it decreased progressively to about 20 mmHg after 1 hour of reperfusion. The increase in EDLVP was significantly ($P < 0.05$) attenuated by the NLRP3 inhibitor only at 60 min reperfusion.

3.2. INF4E Pretreatment Prevents NLRP3 Inflammasome Activation and Downstream Signaling. To confirm the ability of INF4E to interfere with NLRP3 inflammasome complex formation and activation in our experimental model, the expression level and the activation of the downstream signaling of NLRP3 inflammasome were assessed by Western blotting analysis in protein extracts obtained from the apical

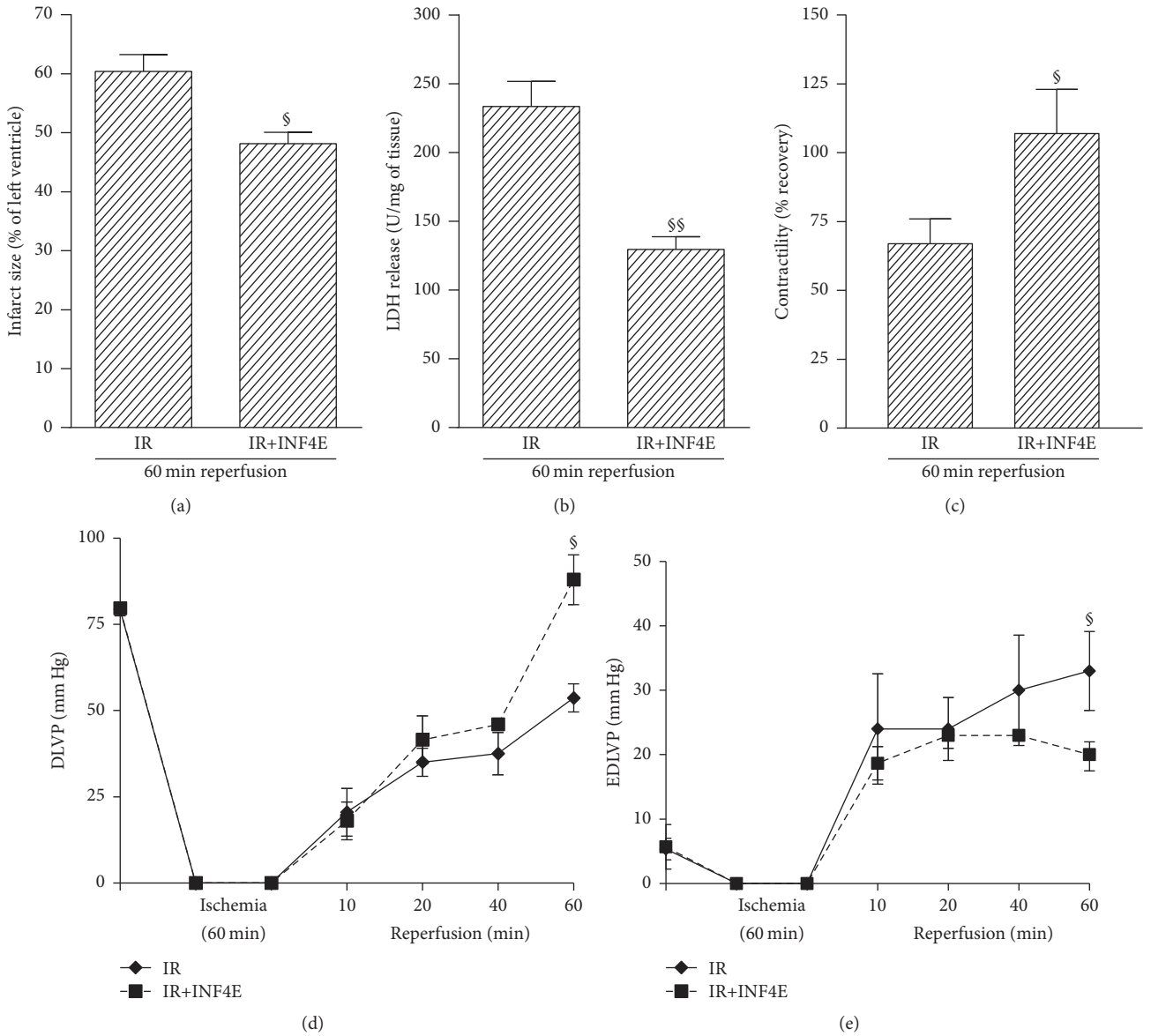

Figure 1: Infarct area, LDH release, and contractility recovery in hearts from rats exposed to 30 min of ischemia plus 60 min of reperfusion, pretreated or not with 50 μM INF4E in the perfusate 20 min before ischemia. (a): infarct size after IR exposition is expressed as a percentage of ischemic tissue (% IS/IT). (b): LDH release in the perfusion effluent during the IR was expressed as units per mg of wet tissue weight. (c)–(e): monitoring of left ventricular pressure (LVP) was used to assess the contractility response to ischemia reperfusion injury. (c) shows the percentage of contractility recovered at the end of 60 min reperfusion. (d) and (e) show the entire time-course of developed LVP (DLVP) and end diastolic LVP (EDLVP), respectively. Data are means of 6 rats ± SEM. $^{\S}P < 0.05$ versus IR. $^{\S\S}P < 0.01$ versus IR.

portion of hearts pretreated or not with INF4E and exposed to IR (Figure 2). Besides, rat hearts were exposed to two different periods of reperfusion, short and long (20 min and 60 min, resp.) to better elucidate the kinetics of the pharmacological modulation of NLRP3 inflammasome and related pathways. As shown in Figure 2, the protein level of NLRP3 was increased in a time-dependent manner, reaching statistical significance only after the 60 min reperfusion. Notably, the INF4E pretreatment effectively reduced its upregulation. Western blotting analysis with an antibody recognizing the C-terminal region of caspase-1 allowed the identification of two bands corresponding to the procaspase-1 and the cleaved active p10 subunit of caspase-1. After 20 min of reperfusion the active form of caspase-1 was markedly increased, without significant changes in the expression of procaspase-1, although the INF4E-pretreated hearts showed a slight nonsignificant trend towards reduced procaspase cleavage. After 60 min of reperfusion, both precursor and active forms of caspase-1 were dramatically increased in the untreated IR group, whereas the INF4E-pretreatment significantly prevented procaspase cleavage. As shown in Figure 2(c), caspase-1 activation is associated with cleavage

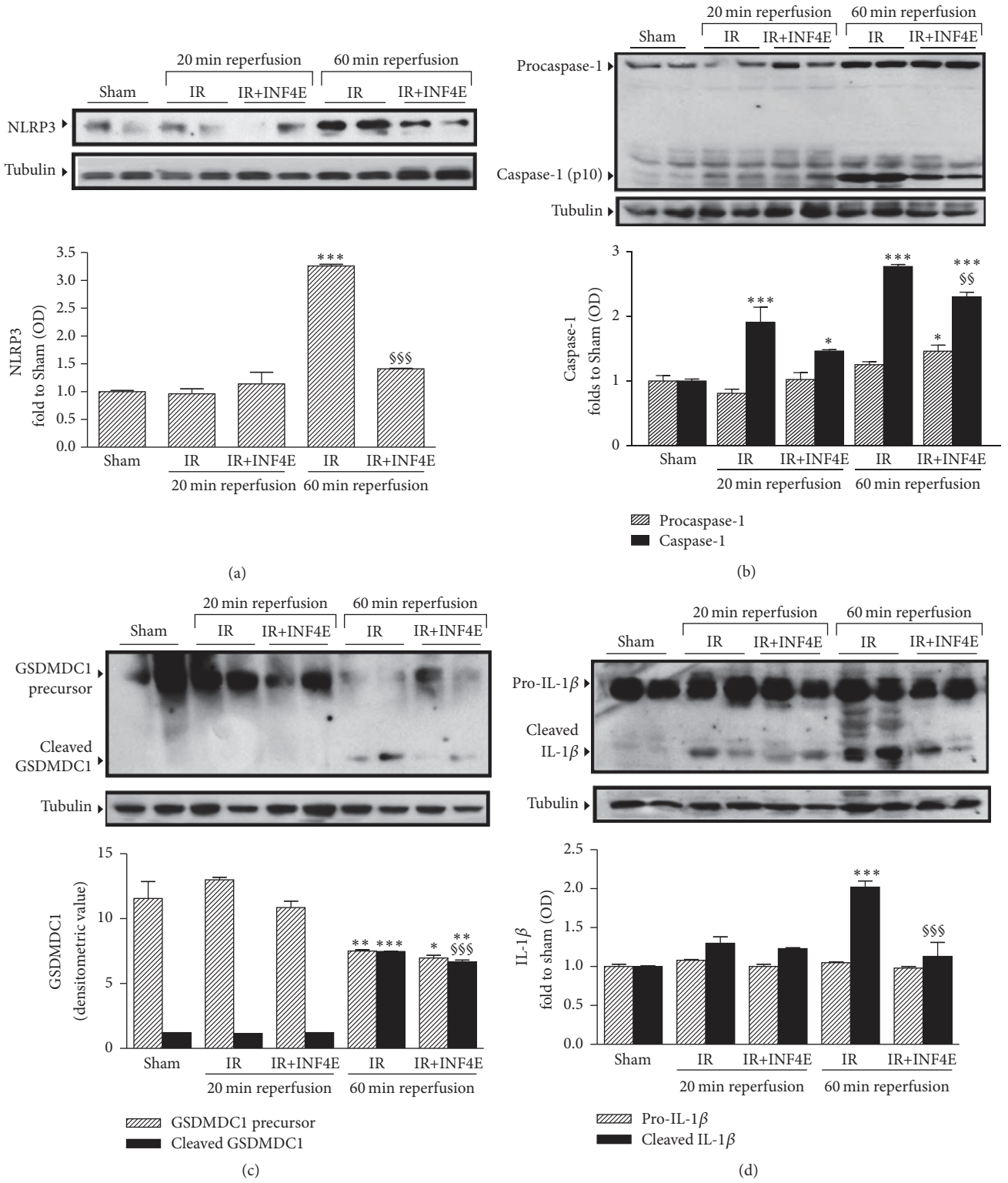

Figure 2: Inflammasome expression and activation in the rat heart exposed to 30 min ischemia plus 20 or 60 min reperfusion, pretreated or not with INF4E. Representative Western blotting showing cardiac levels of NLRP3 and of downstream activation of caspase-1, GSDMDC1, and IL-1β cleavage assessed on heart extracts. Histograms report densitometric analysis normalized for the corresponding tubulin content. Data are means of 6 rats ± SEM. $^{*}P < 0.05$, $^{**}P < 0.01$, and $^{***}P < 0.001$ versus Sham; $^{\S\S}P < 0.01$, $^{\S\S\S}P < 0.001$ versus IR.

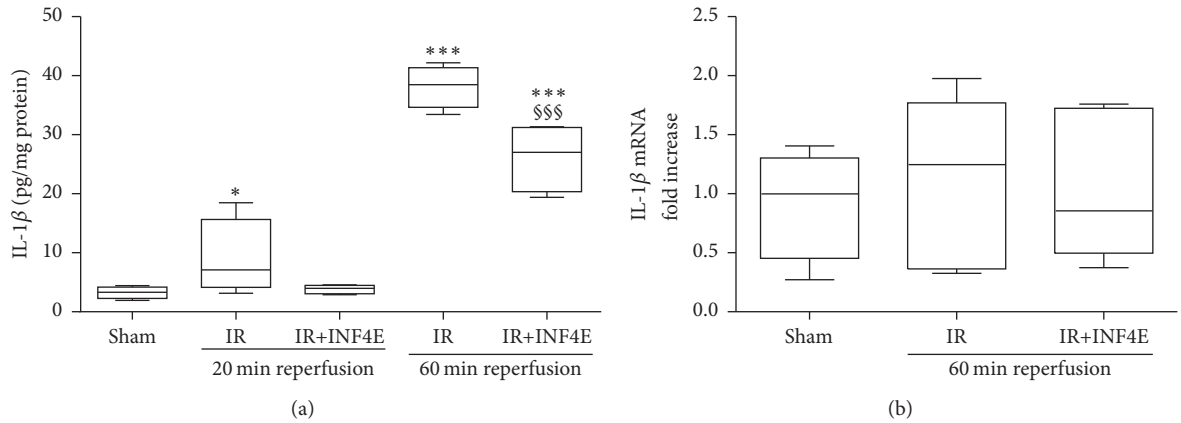

Figure 3: IL-1β concentrations evaluated by ELISA (a) and mRNA levels of IL-1β measured by RT-PCR (b) in extracts of rat hearts exposed to 30 min ischemia plus 20 or 60 min reperfusion, pretreated or not with INF4E. Data are means of 6 rats ± SEM. $^{*}P < 0.05$, $^{***}P < 0.001$ versus Sham; $^{§§§}P < 0.001$ versus IR.

of the GSDMDC1 component of the inflammasome platform, detectable only after the longest reperfusion time. Interestingly, INF4E pretreatment significantly reduced GSDMCD1 cleavage. Accordingly, the protein levels of the active form of IL-1β showed a robust increase after the 60 min reperfusion, as demonstrated by Western blot analysis (Figure 2) and confirmed by ELISA (Figure 3(a)). The INF4E pretreatment prevented the slight increase in IL-1β production due to 20 min of reperfusion and strongly reduced the massive IL-1β release recorded after 60 min of reperfusion (Figures 2 and 3(a)). Interestingly, neither the IR injury nor the drug treatment affected the mRNA levels of IL-1β (Figure 3(b)), thus confirming a selective effect of INF4E on NLRP3 inflammasome-dependent IL-1β cleavage rather than expression.

3.3. INF4E Pretreatment Enhances RISK Pathway Protective Activity. Very recently, a role for NLRP3 inflammasome activation in the modulation of the Reperfusion Injury Salvage Kinase (RISK) pathway has been suggested [20]. Thus, we quantified expression and activity (in terms of phosphorylation) of the key members of this pathway. After 20 min of reperfusion no modulation of the activity and/or expression level of members of the RISK pathway was recorded (Figure 4). On the contrary, the longer IR challenging induced increased phosphorylation rate of both ERK1/2 (Figures 4(a) and 4(b)) and GSK-3β (Figures 4(a) and 4(d)), while phosphorylation of Akt tended to increase, without reaching statistical significance, in untreated hearts exposed to either short or long IR protocol (Figures 4(a) and 4(c)). Interestingly, the INF4E pretreatment further increased the phosphorylation rate of ERK1/2, Akt, and GSK-3β induced by the 60 min reperfusion in untreated hearts (Figures 4(b) and 4(c)), suggesting an enhancement of the activation of this protective pathway by the pharmacological intervention.

3.4. INF4E Pretreatment Improves Mitochondrial Biogenesis and Energy Metabolism. Since mitochondrial metabolism is highly involved in the myocytes response to ischemic insult, and a cross-talk between mitochondria and NLRP3 has been described [21], we analyzed markers of mitochondrial biogenesis after 30 min ischemia and 60 min reperfusion. The MtTFA and the NRF-1 were markedly downregulated by IR. Conversely, mitogenesis was significantly preserved by INF4E pretreatment (Figures 5(a)–5(c)). A crucial physiological reaction of cardiac myocytes to oxygen deprivation is the enhancement of mitochondrial energy production, as suggested in our model by the increased expression of sMtCK after IR (Figures 5(a) and 5(d)). Intriguingly, the INF4E pretreatment further stimulated the expression of sMtCK by 25% with respect to untreated rat hearts (Figures 5(a) and 5(d)).

4. Discussion

The present study improves our understanding on the effects of the NLRP3 inflammasome targeting in acute myocardial infarction. Here we confirmed that myocardial IR induces transcription of all the inflammasome components in a time-dependent way, with slight effect detectable when hearts were exposed to 20 min reperfusion and robust overexpression and activation at the longest reperfusion time (60 min). These data are in agreement with previous papers showing increased expression levels of NLRP3 and procaspase-1 in the infarcted and noninfarcted areas in both cardiomyocytes and nonmyocyte cell, associated with augmentation of caspase-1 activity [13, 22]. We also previously demonstrated that an enhanced susceptibility to a myocardial ischemic insult, due to metabolic derangements, is paralleled by greater NLRP3 inflammasome activation in the heart [12]. However, the potential role of the innate immune NLRP3 protein complex as therapeutic target for cardiac infarction is ill defined. This is mainly due to the contrasting results so far obtained with targeted deletion of the inflammasome components. Few studies demonstrated that the depletion of even one of the inflammasome complex components, either the sensor (NLRP3) or the effector enzyme (caspase-1), can prevent its activation

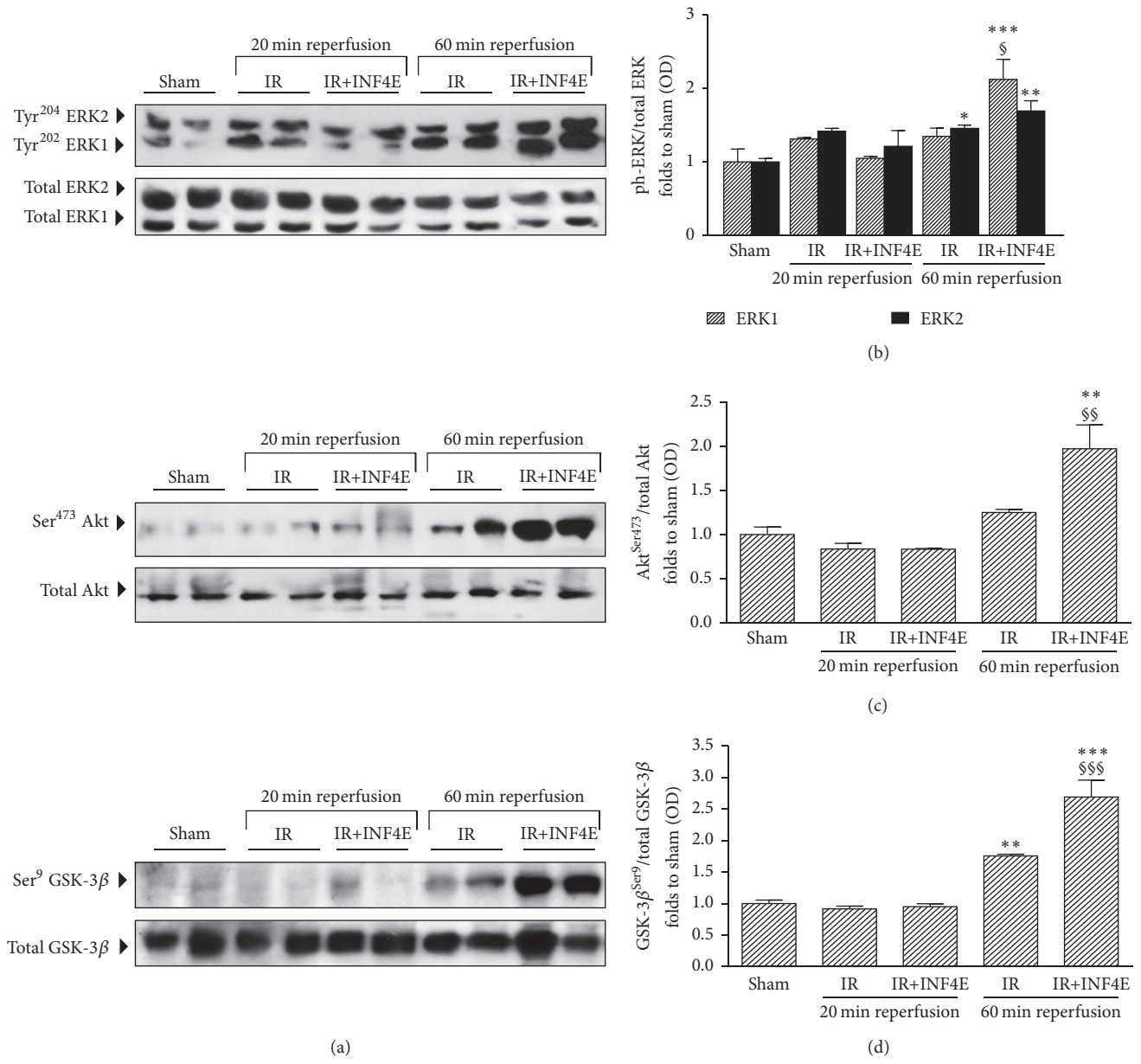

Figure 4: Prosurvival RISK pathway activation in the rat hearts exposed to 30 min ischemia plus 20 or 60 min reperfusion, pretreated or not with INF4E. (a) Representative Western blotting for cardiac levels of total ERK1/2 expression and Thr202/Tyr204 and Thr185/Tyr187 phosphorylation, respectively, total Akt protein expression and Ser473 phosphorylation, and total GSK-3β protein expression and Ser9 phosphorylation, performed on heart extracts. (b)–(d) Histograms report densitometric analysis of the phosphorylated-to-total form ratio. Data are means of 6 rats ± SEM. $^{*}P < 0.05$, $^{**}P < 0.005$, and $^{***}P < 0.001$ versus Sham; $^{\S}P < 0.05$, $^{\S\S}P < 0.005$, and $^{\S\S\S}P < 0.001$ versus IR.

and protect the heart preventing ischemic injury and adverse cardiac remodelling [22–24]. In contrast, Sandanger et al. [20] showed that absence of NLRP3 results in increased myocardial infarct size after *in vivo* IR, whereas Jong et al. [14] concluded that NLRP3 plays no role in acute myocardial infarction due to low cardiac expression. As stated by the same authors, significant differences in the used methodologies as well as in the specific endpoint of interest may help to explain this inconsistency [25]. Besides, a discrepancy in the outcome between NLRP3$^{-/-}$ and ASC$^{-/-}$ mice after cardiac IR has been previously observed [13, 26], suggesting the existence of important inflammasome-independent effects related to targeted genetic deficiency. Thus, only the evaluation of small molecules able to selectively inhibit the NLRP3 inflammasome may allow ultimate elucidation of the potential of NLRP3 inflammasome as pharmacological target for therapeutic intervention in myocardial IR injury. Unfortunately, the lack of highly selective pharmacological inhibitors limits the investigation. INF4E is one of the few compounds that has been demonstrated to directly target

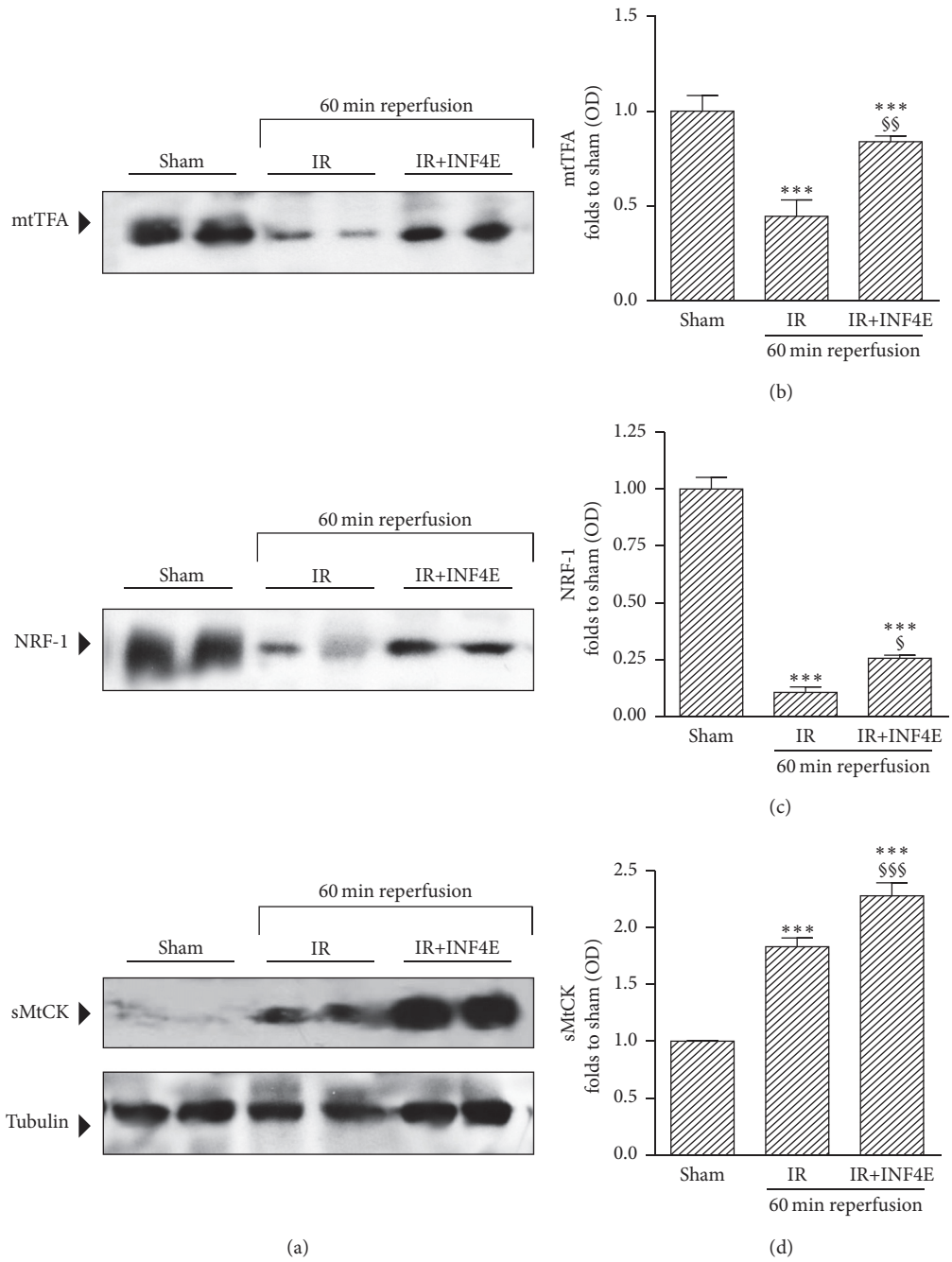

Figure 5: Mitochondrial biogenesis and energy metabolism evaluated in the rat hearts exposed to 30 min ischemia plus 20 or 60 min reperfusion, pretreated or not with INF4E. (a) Representative Western blotting for cardiac levels of MtTFA, NRF-1, and sMtCK performed on heart extracts. (b)–(d) Histograms report densitometric analysis normalized for the corresponding tubulin content. Data are means of 6 rats ± SEM. $^{***}P < 0.001$ versus Sham; $^{\S}P < 0.05$, $^{\S\S}P < 0.005$, and $^{\S\S\S}P < 0.001$ versus IR.

the NLRP3 inflammasome and inhibit the ATPase activity of NLRP3 required for its activation. Although there are clear indications that this drug exerts a specific effect on NLRP3 inflammasome independently of the activating stimulus, the exact mechanism of action has still to be clarified [16]. Here we demonstrate, for the first time, that administration of the NLRP3 inflammasome inhibitor INF4E in a single dose significantly reduces infarct size, the main endpoint to target in cardioprotective studies. Moreover, the pretreatment with INF4E preserves systolic function, an index of reduced myocardial stunning. To the best of our knowledge, so far, only another small molecule acting as NLRP3 inflammasome inhibitor has been tested in models of acute myocardial injury, showing protective effects similar to those recorded in our *ex vivo* model of myocardial IR injury [27, 28]. Interestingly, this compound did not reduce infarct size at

3 h of reperfusion, while it significantly reduced infarct size at 24 h, if administered at the beginning of reperfusion, but not after 3 h reperfusion [29], thus confirming the importance of the first period of reperfusion for IR injury development and the efficacy of pharmacological strategies [5]. Here we documented significant reduction of infarct size even after 60 min of reperfusion, with INF4E administered as pretreatment. It has to be noted that our *ex vivo* model of IR injury may allow excluding the involvement of infiltrating inflammatory cells that usually may affect the reperfusion-related injury as documented in the previous studies investigating the effects of NLRP3 inhibitors when given during reperfusion [28, 29]. Thus, our data further extend the previous findings suggesting that the continuous pharmacological inhibition of NLRP3 inflammasome pathway already during the ischemic period may significantly contribute to the beneficial effects recorded at the end of reperfusion. The kinetics of the reperfusion injury may also affect the entity of the drug target expression and, thus, protection. In fact, when comparing the 20 min reperfusion and the 60 min reperfusion models we observed a progressive expression and activity of NLRP3 inflammasome complex, thus confirming previous findings on the timing of NLRP3 inflammasome formation in the heart during ischemia reperfusion [29].

Very recently, a role for NLRP3 inflammasome activation in the cardioprotective RISK pathway has been faintly suggested, but not convincingly demonstrated [20]. Here we measured the entire RISK pathway, which includes Akt and ERK1/2 activation and GSK3β inhibition through phosphorylation [30]. Our data demonstrate that the activation of ERK/Akt/GSK-3β signaling is further enhanced by pharmacological inhibition of the NLRP3 inflammasome complex and this effect may significantly contribute to its cardioprotective effects. These data confirm our previous findings, showing that pharmacological inhibition of NLRP3 inflammasome significantly potentiates the activity of the prosurvival Akt pathway [31]. Besides, the cross-talk between NLRP3 inflammasome and RISK pathways is further confirmed by the comparative analysis of the expression/activity of members of both pathways, which show robust increase only in the 60 min reperfusion model in both cases.

Although we demonstrated a direct effect of the tested compound on NLRP3 inflammasome activation, we cannot rule out the potential interactions of INF-4E with other signaling pathways, including those involved in the regulation of the expression of NLRP3 and/or activation of the RISK pathway. Thus, a further rigorous evaluation of effects of the tested compound on other signaling pathways affected by IR is needed to better elucidate its pharmacodynamics profile.

The effects of the pharmacological inhibition of NLRP3 inflammasome on the RISK pathway are closely related to those recorded on mitochondrial metabolic response. Indeed, the mitochondrial metabolic dysfunction is crucial for cardiac damage development, as both the block of mitochondrial ATP-sensitive potassium channel (mitoKATP) and the opening of the mitochondrial permeability transition pore (mPTP) are common end effectors of the IR injury. Accordingly, pharmacological strategies which aimed to open the mitoKATP and inhibit mPTP opening effectively reduce myocardial IR injury and improve cardiomyocytes energy homeostasis via modulation of the activity of members of the RISK pathway [32–35]. We and others have demonstrated that the Akt-mediated inactivation of GSK-3β is critical for the prevention of myocardial IR injury, being a key event in the regulation of apoptosis and the enhancement of mitochondrial biogenesis [36–38]. Besides, the use of selective GSK-3β inhibitors evokes protection against IR injury and promotes cell survival by limiting mPTP opening [39, 40]. In agreement with the above-mentioned observations, the INF4E-induced amplification of the RISK pathway activation here described positively impacted on mitochondrial metabolism. In fact, our data clearly demonstrate that markers of mitochondrial biogenesis, suppressed by IR, were significantly upregulated by INF4E administration. Besides, the administered compound enhanced mitochondrial energy metabolism, shown in terms of reinforced expression of the sMtCK, which is a marker of increased mitochondrial ATP production.

Unfortunately, our study does not allow identifying the specific cell types involved in NLRP3-mediated responses. Cardiomyocytes are the most prominent cell type in the heart and loss of contractile tissue is the most important consequence of a myocardial infarction. However, in cardiomyocytes, the activation on NLRP3 inflammasome evokes caspase-1 activation and pyroptosis, but not relevant release of mature IL-1β [22, 41]. In contrast, NLRP3 inflammasome activation in myocardial fibroblasts induces the production of large amounts of mature IL-1β, causing a rapid amplification of the inflammatory response [13, 23, 42]. As cardiomyocytes are crucial target for the IL-1β produced by resident fibroblasts, which impairs contractile function and induces apoptotic cell death, we may speculate that the beneficial effects of INF4E are due, at least in part, to an indirect improvement in cardiomyocytes functionality.

5. Conclusion

Taken together, our results strengthen the crucial role of NLRP3 inflammasome activation even in the early step of myocardial injury caused by IR and show, for the first time, that its pharmacological inhibition by INF4E reduced the organ injury/dysfunction. Preservation of cardiac function by INF4E is, at least in part, attributable to a cardioprotective effect mediated by the activation of the RISK survival pathways and the improvement in mitochondrial function, which, in turn, may improve cardiac function and postischemic outcome. It has to be stressed, however, that the lack of long-term evaluation as well as data on drug effects when administered during reperfusion limit the interpretation of the clinical transferability of our findings. Thus, further rigorous evaluations are needed to gain a better understanding of both efficacy and the mechanism of action of INF4E in the settings of acute myocardial infarction.

Competing Interests

The authors declare that they have no competing interests.

Acknowledgments

This work was supported and funded by the University of Turin (Ricerca Locale 2015 Linea A and Linea B).

References

[1] A. S. Go, D. Mozaffarian, V. L. Roger et al., "Executive summary: heart disease and stroke statistics—2013 update: a report from the American Heart Association," *Circulation*, vol. 127, no. 1, pp. 143–152, 2013.

[2] M. Takahashi, "NLRP3 inflammasome as a novel player in myocardial infarction," *International Heart Journal*, vol. 55, no. 2, pp. 101–105, 2014.

[3] M. G. Perrelli, P. Pagliaro, and C. Penna, "Ischemia/reperfusion injury and cardioprotective mechanisms: role of mitochondria and reactive oxygen species," *World Journal of Cardiology*, vol. 3, no. 6, pp. 186–200, 2011.

[4] C. Penna, M.-G. Perrelli, and P. Pagliaro, "Mitochondrial pathways, permeability transition pore, and redox signaling in cardioprotection: therapeutic implications," *Antioxidants & Redox Signaling*, vol. 18, no. 5, pp. 556–599, 2013.

[5] D. M. Yellon and D. J. Hausenloy, "Myocardial reperfusion injury," *The New England Journal of Medicine*, vol. 357, no. 11, pp. 1121–1135, 2007.

[6] R. Zhou, A. Tardivel, B. Thorens, I. Choi, and J. Tschopp, "Thioredoxin-interacting protein links oxidative stress to inflammasome activation," *Nature Immunology*, vol. 11, no. 2, pp. 136–140, 2010.

[7] R. Zhou, A. S. Yazdi, P. Menu, and J. Tschopp, "A role for mitochondria in NLRP3 inflammasome activation," *Nature*, vol. 469, no. 7329, pp. 221–225, 2011.

[8] J. R. Yaron, S. Gangaraju, M. Y. Rao et al., "K+ regulates Ca2+ to drive inflammasome signaling: dynamic visualization of ion flux in live cells," *Cell Death and Disease*, vol. 6, no. 10, Article ID e1954, 2015.

[9] X. Liu, Z. Zhang, J. Ruan et al., "Inflammasome-activated gasdermin D causes pyroptosis by forming membrane pores," *Nature*, vol. 535, no. 7610, pp. 153–158, 2016.

[10] J. A. Kummer, R. Broekhuizen, H. Everett et al., "Inflammasome components NALP 1 and 3 show distinct but separate expression profiles in human tissues suggesting a site-specific role in the inflammatory response," *Journal of Histochemistry and Cytochemistry*, vol. 55, no. 5, pp. 443–452, 2007.

[11] N. A. Bracey, P. L. Beck, D. A. Muruve et al., "The Nlrp3 inflammasome promotes myocardial dysfunction in structural cardiomyopathy through interleukin-1β," *Experimental Physiology*, vol. 98, no. 2, pp. 462–472, 2013.

[12] R. Mastrocola, M. Collino, C. Penna et al., "Maladaptive modulations of nlrp3 inflammasome and cardioprotective pathways are involved in diet-induced exacerbation of myocardial ischemia/reperfusion injury in mice," *Oxidative Medicine and Cellular Longevity*, vol. 2016, Article ID 3480637, 12 pages, 2016.

[13] Ø. Sandanger, T. Ranheim, L. E. Vinge et al., "The NLRP3 inflammasome is up-regulated in cardiac fibroblasts and mediates myocardial ischaemia-reperfusion injury," *Cardiovascular Research*, vol. 99, no. 1, pp. 164–174, 2013.

[14] W. M. Jong and C. J. Zuurbier, "A role for NLRP3 inflammasome in acute myocardial ischaemia-reperfusion injury?" *Cardiovascular Research*, vol. 99, no. 1, p. 226, 2013.

[15] J. Zhou and W.-J. Chng, "Roles of thioredoxin binding protein (TXNIP) in oxidative stress, apoptosis and cancer," *Mitochondrion*, vol. 13, no. 3, pp. 163–169, 2013.

[16] M. Cocco, D. Garella, A. Di Stilo et al., "Electrophilic warhead-based design of compounds preventing NLRP3 inflammasome-dependent pyroptosis," *Journal of Medicinal Chemistry*, vol. 57, no. 24, pp. 10366–10382, 2014.

[17] M. Cocco, G. Miglio, M. Giorgis et al., "Design, synthesis, and evaluation of acrylamide derivatives as direct NLRP3 inflammasome inhibitors," *ChemMedChem*, vol. 11, no. 16, pp. 1790–1803, 2016.

[18] C. Penna, M. Brancaccio, F. Tullio et al., "Overexpression of the muscle-specific protein, melusin, protects from cardiac ischemia/reperfusion injury," *Basic Research in Cardiology*, vol. 109, no. 4, article 418, 2014.

[19] M. Aragno, R. Mastrocola, C. Ghé et al., "Obestatin induced recovery of myocardial dysfunction in type 1 diabetic rats: underlying mechanisms," *Cardiovascular Diabetology*, vol. 11, article 129, 2012.

[20] Ø. Sandanger, E. Gao, T. Ranheim et al., "NLRP3 inflammasome activation during myocardial ischemia reperfusion is cardioprotective," *Biochemical and Biophysical Research Communications*, vol. 469, no. 4, pp. 1012–1020, 2016.

[21] P. Gurung, J. R. Lukens, and T. D. Kanneganti, "Mitochondria: diversity in the regulation of the NLRP3 inflammasome," *Trends in Molecular Medicine*, vol. 21, no. 3, pp. 193–201, 2015.

[22] E. Mezzaroma, S. Toldo, D. Farkas et al., "The inflammasome promotes adverse cardiac remodeling following acute myocardial infarction in the mouse," *Proceedings of the National Academy of Sciences of the United States of America*, vol. 108, no. 49, pp. 19725–19730, 2011.

[23] M. Kawaguchi, M. Takahashi, T. Hata et al., "Inflammasome activation of cardiac fibroblasts is essential for myocardial ischemia/reperfusion injury," *Circulation*, vol. 123, no. 6, pp. 594–604, 2011.

[24] Y. Liu, K. Lian, L. Zhang et al., "TXNIP mediates NLRP3 inflammasome activation in cardiac microvascular endothelial cells as a novel mechanism in myocardial ischemia/reperfusion injury," *Basic Research in Cardiology*, vol. 109, no. 5, article 415, 2014.

[25] S. Toldo, C. Marchetti, and A. Abbate, "nLRP3 inflammasome activation during myocardial ischemia reperfusion is cardioprotective," *Biochemical and Biophysical Research Communications*, vol. 470, no. 4, pp. 811–812, 2016.

[26] C. J. Zuurbier, W. M. C. Jong, O. Eerbeek et al., "Deletion of the innate immune NLRP3 receptor abolishes cardiac ischemic preconditioning and is associated with decreased IL-6/STAT3 signaling," *PLoS ONE*, vol. 7, no. 7, Article ID e40643, 2012.

[27] C. Marchetti, J. Chojnacki, S. Toldo et al., "A novel pharmacologic inhibitor of the NLRP3 inflammasome limits myocardial injury after ischemia-reperfusion in the mouse," *Journal of Cardiovascular Pharmacology*, vol. 63, no. 4, pp. 316–322, 2014.

[28] C. Marchetti, S. Toldo, J. Chojnacki et al., "Pharmacologic inhibition of the NLRP3 inflammasome preserves cardiac function after ischemic and nonischemic injury in the mouse," *Journal of Cardiovascular Pharmacology*, vol. 66, no. 1, pp. 1–8, 2015.

[29] S. Toldo, C. Marchetti, A. G. Mauro et al., "Inhibition of the NLRP3 inflammasome limits the inflammatory injury following myocardial ischemia-reperfusion in the mouse," *International Journal of Cardiology*, vol. 209, pp. 215–220, 2016.

[30] D. J. Hausenloy, S. Lecour, and D. M. Yellon, "Reperfusion injury salvage kinase and survivor activating factor enhancement

prosurvival signaling pathways in ischemic postconditioning: two sides of the same coin," *Antioxidants and Redox Signaling*, vol. 14, no. 5, pp. 893–907, 2011.

[31] F. Chiazza, A. Couturier-Maillard, E. Benetti et al., "Targeting the NLRP3 inflammasome to reduce diet-induced metabolic abnormalities in mice," *Molecular Medicine*, vol. 21, no. 1, pp. 1025–1037, 2015.

[32] Y. Chen, J. Zhao, J. Du, G. Xu, C. Tang, and B. Geng, "Hydrogen sulfide regulates cardiac sarcoplasmic reticulum Ca^{2+} uptake via K_{ATP} channel and PI3K/Akt pathway," *Life Sciences*, vol. 91, no. 7-8, pp. 271–278, 2012.

[33] M. Najafi, S. Farajnia, M. Mohammadi et al., "Inhibition of mitochondrial permeability transition pore restores the cardioprotection by postconditioning in diabetic hearts," *Journal of Diabetes & Metabolic Disorders*, vol. 13, no. 1, article 106, 2014.

[34] Y. Hu, L. I. Li, W. Yin, L. Shen, B. You, and H. Gao, "Protective effect of proanthocyanidins on anoxia-reoxygenation injury of myocardial cells mediated by the PI3K/Akt/GSK-3β pathway and mitochondrial ATP-sensitive potassium channel," *Molecular Medicine Reports*, vol. 10, no. 4, pp. 2051–2058, 2014.

[35] G. Ikeda, T. Matoba, Y. Nakano et al., "Nanoparticle-mediated targeting of cyclosporine a enhances cardioprotection against ischemia-reperfusion injury through inhibition of mitochondrial permeability transition pore opening," *Scientific Reports*, vol. 6, Article ID 20467, 2016.

[36] A. Kapoor, M. Collino, S. Castiglia, R. Fantozzi, and C. Thiemermann, "Activation of peroxisome proliferator-activated receptor-β/δ attenuates myocardial ischemia/reperfusion injury in the rat," *Shock*, vol. 34, no. 2, pp. 117–124, 2010.

[37] M. Zhang, C. Wang, J. Hu et al., "Notch3/Akt signaling contributes to OSM-induced protection against cardiac ischemia/reperfusion injury," *Apoptosis*, vol. 20, no. 9, pp. 1150–1163, 2015.

[38] D. Sun, S. Li, H. Wu et al., "Oncostatin M (OSM) protects against cardiac ischaemia/reperfusion injury in diabetic mice by regulating apoptosis, mitochondrial biogenesis and insulin sensitivity," *Journal of Cellular and Molecular Medicine*, vol. 19, no. 6, pp. 1296–1307, 2015.

[39] M. Collino, M. Aragno, S. Castiglia et al., "Insulin reduces cerebral ischemia/reperfusion injury in the hippocampus of diabetic rats: a role for glycogen synthase kinase-3beta," *Diabetes*, vol. 58, no. 1, pp. 235–242, 2009.

[40] E. R. Gross, A. K. Hsu, and G. J. Gross, "Delayed cardioprotection afforded by the glycogen synthase kinase 3 inhibitor SB-216763 occurs via a K_{ATP}- and MPTP-dependent mechanism at reperfusion," *American Journal of Physiology—Heart and Circulatory Physiology*, vol. 294, no. 3, pp. H1497–H1500, 2008.

[41] S. Toldo, A. Das, E. Mezzaroma et al., "Induction of microRNA-21 with exogenous hydrogen sulfide attenuates myocardial ischemic and inflammatory injury in mice," *Circulation: Cardiovascular Genetics*, vol. 7, no. 3, pp. 311–320, 2014.

[42] A. Saxena, W. Chen, Y. Su et al., "IL-1 induces proinflammatory leukocyte infiltration and regulates fibroblast phenotype in the infarcted myocardium," *The Journal of Immunology*, vol. 191, no. 9, pp. 4838–4848, 2013.

Hindawi Publishing Corporation
Oxidative Medicine and Cellular Longevity
Volume 2016, Article ID 3128280, 9 pages
http://dx.doi.org/10.1155/2016/3128280

Research Article

Lycopene Ameliorates Transplant Arteriosclerosis in Vascular Allograft Transplantation by Regulating the NO/cGMP Pathways and Rho-Associated Kinases Expression

Yunqiang He,[1] Peng Xia,[2] Hao Jin,[2] Yan Zhang,[2] Bicheng Chen,[1] and Ziqiang Xu[2]

[1]*Zhejiang Provincial Top Key Discipline in Surgery, Wenzhou Key Laboratory of Surgery, Department of Surgery, The First Affiliated Hospital of Wenzhou Medical University, Wenzhou, Zhejiang Province 325000, China*
[2]*Department of Transplantation, The First Affiliated Hospital of Wenzhou Medical University, Wenzhou, Zhejiang Province 325000, China*

Correspondence should be addressed to Bicheng Chen; chenbicheng@hotmail.com and Ziqiang Xu; xzq6641@163.com

Received 2 July 2016; Revised 4 October 2016; Accepted 24 October 2016

Academic Editor: Leopoldo Aguilera-Aguirre

Objective. Transplant arteriosclerosis is considered one of the major factors affecting the survival time of grafts after organ transplantation. In this study, we proposed a hypothesis of whether lycopene can protect grafted vessels through regulating key proteins expression involved in arteriosclerosis. *Methods.* Allogeneic aortic transplantation was performed using Brow-Norway rats as donors and Lewis rats as recipients. After transplantation, the recipients were divided into two groups: the allograft group and the lycopene group. Negative control rats (isograft group) were also established. Histopathological staining was performed to observe the pathological changes, and the expression levels of Ki-67, caspase-3, Rho-associated kinases, intercellular adhesion molecules (ICAM-1), and eNOS were assessed. Western blotting analysis and real-time PCR were also performed for quantitative analysis. *Results.* The histopathological staining showed that vascular stenosis and intimal thickening were not evident after lycopene treatment. The Ki-67, ROCK1, ROCK2, and ICAM-1 expression levels were significantly decreased. However, eNOS expression in grafted arteries and plasma cGMP concentration were increased after lycopene treatment. *Conclusions.* Lycopene could alleviate vascular arteriosclerosis in allograft transplantation via downregulating Rho-associated kinases and regulating key factor expression through the NO/cGMP pathways, which may provide a potentially effective method for transplant arteriosclerosis in clinical organ transplantation.

1. Introduction

Although significant advances in the application of immunosuppressants have significantly increased the success rate of organ transplantation [1], transplant arteriosclerosis (TA) is also considered as one of the major causes of graft failure in a number of transplant patients [2]. Vascular injuries mainly include ischemia-reperfusion injury, the long-term use of immunosuppressive drugs, infiltration of inflammatory cytokines, and acute or chronic graft rejections. In the early stage, these injuries can damage the vascular endothelium, impair the vascular endothelial function, and promote the migration and proliferation of vascular smooth muscle cell (VSMC), which can ultimately lead to arteriosclerosis occlusion [3]. Therefore, vessel protection in grafts has been considered crucial treatment after organ transplantation, which will effectively prevent the occurrence of transplant arteriosclerosis [4].

Lycopene is a natural carotenoid that exists in tomatoes and tomato products. It is considered as one of the most effective singlet oxygen species in carotenoids [5]. Its inactivation capacity is twice that of beta carotene and 100 times that of vitamin E. The study has reported that lycopene can increase the activity and expression level of nitric oxide (NO) [6]. Furthermore, cGMP-dependent protein kinase-I (PKG-I) is considered a critical mediator of the NO/cGMP pathways [7]. It is widely known that lycopene can maintain the normal function of the vascular endothelium by regulating

relevant factors expression through the NO/cGMP pathways. Several studies have found that lycopene has an inhibitory effect on thickening of the intima and media of people who smoke. In addition, lycopene can inhibit the adhesion of inflammatory factors in the vascular intima, reducing damage to the vascular intima [8]. Furthermore, activation of Rho-associated kinases (ROCKs) also plays an important role in vascular arteriosclerosis [9]. Therefore, the detection of ROCKs expression levels was performed in this study to demonstrate the mechanisms involved in the progression of transplant arteriosclerosis.

The aim of this study was to investigate the protective effects of lycopene on grafted vessels. A hypothesis was also proposed: whether lycopene protects grafted vessels after vasotransplantation through regulating the NO/cGMP pathways and Rho-associated kinases expression involved in arteriosclerosis. The results demonstrated that lycopene could alleviate the vascular sclerosis of the transplanted arteries, regulate the expression of key factors in relevant signaling pathways of the blood vessels, and reduce the infiltration of inflammatory factors through its antioxidant effects. This may provide a potentially effective treatment approach for transplant arteriosclerosis in clinical organ transplantation.

2. Materials and Methods

2.1. Animals. Sixteen male Brow-Norway (BN) rats and 32 male Lewis rats at 8 weeks of age (200–220 g) were provided by Vital River Laboratory Animal Technology Co., Ltd. (Beijing, China). All rats were housed with a 12-hour light and 12-hour dark cycle at 24°C ± 1°C, and they were fed ad libitum for a week before the experiments started. All animal procedures were based on the international guidelines and were approved by the Wenzhou Medical University Animal Policy and Welfare Committee.

2.2. Aorta Transplantation. Aorta transplantation was performed based on the previously described methods [10]. Syngeneic aortic transplantation was performed in Lewis rats, and allogeneic aortic transplantation was performed using Brow-Norway (BN) rats as donors and Lewis rats as recipients. These rats were anesthetized by intraperitoneal injection of pentobarbital (60 mg/kg). The abdominal aorta (10–15 mm) was harvested from donors after intravenous heparin injection. After sufficient perfusion with saline, the aortic grafts were transplanted into recipients and anastomosed end to end with the abdominal aorta using noninterrupted 10-0 nylon sutures. The total operation ischemic time was consistently limited to 30 minutes. The operation was considered successful when there was complete patency of the grafted arteries without significant anastomotic bleeding. Then, the recipients were divided into 3 groups. The first group ($n = 8$) was treated for 8 weeks with saline vehicle after an isograft (1 ml/day, isograft group); the second group ($n = 8$) was treated for 8 weeks with saline vehicle after an allograft (allograft group); the third group ($n = 8$) was treated for 8 weeks with lycopene (30 mg/kg/d, lycopene group) after an allograft. After the operations, all recipients were treated with ceftazidime (100 mg/kg) for 3 consecutive days.

2.3. Histopathology. All grafts were harvested 8 weeks after transplantation. Graft vessel tissues were fixed overnight in 4% paraformaldehyde for histopathological staining. After gradient dehydration in ethanol and xylene, the vessel tissues were embedded in paraffin and cut into 5 μm sections by a microtome. After deparaffinization and rehydration, the sections were stained with hematoxylin and eosin (HE staining) for general morphological examination and pathological analysis. The intima area was calculated by subtracting the lumen area from the area enclosed by the internal elastic lamina lining. The degrees of neointimal hyperplasia and arterial stenosis were measured under the optical microscope (original magnification ×200) and analysed by Image-Pro Plus 6.0 image analysis software (Media Cybernetics, Silver Spring, MD). More than 10 fields were evaluated from each section in each group and the mean value was used. All the measurements were performed on blinded slides.

2.4. Enzyme-Linked Immunosorbent Assay (ELISA). Blood samples were collected 8 weeks after transplantation in each group. Rats' plasma cGMP concentrations were quantitatively measured by using an ELISA kit (R&D Systems, Inc., Minnesota, USA) according to the manufacturer's instructions described previously [11]. All the ELISA experiments were repeated at least three times.

2.5. Real-Time Quantitative Reverse Transcription-Polymerase Chain Reaction (Real-Time RT-PCR). According to the protocol that was previously described by Lin et al. [12], total RNA was extracted from the vessel specimens using TRIzol reagent. The primer sequences were as follows: ROCK1, forward 5′-TGGTTGGGACGTACAGTAAAA-3′ and reverse 5′-GTAAGGAAGGCACAAATGAGA-3′; ROCK2, forward 5′-AATGGGTTAGTCGGTTGG-3′ and reverse 5′-CTTGGTTTGTTTGGAGCA-3′; eNOS, forward 5′-GCCAAACAGGCCTGGCGCAA-3′ and reverse 5′-GTGCTGTCCTGCAGTCCCGA-3′; PKG-I, forward 5′-CTTGGAGTGGGAGGTTTC-3′ and reverse 5′-AATGTGTCGTTTCTTGAGG-3′; ICAM-1, forward 5′-TATCCATCCATCCCACAG-3′ and reverse 5′-GTTCGTCTTTCATCCAGTTAGT-3′; β-actin, forward 5′-TACAACTCCTTGCAGCTCC-3′ and reverse 5′-ATCTTCATGAGGTAGTCAGTC-3′. The ROCK1, ROCK2, eNOS, PKG-I, and ICAM-1 levels were normalized to that of β-actin. The gene expression was determined by real-time quantitative monitoring of PCR reactions with LightCycler System (Roche, Indianapolis, IN, USA). All PCR experiments were performed in at least three independent treatments.

2.6. Immunohistochemistry. The paraffin tissue sections were dewaxed in xylene and rehydrated in gradient alcohol. Then, the sections were washed with distilled water, and endogenous peroxidase was blocked by 3% hydrogen peroxide. The heat-mediated antigen retrieval was performed with citrate buffer at pH 6 before starting the IHC staining protocol. Then, the sections were blocked for 60 min with 5% goat sera. Indirect immunoperoxidase staining of tissue sections was performed, and the samples were incubated overnight with

primary antibodies against Ki-67, ICAM-1, (Cambridge, MA, USA), eNOS, activated caspase-3 (Sigma-Aldrich, USA), and ROCK1 and ROCK2 (Proteintech, USA) at 4°C. Then, the tissue sections were washed with phosphate-buffered saline (PBS, 0.01 M), incubated with secondary antibodies, and visualized with diaminobenzidine (DAB, brown color, ZSGB-BIO, Beijing, China) and hematoxylin counterstaining under a microscope. The intensity of positive staining was measured by IOD/area with Image-Pro Plus 6.0 image analysis software (Media Cybernetics, Silver Spring, MD).

2.7. Western Blot Analysis. The protein expression of PKG-I was examined by Western blot assays. Briefly, vessel tissues were homogenized in lysis buffer, and the supernatants were collected by centrifugation at 12000 rpm for 15 min at 4°C. After determining the total protein concentration, 50 micrograms of protein per specimen was run on 10% SDS-polyacrylamide gel electrophoresis and transferred to nitrocellulose membranes. After blocking with 5% skim milk for 1 h at room temperature, the membranes were incubated with primary antibodies at 4°C overnight. Then, the membranes were washed with Tris-buffered saline containing 0.05% Tween 20, and they were incubated with secondary horseradish peroxidase-conjugated antibody for 1 h at room temperature. Antigen-antibody complexes were then visualized using an enhanced chemiluminescence kit (Amersham, USA), and the intensity of the protein bands was quantified with Quantity One software (version 4.6.2, Bio-Rad, USA). Rabbit polyclonal antibody PKG-I and mouse monoclonal antibody β-actin were purchased from Abcam (Cambridge, MA, USA).

2.8. Statistical Analysis. SPSS software (version 19.0; SPSS, Chicago, IL, USA) was used for statistical analyses. All statistical data are presented as the means ± standard error of the mean (SEM). Statistical analyses were performed using one-way analysis of variance. The differences between groups were considered significant at $P < 0.05$.

3. Results

3.1. Model Building. The aortic transplantation model was considered successfully established when there was complete patency of the grafted arteries without significant anastomotic bleeding 3 days after transplantation. The mean operative duration of surgical vascular transplantation was 41.5 ± 7.5 min. The ischemic time was consistently less than 30 minutes. An abdominal longitudinal incision was performed to observe the grafted vessels 3 days after surgery. In this study, the surgical success percentage was 87.5% (21/24). Eight weeks after transplantation, the blood flow at both the proximal and the distal anastomotic sites was observed. The patency of all successful grafted vessels was adequate.

3.2. Lycopene Ameliorated Allograft Arteriosclerosis and VSMCs Proliferation. Lycopene could remarkably alleviate neointimal hyperplasia and arteriosclerosis of the aortic grafts. As shown in Figures 1(a1)–1(a3), the HE staining of grafted vessels in each group showed that vascular stenosis and intimal thickening were significant in the allograft group (Figure 1(a2)) compared with the isograft group (a1). This pathological staining also revealed that the inflammatory cells accumulation and leukocyte infiltration were evident in the allograft group. We also measured the degree of vessel stenosis in each group and found that it was more significant in the allograft group. However, these features were not obvious in the lycopene group (Figure 1(a3)). The thickness of the intima in the lycopene group (89.09 ± 4.13 μm) was significantly decreased compared with the allograft group (131.01 ± 5.69 μm; $P < 0.05$). Furthermore, the Ki-67 expression (Figures 1(b1)–1(b3)) in VSMCs was also significantly decreased in the lycopene group compared with that in the allograft group. This indicated that VSMCs proliferation was reduced in grafted vessels after lycopene treatment. However, there was no obvious improvement in the caspase-3 expression (Figures 1(c1)–1(c3)), which indicated that the proapoptosis effects of lycopene were not significant in this study. The ratio of Ki-67/caspase-3 positive cells was analysed to evaluate the proliferation and apoptosis levels of the intimal cells. The ratio in the lycopene group (3.41 ± 0.21) was significantly lower than in the allograft group (7.16 ± 0.29).

3.3. Downregulation of ROCK1 and ROCK2 Expression Levels in Allograft Vessels after Lycopene Treatment. ROCKs activation was also critical in the progression of vascular arteriosclerosis. The ROCK1 and ROCK2 immunohistochemical staining was performed in our study to demonstrate the link between the upregulated ROCKs expression and arteriosclerosis. As shown in Figures 2(a1)–2(a3) and 2(b1)–2(b3), the ROCK1 and ROCK2 expression levels in VSMCs were significantly decreased in the lycopene group ((a3) and (b3)) compared with the allograft group ((a2) and (b2)). The decreased IOD/area means (integrated optical density/area) of ROCK1 and ROCK2 in the lycopene group ((a4) and (b4)) coincided with the immunohistochemical staining results. Real-time quantitative PCR analysis also revealed that the relative mRNA expression of ROCK1 and ROCK2 ((a5) and (b5)) was significantly lower than that in the allograft group (both P values < 0.05).

3.4. Lycopene Inhibited ICAM-1 Expression in Allograft Vessels. We assessed whether lycopene inhibited inflammation in the grafted vessels, which was also considered to play a key role in the progress of allograft arteriosclerosis. In this study, immunohistochemical staining of grafted vessels was performed, and the results are shown as the IOD/area means (Figure 3(a4)). As shown in Figure 3, there is a significant decrease in the ICAM-1 expression in the lycopene group (a3) compared with the allograft group vessels (a2). The real-time quantitative PCR results (a5) also demonstrated that the relative mRNA expression of ICAM-1 in the lycopene group was significantly lower than that in the allograft group.

3.5. Lycopene Increased eNOS and PKG-I Protein Expression in Aortic Allografts. eNOS is an important factor which has a protective function in the cardiovascular system and is

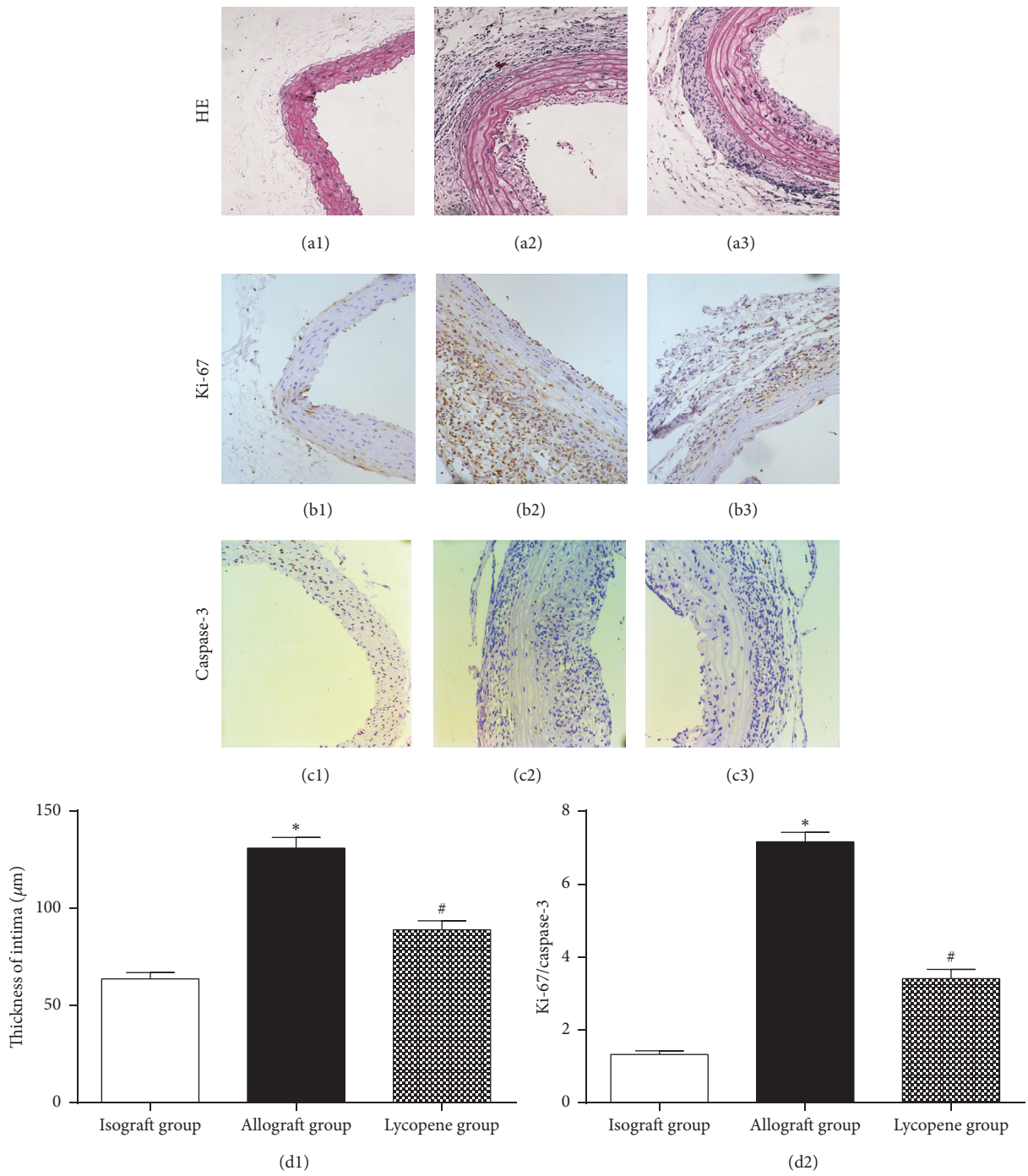

Figure 1: Histopathological staining of grafted vessels and analysis of cell proliferation and apoptosis under light microscopy (original magnification ×200). (a1)–(a3) Hematoxylin-eosin (HE) staining of grafted aortic specimens obtained 8 weeks after transplantation. (b1)–(b3) Immunohistochemical staining of Ki-67 in arterial grafts. (c1)–(c3) Immunohistochemical staining of caspase-3 in grafted arteries. (d1) Thickness of intima in each group (μm, original magnification ×200), $^{*}P < 0.001$, allograft group compared with the isograft group; $^{\#}P = 0.017$, lycopene group compared with the allograft group. (d2) The positive cells ratio of Ki-67/caspase-3 in each group, $^{*}P < 0.001$, $^{\#}P < 0.001$. ((a1), (b1), and (c1)) Isograft group; ((a2), (b2), and (c2)) allograft group; ((a3), (b3), and (c3)) lycopene group.

attributed to the production of NO in vascular endothelial cells. In this study, eNOS expression level was measured by immunohistochemical staining of grafted vessels in each group (Figures 3(b1)–3(b3)). The positive staining was evident in the isograft group (b1) and lycopene group (b3), while, in the allograft group (b2), it was significantly decreased. The IOD/area means analysis (Figure 3(b4)) and real-time quantitative PCR measurements (b5) both demonstrated the results of the immunohistochemical staining. All these data revealed that eNOS expression level in arterial transplantation

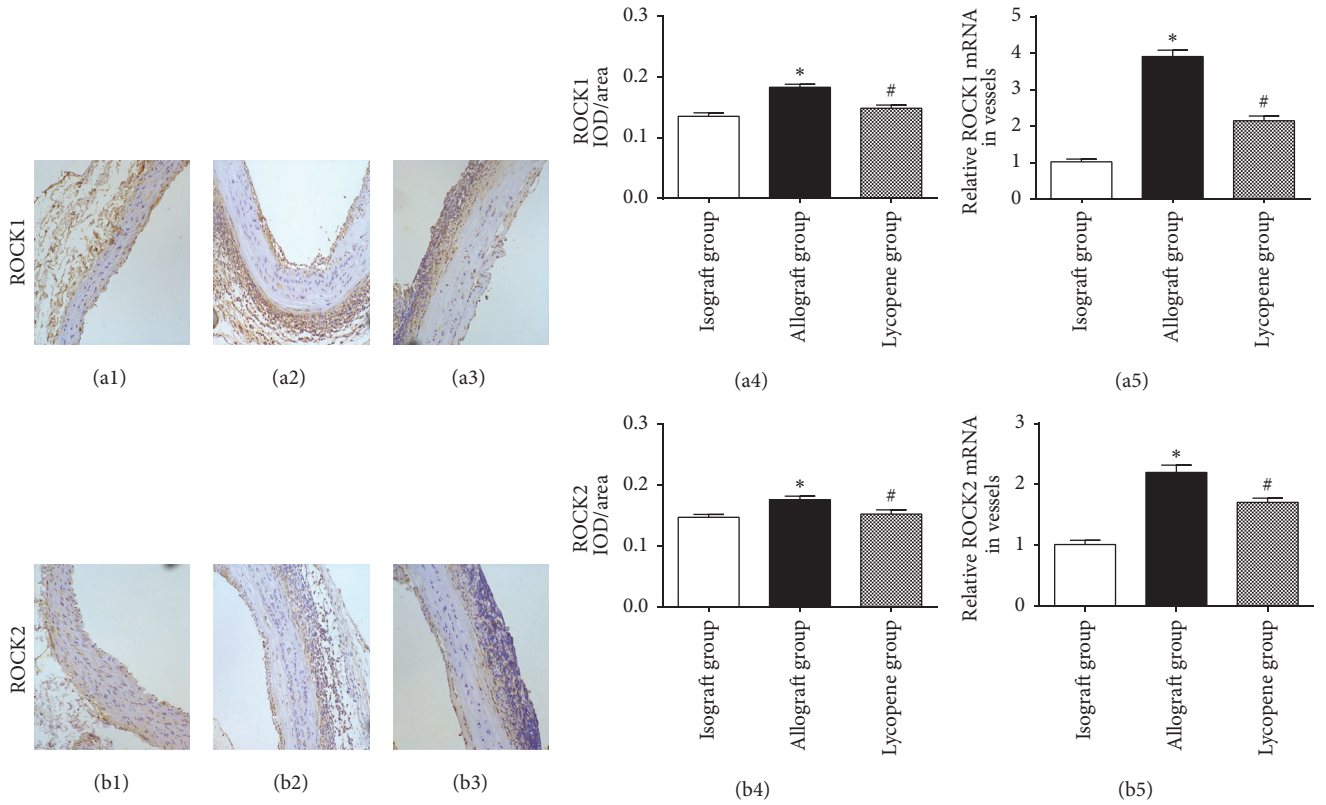

Figure 2: Expression of ROCK1 and ROCK2 in each group. ((a1)–(a3) and (b1)–(b3)) Immunohistochemical staining of ROCK1 and ROCK2 in grafted arteries (original magnification ×200). ((a4) and (b4)) The mean of the IOD/area of ROCK1 and ROCK2 in each group. IOD/area: integrated optical density/area; the mean of the IOD/area of positive staining was used to accurately measure the degree of positive expression in immunohistochemical staining. $^{*}P < 0.01$ for the isograft group compared with the allograft group; $^{\#}P < 0.05$ for the lycopene group compared with the allograft group. ((a5) and (b5)) Real-time quantitative PCR analysis of ROCK1 and ROCK2 mRNA expression in each group. $^{*}P < 0.001$ and $^{\#}P < 0.05$. ((a1) and (b1)) Isograft group; ((a2) and (b2)) allograft group; ((a3) and (b3)) lycopene group.

could be increased after lycopene treatment. Meanwhile, PKG-I plays a critical role in regulating vascular smooth cells by regulating Rho A activation. Western blot analysis was performed to evaluate the protein expression of PKG-I in grafted vessels. As shown in Figure 4(a), the results of Western blot analysis revealed the different expression of PKG-I protein in aortic grafts between the 3 groups. In the lycopene group, the PKG-I expression was markedly increased compared with the allograft group ($P < 0.05$). The result also coincided with the real-time quantitative PCR analysis of PKG-I mRNA expression in the grafted vessels (Figure 4(b)).

4. Discussion

Transplant vasculopathy is one of the major causes of graft failure in organ transplantation. The protection of transplant vessels has become an important issue in maintaining the normal functions of the grafts [13, 14]. In this study, we investigated the preventive and therapeutic effects of lycopene in treating transplant vasculopathy. The results of our study demonstrated that intimal hyperplasia and smooth muscle cell proliferation were remarkably reduced by the administration of lycopene at 8 weeks after allogeneic aortic transplantation. Furthermore, we also found that lycopene could increase the expression of PKG-I and eNOS, downregulate the expression of ROCK1, ROCK2, and ICAM-1, and inhibit the infiltration of inflammatory cell in allograft vessels. However, in the vascular intima and media, the immunohistochemical staining showed that there was no significant increase in the cell apoptosis after lycopene treatment. This indicated that the proapoptosis effect of lycopene was not obvious in this study, and its ameliorative effects on the transplant arteriosclerosis were not based on the proapoptosis mechanisms. Furthermore, the plasma cGMP concentration was also detected in this study to evaluate the expression levels of cGMP signaling pathways. After lycopene treatment, it exhibited a significant increase when compared with the allograft group. All the data in this study demonstrated that arteriosclerosis in vascular allograft transplantation could be ameliorated by lycopene through regulating NO/cGMP pathways and Rho-associated kinases expression.

Endothelial cells are extremely important in regulating vascular tone and maintaining vascular structure [15]. However, the immune and nonimmune injuries that chronically occur in endothelial cells (ECs) may trigger endothelial activation and dysfunction in patients after organ transplantation [16]. These can result in intimal hyperplasia, smooth muscle cell (SMC) proliferation, and extracellular matrix

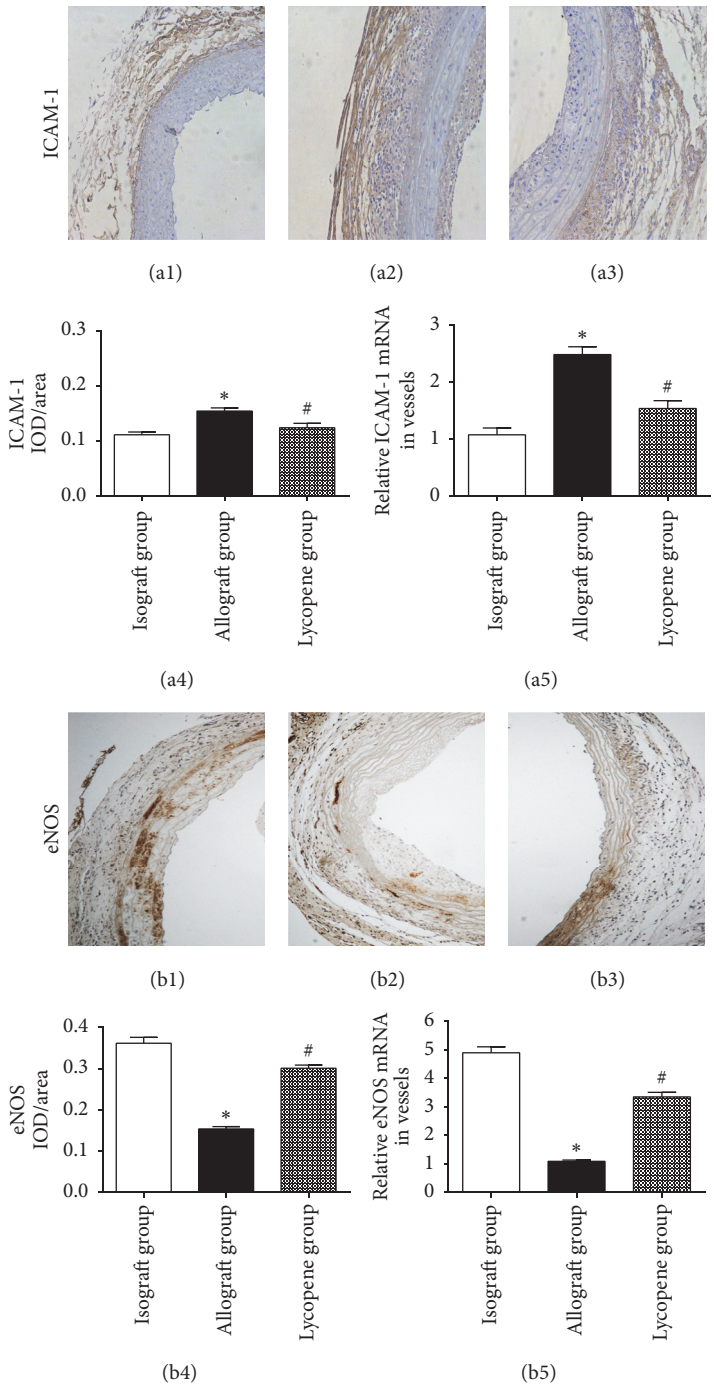

Figure 3: Expression levels of ICAM-1 and eNOS were determined by immunohistochemical staining and real-time quantitative PCR analysis. ((a1)–(a3) and (b1)–(b3)) Immunohistochemical staining of ICAM-1 and eNOS in grafted arteries (original magnification ×200). ((a4) and (b4)) The mean of IOD/area of ICAM-1 and eNOS immunohistochemical staining in each group. (a4) $^{*}P = 0.001$, allograft group compared with the isograft group; $^{\#}P = 0.019$, lycopene group compared with the allograft group. (b4) $^{*}P < 0.001$, $^{\#}P < 0.001$. ((a5) and (b5)) Real-time quantitative PCR analysis of ICAM-1 and eNOS mRNA expression in each group. (a5) $^{*}P < 0.001$, $^{\#}P = 0.003$. (b5) $^{*}P < 0.001$ and $^{\#}P < 0.001$. ((a1) and (b1)) Isograft group; ((a2) and (b2)) allograft group; ((a3) and (b3)) lycopene group.

synthesis, which is accompanied by resulting gradual decline in graft function. Nitric oxide (NO) is the primary mediator of endothelial function, and it can cause vasodilation by upregulating guanylyl cyclases on subjacent vascular SMC and inhibiting vascular SMC proliferation and migration [17, 18]. However, ischemia-reperfusion (I/R) injury, oxidative stress, and immunosuppressive drugs can generate excessive O_2^-, which can rapidly inactivate NO in allografts and lead to the occurrence and progression of graft vasculopathy [19]. In this study, the eNOS immunohistochemical staining

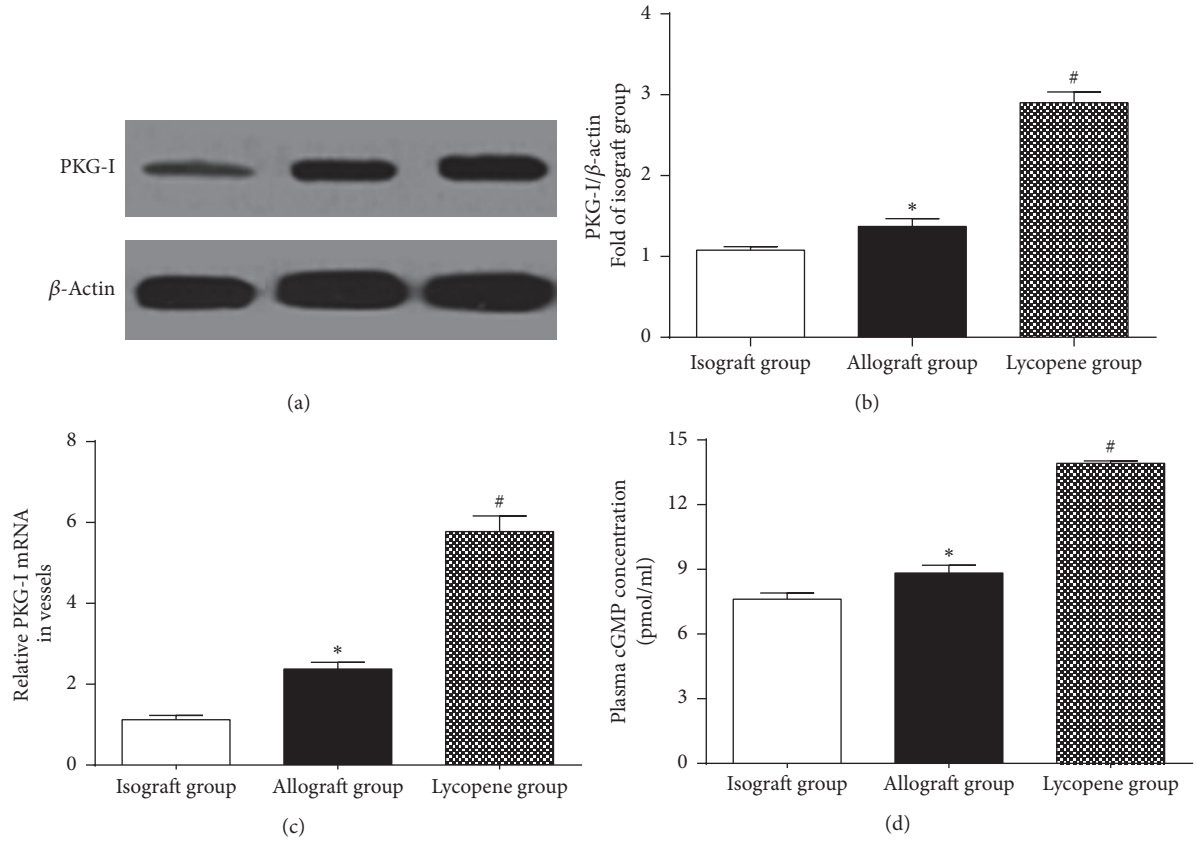

Figure 4: Analysis of PKG-I protein expression in grafted arteries and plasma cGMP concentration detection in each group. ((a) and (b)) Western blot analysis of PKG-I protein expression in each group; $^{*}P < 0.05$, allograft group compared with the isograft group; $^{\#}P < 0.001$, lycopene group compared with the allograft group. (c) Real-time quantitative PCR analysis of PKG-I mRNA expression; $^{*}P < 0.001$; $^{\#}P < 0.001$. (d) Determination and analysis of the plasma cGMP concentration in each group; $^{*}P < 0.05$; $^{\#}P < 0.001$.

was performed in grafted vessels to analyse the expression levels of NO *in vivo*. eNOS has a protective effect on the cardiovascular system and is considered to be attributed to NO production in the vascular endothelial cell. Its activation and expression play important roles in regulating the NO production. Lycopene is the most potent single oxygen quencher among the natural carotenoids. Di Tomo et al. demonstrated that lycopene suppresses reactive oxygen species (ROS) generation and increases the NO expression level and bioavailability in human umbilical vein endothelial cells [6]. The authors also reported that lycopene regulates the NO expression level and bioavailability by directly reducing molecules. The results of our study showed that neointimal hyperplasia was alleviated, and the Ki-67 expression was downregulated in the lycopene group. In addition, these results coincided with the experimental design proposed in this study that lycopene can improve the graft vasculopathy by antioxygenation. Cells apoptosis dysfunction of vascular smooth muscle cell is considered another important factor that causes neointimal hyperplasia and intimal thickening during the progression of vascular atherosclerosis [20]. The proapoptosis effect of lycopene was not obvious in our study which indicated that lycopene ameliorated vascular atherosclerosis through regulating other signaling pathways, and this is in agreement with our experimental hypothesis.

Migration of vascular smooth muscle cell from the media to intima plays a crucial role during the formation of atherosclerotic plaques and vascular restenosis in graft vasculopathy. Rho-associated kinases (ROCKs) are typical downstream effectors of the small GTPase Rho family [21]. ROCKs can be activated by upstream regulator Rho A, phosphorylating and inactivating myosin light chain (MLC) phosphatase, and subsequently enhancing MLC phosphorylation, resulting in vasoconstriction [22, 23]. Additionally, ROCKs can regulate the actin cytoskeleton reorganization of endothelial cells (ECs) and SMC, which is associated with vascular remodeling [9]. In a porcine model, long-term inhibition of Rho kinase results in regression of the arteriosclerotic lesions [24]. ROCK1 and ROCK2 are two representative subtypes of the ROCK family. They have high homology, and 65 percent of the amino acid sequences are the same. In addition, both help regulate many important basic functions of cells, such as cell adhesion, migration, proliferation, apoptosis, and transcription regulation. The upregulated ROCK1 and ROCK2 expression levels are considered to play an important role in the progression of transplant vascular atherosclerosis [24]. The results of our study also demonstrated that ROCK1 and ROCK2 expression levels were significantly decreased after lycopene treatment, which improved the grafted vessels. Piera-Velazquez et al. showed

that ROCK1 inhibition can decrease foam cell formation and inhibit the pathological process of atherosclerosis [25]. However, the specific regulatory mechanisms of ROCK1 and ROCK2 in ameliorating graft atherosclerosis remain unclear. In addition, PKG-I is a critical mediator of the NO/cGMP pathway that plays an important role in regulating vascular smooth cell by regulating Rho A activation [26]. PKG-I phosphorylates Rho A at Ser188, which inhibits its membrane association and prevents the activation of Rho kinases [27]. Our data showed that lycopene could increase the PKG-I level and downregulate ROCK1 and ROCK2 expression in grafted vessels. The increased plasma cGMP concentration also indicated the upregulated expression of cGMP signaling pathway after lycopene treatment.

Vessel inflammation is also an early and important event in the process of allograft atherosclerosis [28]. It is now widely accepted that both the production of intercellular adhesion molecules (ICAM-1) and their shedding onto endothelial and leukocytic surfaces play a pivotal role in mediating the interaction between endothelial cells and blood constituents at the early stage of atherosclerosis [29, 30]. In addition, ICAM-1 increased the thrombotic potential by influencing the migration and proliferation of SMCs in the vessel blood. In addition, it is reported that TNF-α can upregulate ICAM-1 expression on the endothelium during atherogenesis via NF-κB binding to the promoter. It has been reported that lycopene can inhibit TNF-α-induced ICAM-1 protein expression through affecting the NF-κB signaling pathway [31], which explains how lycopene has protective effects on allograft atherosclerosis through anti-inflammatory activity.

In conclusion, the results of our study demonstrated that lycopene had significant therapeutic effects on the occurrence and progression of transplant vascular atherosclerosis. It could ameliorate allograft atherosclerosis by regulating the expression of the NO/cGMP pathway and affecting many critical factors. This may provide new possibilities for preventing the formation of grafts atherosclerosis during clinical organ transplantation.

Competing Interests

All authors declare that there are no financial or nonfinancial competing interests regarding the publication of this paper.

Authors' Contributions

Yunqiang He and Peng Xia contributed equally to this work.

Acknowledgments

This project was supported by grants from the National Natural Science Foundation of China (81501382 and 81572087), Natural Science Foundation of Zhejiang Province (LQ16H100002, LQ13H100003, and LY16H050007), Science and Technology Agency of Zhejiang Province (2015C33186), and Science and Technology Department of Wenzhou (Y20120157).

References

[1] O. Bamgbola, "Metabolic consequences of modern immunosuppressive agents in solid organ transplantation," *Therapeutic Advances in Endocrinology and Metabolism*, vol. 7, no. 3, pp. 110–127, 2016.

[2] Y. Zhang, M. Yang, S. Gong et al., "Cordyceps sinensis extracts attenuate aortic transplant arteriosclerosis in rats," *Journal of Surgical Research*, vol. 175, no. 1, pp. 123–130, 2012.

[3] Y. Sun, K. Wang, P. Ye et al., "MicroRNA-155 promotes the directional migration of resident smooth muscle progenitor cells by regulating monocyte chemoattractant protein 1 in transplant arteriosclerosis," *Arteriosclerosis, Thrombosis, and Vascular Biology*, vol. 36, no. 6, pp. 1230–1239, 2016.

[4] M. A. Soares, O. C. Ezeamuzie, M. J. Ham et al., "Targeted protection of donor graft vasculature using a phosphodiesterase inhibitor increases survival and predictability of autologous fat grafts," *Plastic and Reconstructive Surgery*, vol. 135, no. 2, pp. 488–499, 2015.

[5] G. Britton, "Structure and properties of carotenoids in relation to function," *The FASEB Journal*, vol. 9, no. 15, pp. 1551–1558, 1995.

[6] P. Di Tomo, R. Canali, D. Ciavardelli et al., "β-Carotene and lycopene affect endothelial response to TNF-α reducing nitro-oxidative stress and interaction with monocytes," *Molecular Nutrition and Food Research*, vol. 56, no. 2, pp. 217–227, 2012.

[7] L. Borysova and T. Burdyga, "Evidence that NO/cGMP/PKG signalling cascade mediates endothelium dependent inhibition of IP3R mediated Ca^{2+} oscillations in myocytes and pericytes of ureteric microvascular network in situ," *Cell Calcium*, vol. 58, no. 6, pp. 535–540, 2015.

[8] X. Liu, D. Qu, F. He, Q. Lu, J. Wang, and D. Cai, "Effect of lycopene on the vascular endothelial function and expression of inflammatory agents in hyperhomocysteinemic rats," *Asia Pacific Journal of Clinical Nutrition*, vol. 16, supplement 1, pp. 244–248, 2007.

[9] G. K. Kolluru, S. Majumder, and S. Chatterjee, "Rho-kinase as a therapeutic target in vascular diseases: striking nitric oxide signaling," *Nitric Oxide*, vol. 43, pp. 45–54, 2014.

[10] G. Onuta, H. Rienstra, J. F. de Boer et al., "Rosiglitazone attenuates transplant arteriosclerosis after allogeneic aorta transplantation in rats," *Transplantation*, vol. 84, no. 4, pp. 517–526, 2007.

[11] F. Song, H. Sun, Y. Wang et al., "Pannexin3 inhibits TNF-α-induced inflammatory response by suppressing NF-κB signalling pathway in human dental pulp cells," *Journal of Cellular and Molecular Medicine*, 2016.

[12] C.-L. Lin, F.-S. Wang, Y.-C. Hsu et al., "Modulation of Notch-1 signaling alleviates vascular endothelial growth factor-mediated diabetic nephropathy," *Diabetes*, vol. 59, no. 8, pp. 1915–1925, 2010.

[13] A. von Rossum, I. Laher, and J. C. Choy, "Immune-mediated vascular injury and dysfunction in transplant arteriosclerosis," *Frontiers in Immunology*, vol. 5, article 684, 2014.

[14] K. Lietz and L. W. Miller, "Current understanding and management of allograft vasculopathy," *Seminars in Thoracic and Cardiovascular Surgery*, vol. 16, no. 4, pp. 386–394, 2004.

[15] E. Osto, F. Tona, E. De Bon, S. Iliceto, and G. Cella, "Endothelial dysfunction in cardiac allograft vasculopathy: potential pharmacological interventions," *Current Vascular Pharmacology*, vol. 8, no. 2, pp. 169–188, 2010.

[16] Q. Zhou and J. K. Liao, "Rho kinase: an important mediator of atherosclerosis and vascular disease," *Current Pharmaceutical Design*, vol. 15, no. 27, pp. 3108–3115, 2009.

[17] C. P. Tiefenbacher and J. Kreuzer, "Nitric oxide-mediated endothelial dysfunction-is there need to treat?" *Current Vascular Pharmacology*, vol. 1, no. 2, pp. 123–133, 2003.

[18] T. Largiadèr, M. Eto, S. K. Payeli et al., "Endothelial nitric oxide synthase gene transfer inhibits human smooth muscle cell migration via inhibition of Rho A," *Journal of Cardiovascular Pharmacology*, vol. 52, no. 4, pp. 369–374, 2008.

[19] I. Fleming, "Molecular mechanisms underlying the activation of eNOS," *Pflugers Archiv European Journal of Physiology*, vol. 459, no. 6, pp. 793–806, 2010.

[20] S. Kang, K. Kim, J. Noh et al., "Simvastatin induces the apoptosis of normal vascular smooth muscle through the disruption of actin integrity via the impairment of RhoA/Rac-1 activity," *Thrombosis and Haemostasis*, vol. 116, no. 3, pp. 496–505, 2016.

[21] K. Riento and A. J. Ridley, "Rocks: multifunctional kinases in cell behaviour," *Nature Reviews Molecular Cell Biology*, vol. 4, no. 6, pp. 446–456, 2003.

[22] M. Noda, C. Yasuda-Fukazawa, K. Moriishi et al., "Involvement of rho in GTPγS-induced enhancement of phosphorylation of 20 kDa myosin light chain in vascular smooth muscle cells: inhibition of phosphatase activity," *FEBS Letters*, vol. 367, no. 3, pp. 246–250, 1995.

[23] K. Kimura, M. Ito, M. Amano et al., "Regulation of myosin phosphatase by Rho and Rho-associated kinase (Rho-kinase)," *Science*, vol. 273, no. 5272, pp. 245–248, 1996.

[24] H. Shimokawa, K. Morishige, K. Miyata et al., "Long-term inhibition of Rho-kinase induces a regression of arteriosclerotic coronary lesions in a porcine model in vivo," *Cardiovascular Research*, vol. 51, no. 1, pp. 169–177, 2001.

[25] S. Piera-Velazquez, Z. Li, and S. A. Jimenez, "Role of endothelial-mesenchymal transition (EndoMT) in the pathogenesis of fibrotic disorders," *American Journal of Pathology*, vol. 179, no. 3, pp. 1074–1080, 2011.

[26] M. Kato, R. Blanton, G.-R. Wang et al., "Direct binding and regulation of RhoA protein by cyclic GMP-dependent protein kinase Iα," *Journal of Biological Chemistry*, vol. 287, no. 49, pp. 41342–41351, 2012.

[27] F. Hofmann, "The biology of cyclic GMP-dependent protein kinases," *Journal of Biological Chemistry*, vol. 280, no. 1, pp. 1–4, 2005.

[28] G. K. Hansson, "Inflammation, atherosclerosis, and coronary artery disease," *The New England Journal of Medicine*, vol. 352, no. 16, pp. 1626–1695, 2005.

[29] Y. Luo, J. Feng, Q. Xu, W. Wang, and X. Wang, "NSun2 deficiency protects endothelium from inflammation via mRNA methylation of ICAM-1," *Circulation Research*, vol. 118, no. 6, pp. 944–956, 2016.

[30] T. Noguchi, K. Nakagome, T. Kobayashi et al., "Effect of LTRA on IP-10-induced eosinophil adhesion to ICAM-1," *Allergology International*, vol. 65, pp. S62–S64, 2016.

[31] C.-F. Hung, T.-F. Huang, B.-H. Chen, J.-M. Shieh, P.-H. Wu, and W.-B. Wu, "Lycopene inhibits TNF-α-induced endothelial ICAM-1 expression and monocyte-endothelial adhesion," *European Journal of Pharmacology*, vol. 586, no. 1–3, pp. 275–282, 2008.